Available online at www.sciencedirect.com

ScienceDirect

Journal of Magnesium and Alloys 9 (2021) 705–747

www.elsevier.com/locate/jma

Review

Research advances in magnesium and magnesium alloys worldwide in 2020

Yan Yang[a,b,*], Xiaoming Xiong[a], Jing Chen[a], Xiaodong Peng[a,b,*], Daolun Chen[c], Fusheng Pan[a,b,*]

[a] *National Engineering Research Center for Magnesium Alloys, Chongqing University, Chongqing 400044, China*
[b] *State Key Laboratory of Mechanical Transmissions, College of Materials Science and Engineering, Chongqing University, Chongqing 400044, China*
[c] *Department of Mechanical and Industrial Engineering, Ryerson University, Toronto, Ontario M5B 2K3, Canada*

Received 26 March 2021; received in revised form 28 April 2021; accepted 28 April 2021
Available online 19 May 2021

Abstract

Research on magnesium alloys continues to attract great attention, with more than 3000 papers on magnesium and magnesium alloys published and indexed in SCI in 2020 alone. The results of bibliometric analyses show that microstructure control and mechanical properties of Mg alloys are continuously the main research focus, and the corrosion and protection of Mg alloys are still widely concerned. The emerging research hot spots are mainly on functional magnesium materials, such as Mg ion batteries, hydrogen storage Mg materials, and bio-magnesium alloys. Great contributions to the research and development of magnesium alloys in 2020 have been made by Chongqing University, Chinese Academy of Sciences, Central South University, Shanghai Jiaotong University, Northeastern University, Helmholtz Zentrum Geesthacht, etc. The directions for future research are suggested, including: 1) the synergistic control of microstructures to achieve high-performance magnesium alloys with concurrent high strength and superior plasticity along with high corrosion resistance and low cost; 2) further development of functional magnesium materials such as Mg batteries, hydrogen storage Mg materials, structural-functional materials and bio-magnesium materials; 3) studies on the effective corrosion protection and control of degradation rate of magnesium alloys; 4) further improvement of advanced processing technology on Mg alloys.
© 2021 Chongqing University. Publishing services provided by Elsevier B.V. on behalf of KeAi Communications Co. Ltd.
This is an open access article under the CC BY-NC-ND license (http://creativecommons.org/licenses/by-nc-nd/4.0/)
Peer review under responsibility of Chongqing University

Keywords: Bibliometric analysis; Magnesium alloys; Functional magnesium materials; Corrosion and protection; Microstructure; Mechanical properties; Mg battery; Degradation.

1. Introduction

Magnesium (Mg) is considered to be the best green material in the 21st century [1]. Mg alloys have excellent physical and chemical properties such as low density, high specific strength and stiffness, good damping performance, good biocompatibility, large hydrogen storage capacity, and high theoretical specific capacity for battery, etc. Thus magnesium and its alloys have attracted more and more attention and possess great application potential in the field of aerospace, automotive, 3C (computers, communications, and consumer electronics), biomedical and energy sectors, etc., in the world [2-4]. However, a lot of difficulties still need to be overcome to broaden the further applications of magnesium alloys. The relatively low strength, poor plasticity, and inferior corrosion resistance of magnesium alloys hinder the structural applications, while the problems on the fast degradation rate of Mg alloys and narrow hydrogen charging and discharging window need to be solved in functional materials to broaden the future application of Mg alloys [5].

In the past year of 2020, despite the challenges faced, there were still a lot of studies on magnesium and its alloys including alloy design and optimization, characterization and observation of microstructures, functional materials such as

* Corresponding authors.
E-mail addresses: yanyang@cqu.edu.cn (Y. Yang), pxd@cqu.edu.cn (X. Peng), fspan@cqu.edu.cn (F. Pan).

https://doi.org/10.1016/j.jma.2021.04.001
2213-9567/© 2021 Chongqing University. Publishing services provided by Elsevier B.V. on behalf of KeAi Communications Co. Ltd. This is an open access article under the CC BY-NC-ND license (http://creativecommons.org/licenses/by-nc-nd/4.0/) Peer review under responsibility of Chongqing University

bio-magnesium alloys and Mg batteries, which is beneficial to promoting the applications of magnesium and its alloys. Using "magnesium" as the title to search in the authoritative database of "Web of Science Core Collection", 3034 papers containing magnesium in the title were published in the past year alone. Based on such a literature search, the research trends and hotspots of magnesium alloys were analyzed. The present work aims to review the important advances of magnesium and its alloys worldwide in 2020, so as to enhance the spread of scientific research of magnesium alloys and promote the development and application of magnesium alloys globally.

2. Overview of Mg research in 2020

2.1. Overall status of Mg research

The "Mg or magnesium alloy" was used as a keyword to search in the Science Citation Index Expanded and Emerging Sources Citation Index of Web of Science (WoS) Core Collection with a time limit of 2020 only on January 5, 2021 and 3034 papers were found. The VOSviewer software was used to analyze the data of Mg alloy papers in 2020.

The distributions of countries and organizations that published Mg papers were analyzed based on the above-mentioned literature search results. Fig. 1 shows the statistical analysis result of the distribution of countries with at least 5 Mg papers published in 2020. Fig. 1(a) shows the paper percentage in different countries (regions). The top five countries (regions) that published Mg papers are China, the USA, India, Germany, and Japan. China publishes the most Mg papers with 43.78% while the second country is the USA with 7.68%. Fig. 1(b) shows the network visualization among different countries. The circle area size represents the number of published papers while the width of the link lines among different countries (regions) indicates the collaboration activity. About 57.05% of Mg papers are published based on international collaborations. A lot of international collaborations are seen among China, USA, Germany, Australia, and England. The statistical data indicates that international collaborations can effectively accelerate the research and development of Mg alloys.

Fig. 2 shows the statistical analysis result of organizations that published at least 15 Mg papers in 2020. Fig. 2(a) shows the top 20 organizations that published Mg papers in 2020. Chongqing University has published the most Mg papers, followed by Chinese Academy of Sciences, Central South University, Shanghai Jiaotong University, Northeastern University, and Helmholtz Zentrum Geesthacht, etc. Fig. 2(b) shows the network visualization among different organizations. The circle area size represents the number of published papers, while the width of the link lines among different organizations indicates the collaboration activity. There is a lot of collaborations among different organizations. More than 63.10% of Mg papers are published based on collaborations, which suggests that collaborations among different organizations can significantly accelerate Mg research. International collaborations among different institutions is conducive to the dissemination and enhanced impact of academic achievements in the field of Mg alloys.

Table 1
Top 20 journals with Mg papers worldwide in 2020.

Journals	Impact Factor	Number of Magnesium Papers
Materials Science and Engineering A	4.652	176
Journal of Alloys and Compounds	4.650	175
Journal of Magnesium and Alloys	7.115	111
Materials	3.057	101
Metals	2.117	78
Journal of Materials Engineering and Performance	1.652	66
Journal of Materials Research and Technology-JMR&T	5.289	62
Materials Characterization	3.562	62
Metals and Materials International	1.990	59
Journal of Materials Science & Technology	6.155	58
Materials Research Express	1.929	54
Surface & Coatings Technology	3.784	53
Materials Letters	3.204	50
International Journal of Hydrogen Energy	4.939	47
Rare Metal Materials and Engineering	0.485	46
Acta Metallurgica Sinica-English Letters	2.090	41
Corrosion Science	6.479	40
Metallurgical and Materials Transactions A	2.050	38
Materials and Design	6.289	34
Journal of the Electrochemical Society	3.721	32

2.2. Statistics and analysis of journals publishing Mg papers

According to the number of magnesium papers published in 2020, the top 20 journals are listed in Table 1. The top three journals are Materials Science and Engineering A, Journal of Alloys and Compounds, and Journal of Magnesium and Alloys. The network visualization among different journals that published at least 10 Mg papers in 2020 is shown on Fig. 3. The relatedness among different journals is determined based on the number of times they cite each other. In general, the closer the two journals locate to each other, the stronger their relatedness. The mutual citation links between journals are also represented by lines. The results indicate that there are a lot of mutual citation connections among different journals. The correlations among the Journal of Magnesium and Alloys, Materials Science and Engineering A, and Journal of Alloys and Compounds are quite close.

Journal of Magnesium and Alloys (JMA, ISSN 2213–9567) launched in 2013 is an English journal focused on magnesium and its alloys in the world. JMA provides an international medium to publish theoretical and experimental studies on magnesium in the field of science and engineering. JMA covers all aspects of magnesium, magnesium alloys, and their products. JMA has achieved a good reputation with great influence in the world. Through the fast development for several years by publishing high-quality papers, the IF of JMA increases rapidly from 4.523 in 2018 to 7.115 in 2019, ranking at No. 2 among the 79 journals in Metallurgy & Metallurgical

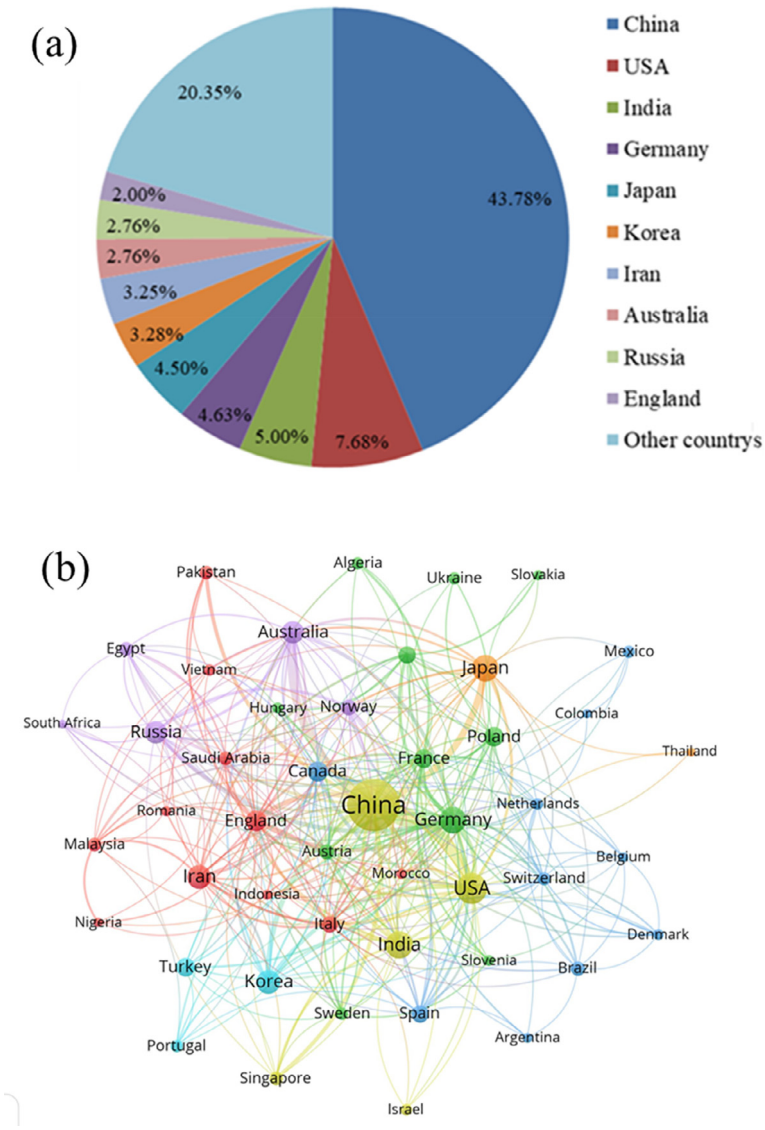

Fig. 1. Statistical analysis of the distribution of countries with at least 5 Mg papers published in 2020: (a) Paper percentage in different countries (regions); (b) network visualization among different countries.

Engineering category (JCR Q1). 111 papers were published in the JMA in 2020, with an increase of 58.57% compared to 2019. Statistical analysis of the countries (regions) and institutions of the JMA articles revealed the extent of international, national and institutional collaborations involved in JMA publications. Fig. 4 shows the statistical analysis result of country (region) distribution of Mg papers published in the JMA in 2020. Fig. 4(a) indicates the paper percentage in different countries (regions). The top five countries that published Mg papers in the JMA are China, the USA, Germany, Australia and Korea, respectively. The country (region) distribution of the papers published in the JMA is similar to that of all published Mg papers worldwide in 2020 as shown in Fig. 1(a). The number of collaborations among different institutions was 68, accounting for 61.26%. More than half of the articles in the JMA involved institutional collaborations, which is also similar to the whole trend. The statistical results confirm that the JMA enjoys greater importance to academic achievements resulting from collaborations between researchers and organizations. The academic value of JMA is effectively guaranteed by strictly controlling the academic level of the articles. The Mg papers published in the JMA have been highly recognized by many experts in the Mg field, and can effectively reflect the current status of Mg research and promote Mg research in the future.

2.3. Research hotspots in 2020 based on bibliometric analysis

The top 150 keywords by relevance, based on the 3034 magnesium articles published in 2020 are shown in Fig. 5. “Microstructure” appears 992 times while “Mechanical properties” appear 820 times, which means the microstructure and mechanical properties of magnesium alloys are still the re-

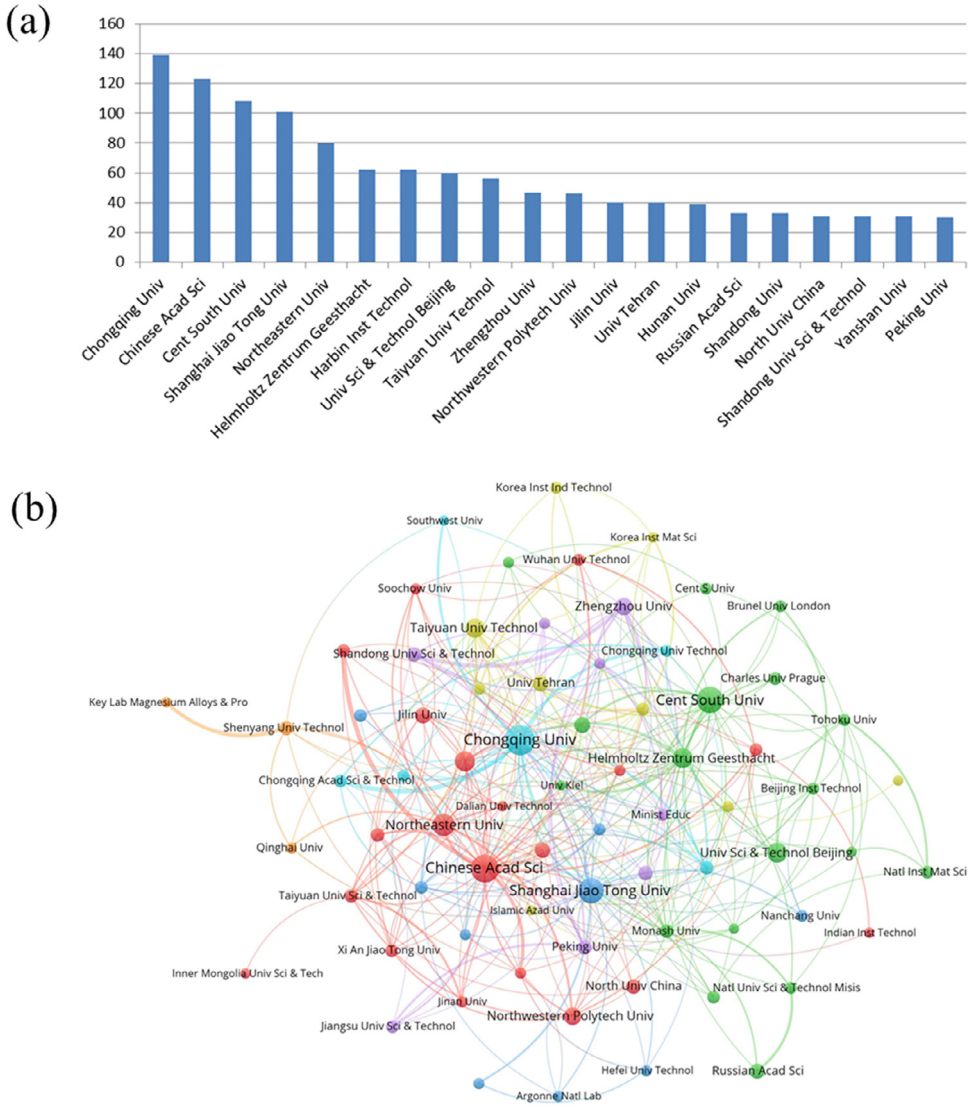

Fig. 2. Statistical analysis of organizations publishing at least 15 Mg papers in 2020: (a) Top 20 organizations; (b) network visualization among different organizations.

search hotspots. The microstructure is the foundation of magnesium alloy research. The microstructure of magnesium and its alloys directly influences their properties and performance. The studies on the microstructure mainly focus on the precipitation, grain refinement, dynamic recrystallization, texture, twinning, stacking ordered phase, and microstructure prediction. The above microstructural studies have laid the research foundation and become a research hotspot for magnesium alloys. Thus, the microstructure is the most frequently used keyword in Mg-related papers. As the lightest metallic structural material, the studies on the improvement of mechanical properties have never been stopped. The improvement of mechanical properties of magnesium alloys by adding alloying elements and applying a variety of plastic deformation routes is a common research topic for scientists.

By classifying the keywords and analyzing the related literature, the research on magnesium alloys could be generally grouped into three main categories: 1) traditional cast and wrought Mg alloys mainly focused on microstructure and mechanical properties, 2) corrosion and bio-Mg materials, and 3) functional materials including Mg battery and hydrogen materials, etc. Functional Mg materials have been noticed to attract more and more attention of scientific community recently.

3. Cast Mg alloys

3.1. Rare-earth (RE) containing cast Mg alloys

In 2020, high performance Mg-RE based cast alloys, especially Mg-Gd, Mg-Y based alloys are still a research hotspot due to their superior mechanical properties. However, the high content of RE additions results in a high cost, which hinders its automotive applications. Thus, more effort was put into developing the cast magnesium alloys with low RE additions in the past year. The mechanical properties of some new types of cast magnesium alloys developed worldwide are listed in

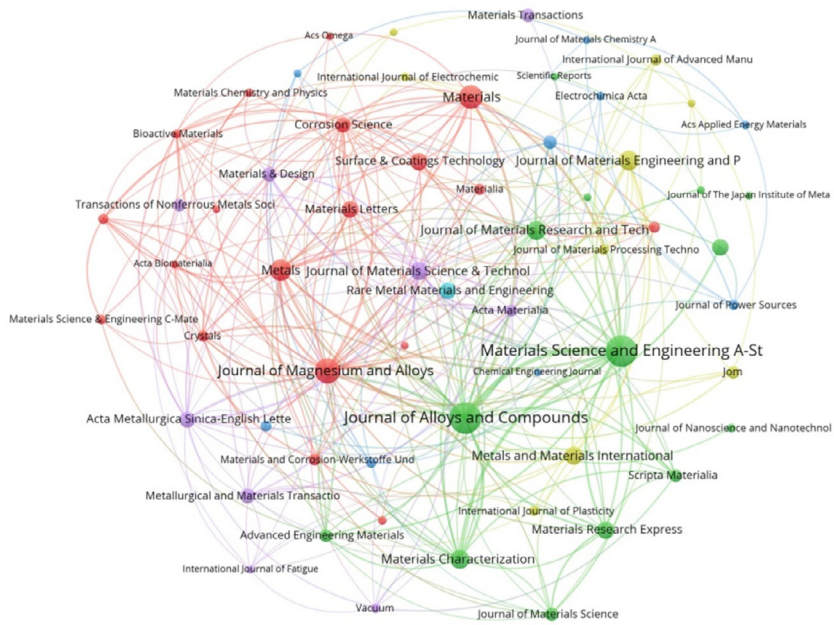

Fig. 3. Network visualization among different journals published at least 10 Mg papers in 2020.

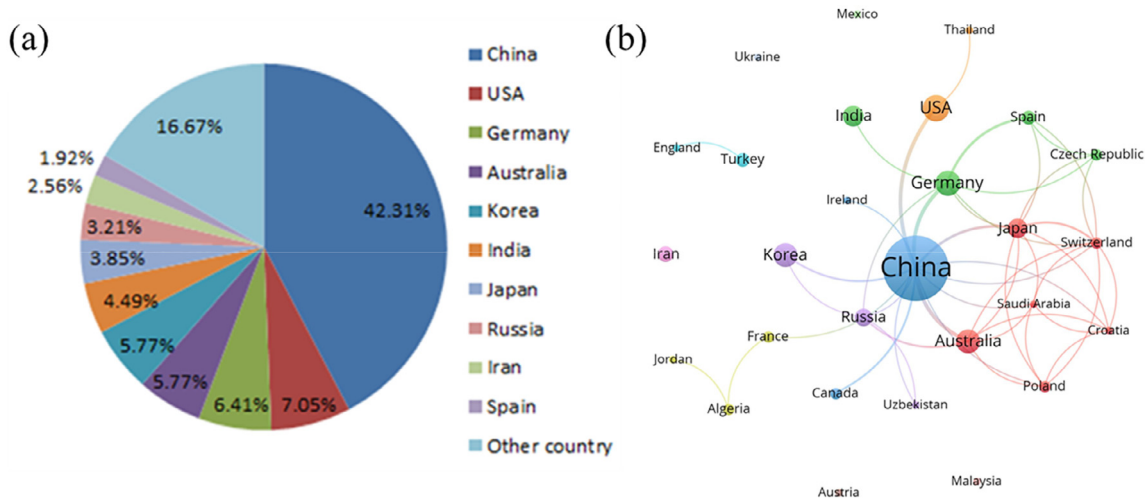

Fig. 4. Statistical analysis of county (region) distribution of Mg papers published in the Journal of Magnesium and Alloys in 2020: (a) Paper percentage in different countries (regions); (b) network visualization among different countries.

Table 2. The ultimate tensile strength (UTS) and the yield strength (YS) reach 340 MPa and 251 MPa respectively with an elongation (EL) of 6.2% for a sand-cast and heat treated Mg alloy with a relatively low Gd addition [6]. The UTS of some permanent mold cast and high-pressure die casting Mg alloys can be raised to above 250 MPa with relatively better ductility as well [7-9].

Wencai Liu and Wenjiang Ding et al. [6] prepared a Mg-6Gd-3Y-0.5Zr (GW63) alloy by sand-casting. To simulate the thermal cycling under extreme service conditions (e.g., space or moon environments), the sand-cast and T6 treated GW63 alloys were subjected to thermal cycling treatment which consists of deep cryogenic-elevated temperature cycling treatment (DCET) and deep cryogenic cycling treatment (DCT). They found that there was no obvious influence of DCT on the mechanical properties of the tested GW63 alloys as shown in Fig. 6. However, after the sand-cast and T6 treated bars were subjected to 3 cycles of the deep cryogenic-elevated temperature cycling treatment (T6-DCET-3C, DCET at ±196 °C), the YS and UTS first increased and then decreased, and the highest values appeared in the three cycles, 251 MPa and 340 MPa, with an increase by 5.9% and 10.0%, respectively, compared with the untreated alloy. The elevated temperature process of DCET plays a crucial role in improving the age-hardening responses and releasing the stress concentration brought by DCT to a great extent, leading to overcome the obstacle of essential phase transformation. Overall, Mg-6Gd-3Y-0.5Zr alloys have stable mechanical properties and there are no big

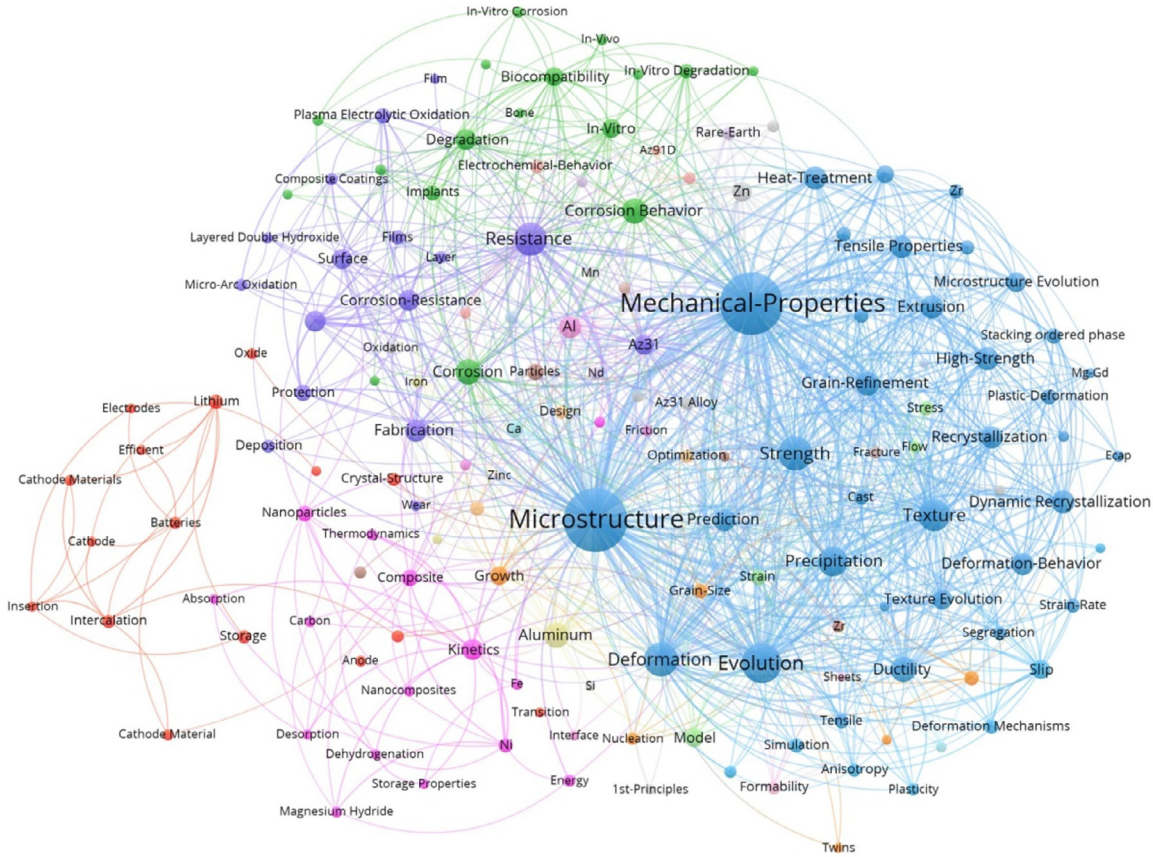

Fig. 5. Network visualization among different key words in Mg related papers.

Table 2
Mechanical properties of RE-containing cast magnesium alloys.

Alloy (wt.%)	Cast method	Heat treatment	YS (MPa)	UTS (MPa)	EL (%)	Ref.
Mg-6Gd-3Y-0.5Zr	Sand cast	T6-DCET-3C	251	340	6.2	[6]
Mg-6Zn-8.16Y-2.02Mn-0.3Mo	Permanent mold cast	–	–	265	13.5	[7]
Mg-4Y-4Zn	Permanent mold cast	–	122	232	–	[10]
Mg-2Y-2Zn	Permanent mold cast	500 °C × 12 h + 225 °C × 8 h	145	256	5.7	[11]
Mg-1Zn-1.5Y-1Mn-0.5Ni-0.1Bi	Permanent mold cast	–	167	239	12	[12]
Mg-7Y-1Nd-0.5Zr	Permanent mold cast	537 °C × 126 h	144	181	5.5	[13]
Mg-1.8Zn-0.4Zr-1.74Gd-0.5Y	Permanent mold cast	–	99	175	15.8	[14]
Mg-4Al-3La-0.3Mn-2Gd	High-pressure die casting	–	181	284	14	[8]
AE44–2	High-pressure die casting	–	152	260	19.6	[9]
Mg-4Zn-1La	Low-pressure die casting	400 °C × 12 h + water quenching	108	199	8.2	[15]
Mg-8Gd-4Y-1Zn-Mn	Semi-continuous casting	T6	214	268	1.8	[16]

changes after cycling treatment. GW63 alloy shows great potential in the field of spaceflight.

Mingxing Zhang's group studied the influence of Nd and Mn additions on the creep resistance of a Mg-3Gd-2Ca (wt.%) alloy at both 180 °C and 210 °C. They observed that the modified Mg-2Gd-1Nd-2Ca-0.5Mn alloy with less RE addition after solid solution treatment exhibited an outstanding creep resistance, which is superior to the commercial creep-resistant Mg alloy. The creep properties of newly developed Mg alloys were strengthened via a combination of improved solid solution strengthening by Nd and increased precipitation hardening by Mn addition as shown in Fig. 7 [17].

The appropriate amount of Mo was beneficial to grain refinement and the formation of long-period stacking ordered (LPSO) structure with a continuous distribution, which was advantageous to the improvement of mechanical properties and corrosion resistance. The Mg-6Zn-8.16Y-2.02Mn-0.3Mo alloy possesses the UTS and elongation of 265 MPa

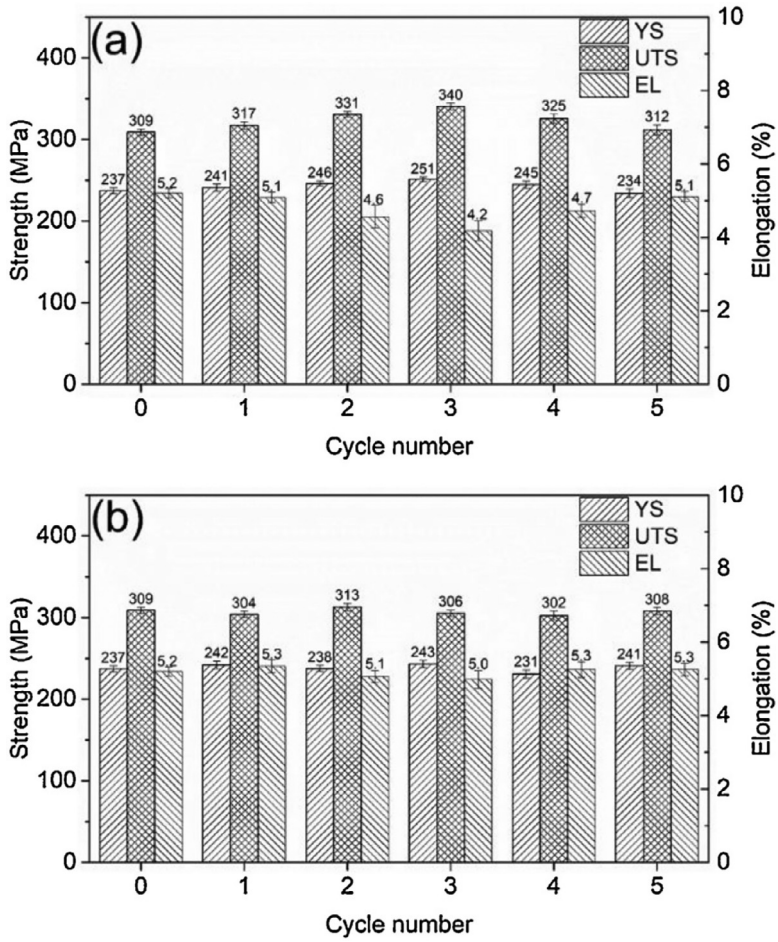

Fig. 6. Tensile properties of the T6 treated GW63 alloys treated by different cycle numbers of thermal cycling: (a) DCET; (b) DCT [6].

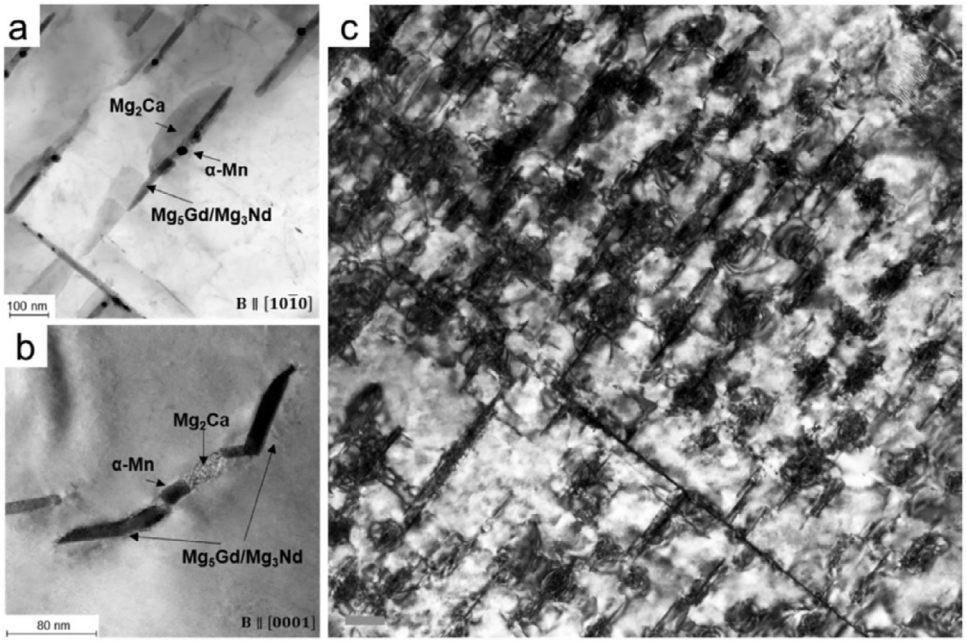

Fig. 7. TEM bright-field image showing (a and b) typical morphology of the dynamic co-precipitates in the #3 Mg-2Gd-1Nd-2Ca-0.5Mn alloy and (c) strong interactions of dislocations with those co-precipitates upon creep [17].

Table 3
Mechanical properties of some new types of RE-free cast Mg alloys.

Alloy (wt.%)	Cast method	Heat treatment	YS (MPa)	UTS (MPa)	EL (%)	Creep rate (s^{-1})	Ref.
Mg-1Zn-0.1Mn-0.2Ca	Gravity casting	420 $°C \times 18h$ + water quenched	68	182	9.2	–	[18]
Mg-6Al-0.2Mn-2Ca-0.3Si	Die casting	–	–	–	–	0.65×10^{-9} 150 °C/50 MPa/100 h)	[19]
Mg-7Sn-1Si	Sand cast	Aged at 250 °C/72 h	115	145	2.8	3.40×10^{-8} (200 °C/45 MPa/>110 h)	[20]

and 13.5%, respectively, with the lowest weight loss rate in Hank's solution [7]. As-cast low RE $Mg_{96.5}Zn_1Y_{1.5}Mn_1$ alloy with LPSO phase by Ni and Bi microalloying exhibits superior mechanical properties with YS, UTS, and elongation of 167 ± 1 MPa, 239 ± 1.6 MPa, and $12.0 \pm 0.45\%$, respectively [12].

In general, RE-containing cast Mg alloys are still the research hotspot and some progress has been made over the past year. However, the mechanical properties of cast Mg alloys with low RE additions still need to be further improved in the future.

3.2. Low-cost RE-free cast Mg alloys

Cost generally plays a determining role in the commercialization of cast magnesium alloys. As described above, magnesium alloys containing RE elements usually exhibit good creep resistance and good tensile properties at ambient temperature. However, the high cost of rare earth elements has led to the studies on the creep resistance of Mg alloys with inexpensive alloying elements (Sn, Ca, Si) that could be used to substitute RE elements. It is of great significance to develop low-cost and high-performance magnesium alloys in the absence of costly RE elements. The mechanical properties of some new types of low-cost and RE-free cast Mg alloys reported in 2020 are summarized in Table 3.

Tomasz Rzychoń investigated the effect of Si and Al on the creep resistance of Mg-7Sn alloy. The addition of Si and Al to Mg-7Sn alloy leads to the improvement of the creep resistance due to existence of Mg2Sn phase and the appearance of Mg2Si phase at grain boundary [20].

Xiaoping Lin et al. [21] studied the microstructure and mechanical properties of Mg-5.88Zn-0.53Cu-0.16Zr (wt.%) alloy solidified at 2–6 GPa using high-pressure solidification technology. They found that the microstructure was refined and the secondary dendrite spacing changed from 35 μm at atmospheric pressure to 10 μm at 6 GPa gradually. The shape of eutectic phases is improved by high-pressure solidification technology. The maximum compression strength reached 430 MPa, which means that high-pressure solidification technology could improve the mechanical properties of cast alloys.

However, the mechanical properties of RE-free cast Mg alloys are in general still much lower than those of Mg-RE bases alloys, which need to be improved in the future. In order to further broaden the application of cast Mg alloys, it is necessary to develop new cast magnesium alloys with high strength and elongation at a low cost. The strength and elongation should not be lower than 280 MPa and 7%, respectively. A lot of work still needs to be done to develop high-performance cast magnesium alloys with low cost in the future [5].

3.3. Microstructure of cast magnesium alloys

3.3.1. Microstructural characterization of cast magnesium alloy

The microstructure has a great influence on the performance of as-cast magnesium alloys. In 2020, the research on the microstructure of cast Mg alloys mainly focused on Mg-Ag-Al, Mg-Gd, Mg-Al-Zn-Sn, Mg-4Al-2La-2Ca-0.3Mn, Mg-RE-TM (TM=Zn, Cu, Ni, Mn) alloys.

Fanzhi Meng et al. [22] studied the aggregated eutectic intermetallic phases in a cast Mg-Ag-Al alloy, where ε-Mg_3Ag, β-$Mg_2(Al, Ag)_3$, γ-$Mg_{17}Al_{12}$ were observed to aggregate together following certain crystallographic orientation relationships as shown in Fig. 8. The numerous fine particles with the special intermetallic phase composition and many semi-coherent interphase boundaries lead to high-strength and high-ductility for the cast Mg-Ag-Al alloy.

Jian Meng et al. [23] found that Ca segregated at Mg-$Al_{11}La_3$ interphase boundaries in a die-cast Mg-4Al-2La-2Ca-0.3Mn alloy. The $Al_{11}La_3$ phase was decomposed into Al_2(Ca, La) phase through Ca atoms substituting the La atoms of $Al_{11}La_3$. The decomposition of $Al_{11}La_3$ is attributed to the fact that the interphase boundary segregation of Ca and the diffusion of Ca into $Al_{11}La_3$ change its thermodynamic stability.

The temperature dependence of prismatic slip in a LPSO $Mg_{85}Zn_6Y_9$ alloy was determined by micro-double-shear tests in the temperature range of 298–673 K. The room-temperature critical resolved shear stress (CRSS) for the prismatic slip was measured to be ~261 MPa, which is higher than that of the basal plane (~28 MPa); the CRSS for the prismatic slip had a gradual transition over 523 K, decreasing to ~110 MPa at 673 K. The prismatic slip was promoted through cross-slip onto the basal plane over the transition temperature as shown in Fig. 9 [24].The results point to the reason for the good ductility of Mg alloys at high temperatures.

3.3.2. Influence of casting parameters on the microstructure of cast magnesium alloys

The casting process has a significant influence on the microstructure of cast Mg alloys, which determines the mechan-

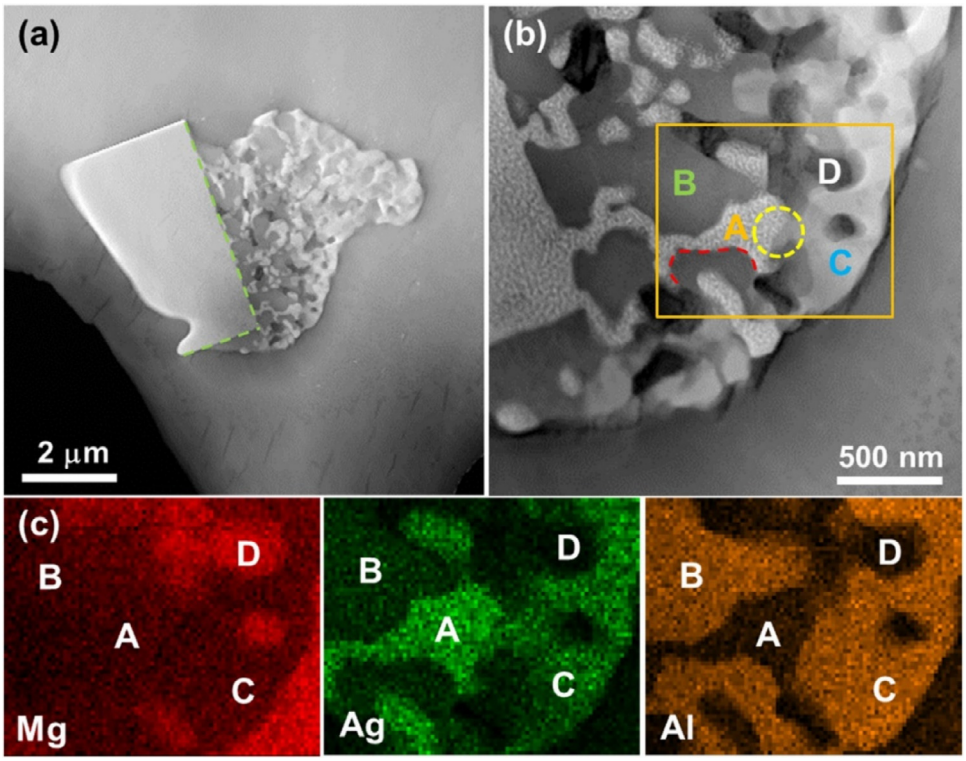

Fig. 8. (a, b) HAADF STEM images for the eutectic particle in a Mg-Ag-Al alloy simultaneously containing four phases, and (c) the EDS mappings of Mg, Ag and Al for the region marked by an orange box in (b) [22].

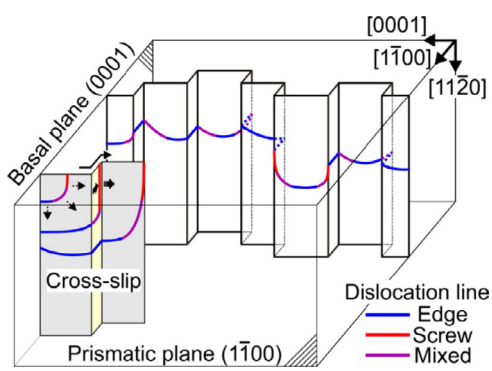

Fig. 9. Schematic illustration of possible mechanisms of prismatic slip related to double cross slipping in the 18R LPSO structure over 573 K [24].

ical properties of cast Mg alloy. The influence of casting parameters on the microstructure of cast Mg alloys was studied and the relationship between porosity and ductility was identified in 2020 [25-27].

Yuansheng Yang's group [25] reported the influence of cooling rate on the microstructure and micro-segregation in a new type of Mg-6Al-4Zn-1.2Sn alloy. The secondary dendrite arm spacing and the average grain size decrease from 14.3 μm to 2.9 μm and from 187 μm to 78 μm, respectively, with increasing cooling rate from 4.5×10^1 °C/s to 2.3×10^3 °C/s as shown in Fig. 10. The micro-segregation ratio of Al, Zn, and Sn elements decreases significantly with increasing cooling rate. The research on the sub-rapid solidification of Mg-6Al-4Zn-1.2Sn alloy reveals the changes of the microstructures at different cooling rates and provides essential information for the application of the alloy, including the thin-wall castings.

Yongbiao Wang and Liming Peng et al. [26] investigated the effect of a low cooling rate with a fixed temperature gradient during directional solidification on the microstructure of Mg-Gd alloys by coupling in situ X-ray synchrotron radiography and phase-field method. The dendritic morphology of Mg-6Gd (wt.%) alloy at different cooling rates is shown in Fig. 11. The primary dendrite spacing decreases with increasing cooling rate, and the relationship between the logarithm of primary dendrite arm spacing and the logarithm of cooling rate is linear. The simulation is in good agreement with the experimental results, which means that the phase-field method can be used to simulate the solidification process and predict the microstructure of alloy in the future.

Porosity also strongly affects the ductility of magnesium alloys prepared by high-pressure die castings. Jiang Zheng and Weijian Han et al. [27] studied the inter-relationship between various pore characteristics and the ductility in a thin-wall HPDC AM60 alloy. The result indicates that the ductility can be considered as a function of the local porosity in the fracture segment. Ductility can be linked to the highest local porosity in the gage section.

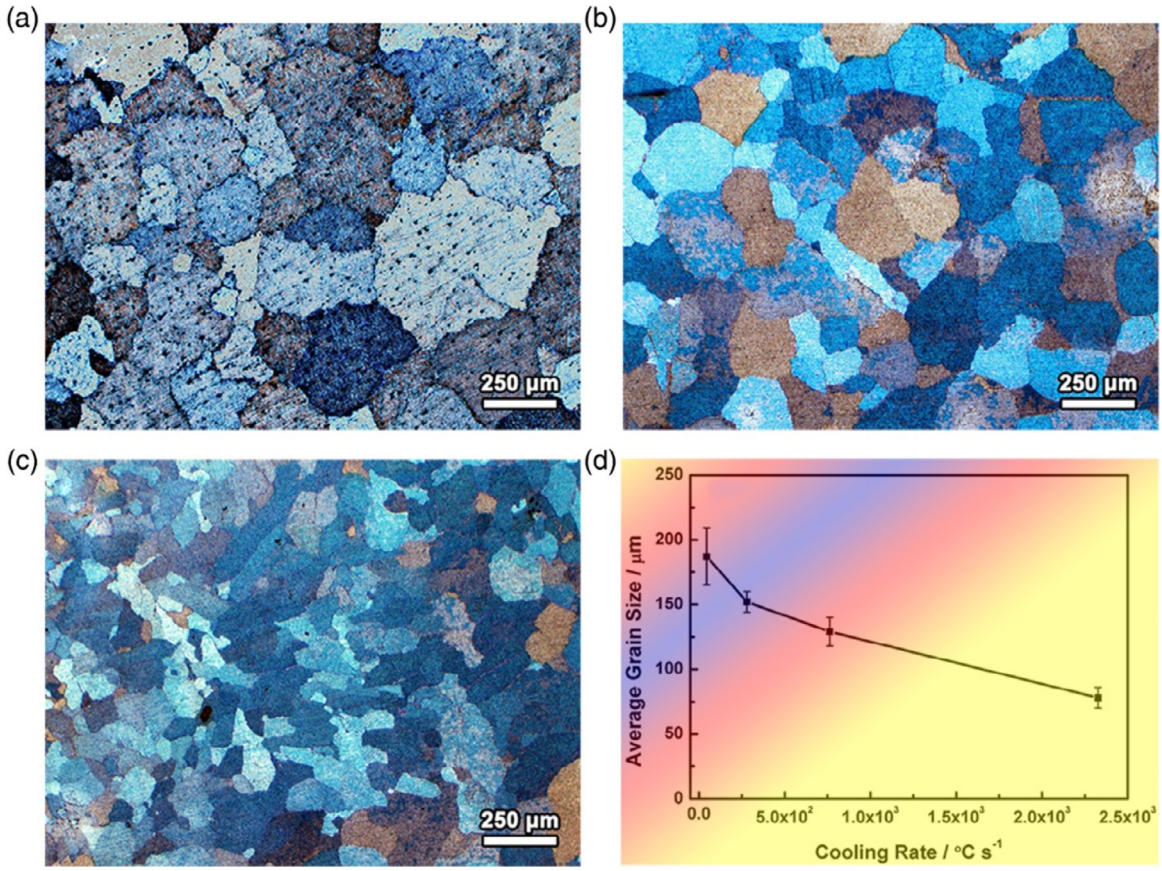

Fig. 10. Optical micrographs of grains that solidified at different cooling rates: (a) 4.5×10^1 °C/s; (b) 7.6×10^2 °C/s; c) 2.3×10^3 °C/s; and d) the average grain size as a function of cooling rate [25].

4. Wrought Mg alloys

4.1. Traditional commercial wrought Mg alloys

In 2020, the studies on traditional commercial wrought Mg alloys mainly focus on the evolution of microstructure and crystal orientation. For example, the research of AZ31 alloy mainly focuses on the effect of the deformation process on the texture evolution [28-32], microstructure, and mechanical properties of magnesium alloys [33-36]. Feng Li et al. [37] studied unusual texture formation and mechanical properties in AZ31 magnesium alloy sheets processed by the continuous variable channel direct extrusion (CVCDE). When the AZ31 sheets were extruded by CVCDE using two interim dies, there were obvious triple grain boundaries, low dislocation density in the crystal, and the weaker basal texture. In addition, they [29] also investigated the effect of extrusion ratio on the microstructure and texture evolution of AZ31 magnesium alloy by the staggered extrusion (SE). After the SE process, the extruded fiber texture of the AZ31 bending products is obvious, and the deformed texture is a mixed texture of {0001}[10–10] deformation texture and {10–11}[11–20] recrystallization texture. Li Hu and Tao Zhou et al. [38] investigated the effects of final rolling temperature on the microstructures, texture, and mechanical properties of AZ31 Mg alloy sheets prepared by equal channel angular rolling and continuous bending. They found that the annealing recrystallization texture becomes a non-basal (pyramidal) texture with double peaks tilting away from normal direction (ND) to rolling direction (RD). The tilted angle of double peaks of annealing recrystallization non-basal texture increases with increasing final rolling temperature. Fusheng Pan et al. [39] investigated that the reorientation of the texture during the biaxial compression was different from that during the uniaxial compression. Bin Jiang et al. [40] found that the novel integrated extrusion with side direction strain could promote the local accumulation of dynamically recrystallized grains and increase the random high-angle boundaries to achieve weak (0002) basal texture.

Deformation twinning has been observed to play a very important role in Mg alloys deformation. Chaitanya Paramatmuni et al. [41] reported that the rate of twin growth was influenced by its crystallographic orientation instead of the global Schmid factor (which was based on parent grain orientation). Pingli Mao et al. [42] identified that extruded AZ31 magnesium alloy showed obvious anisotropic and asymmetric behavior under high strain rate deformation and the anisotropy caused by the different roles of {10–12} extension twinning. Soong-Keun Hyun et al. [43] indicated that the planar defects such as twinning and slip traces could be formed pe-

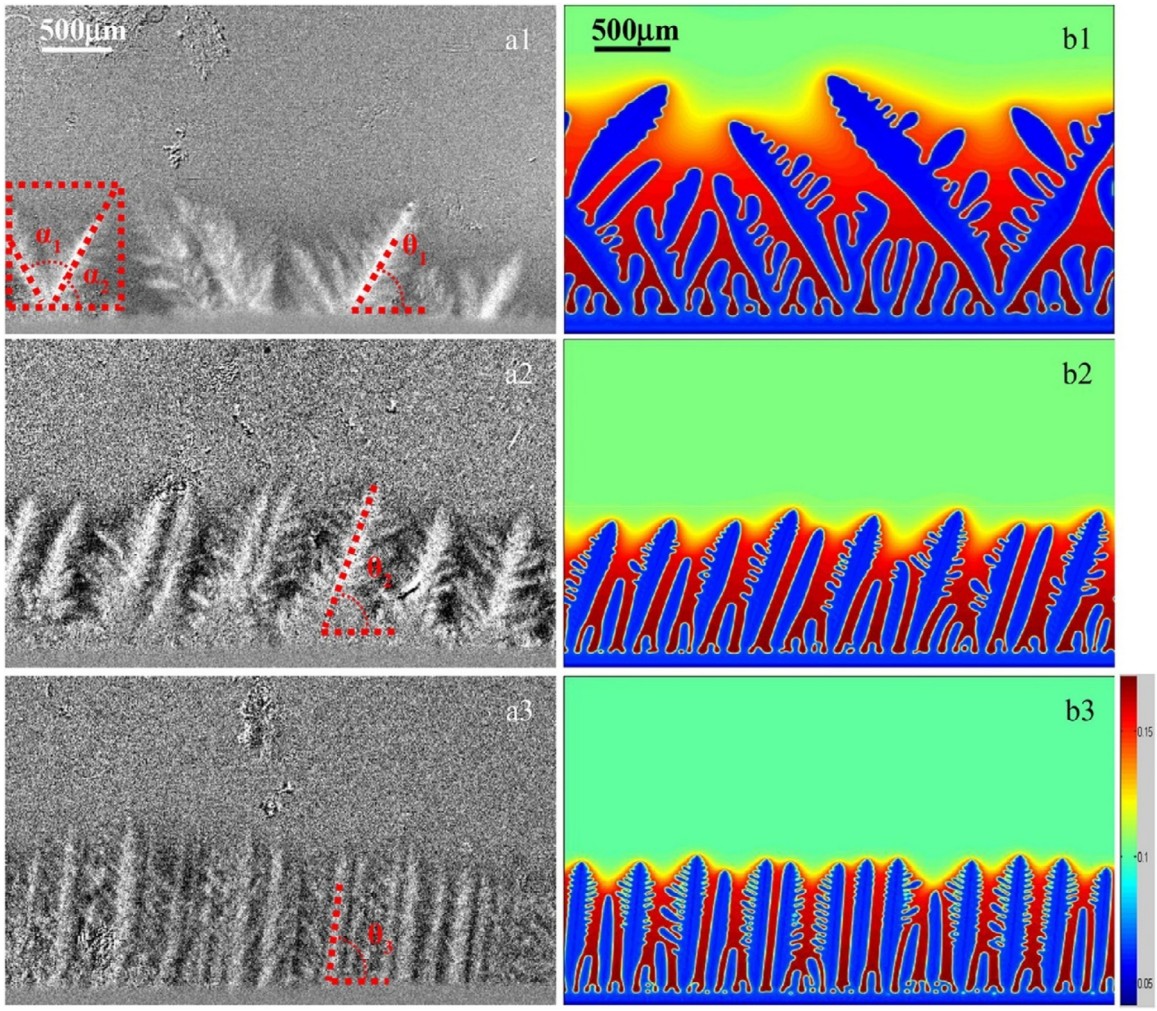

Fig. 11. The dendritic morphology of Mg-6Gd (wt.%) alloy at three different cooling rates $R = 0.033$ K/s, $R = 0.1$ K/s and $R = 0.25$ K/s in directional solidification from the top to bottom respectively: experimental results (a1-a3), and simulated results (b1-b3) [26].

riodically along serrated grain boundaries due to a rotational stress in the cold-shear-strained serrated grain boundaries. Jun Jiang et al. [44] investigated the effects of twin-twin interactions and deformation bands on the nucleation of recrystallization in AZ31 magnesium alloy. The results show that substantial twin boundaries, especially twin-twin interactions provide abundant nucleation sites for recrystallization, which contribute to the formation of homogenous microstructure with a weak texture and fine grains in the annealed LNT-rolled sample.

In addition, some studies focused on improving the properties of commercial alloys by alloying and processing technology. For example, Yb was added to ZK60 alloy to alter the dynamic recrystallization process and improve the strength [45]. A small amount of Sm addition is beneficial to improve the strength and plasticity of ZK60 and AZ31 due to the formation of the micro-scale phase [46,47]. Jianfeng Fan et al. [48] reported that the mechanical properties of AZ61 alloy were improved by a combination of two-step equal-channel angular pressing (TS-ECAP) and electropulsing treatment (EPT) processing. The ultimate strength of the AZ61 alloy reached 426 MPa, and the elongation was greatly improved from 6.8% to 18.3%. Aibin Ma et al. [28] combined processing of hot extrusion with multi-pass rotary die equal channel angular pressing (RD-ECAP) to improve its strength and ductility of AZ91 alloy.

In general, the composition of traditional commercial magnesium alloys is still continuously optimized. Through the use of trace rare earth elements, the basal texture is weakened and the recrystallized structure is improved, which can effectively improve its mechanical properties. The processing technology is also continuously improved. The flow channel shape increases strain, which is good at the improvement of mechanical properties and anisotropy. Future work in this area still needs to continue.

4.2. High strength wrought Mg alloys

In 2020, Mg alloys with high strength-ductility synergy mainly focus on low-alloy and rare earth (RE) wrought alloys. The mechanical properties of ultra-high strength wrought magnesium alloys are summarized in Table 4.

Table 4
Mechanical properties of high strength wrought Mg alloys at room temperature in 2020.

Alloys	Process	YS (MPa)	UTS (MPa)	EL (%)	Ref.
Mg-8Gd-3Y-0.4Zr	Rotary swaging+ aging	650	710	4.5	[49]
Mg-12Gd-1Er-1Zn-0.9Zr	Hot extrusion combined with pre-deformation and two-stage aging treatment	506	549	8.2	[50]
Mg-13.1Gd-1.6Ag-0.4Zr	Extrusion+ cold rolling and aging	421	515	3.1	[51]
Mg-13Gd	Extrusion+ aging	470	508	2.5	[52]
Mg-1.0Ca-1.0Al-0.2Zn-0.1Mn	As-extruded	~425		~11	[53]
Mg-9Gd-3Nd-1Zn-1Sn-0.5Zr	Extrusion+ aging	391	462	4.2	[54]
Mg-10.6Gd-2Ag	ECAP+ aged	396	460	8.9	[55]
Mg-9.2Gd-4.4Y-1.0Zn-0.8Mn	Extrusion+ aging	382	455	11	[56]
Mg-6.0Zn-2.0Yb-0.5Zr	Axisymmetric hot extrusion	~380	~436	~14.1	[57]
Mg-13Gd-4Y-2Zn-0.5Zr	Multi-directional forged	308	399	14.1	[58]
Mg-6Zn-1Mn-0.2Gd	Extrusion+ aging	360	390	8.3	[59]
AZ91D	Extrusion	320	382	13.8	[60]
Mg-9Al	Multi-directional forging	216	352	17	[61]

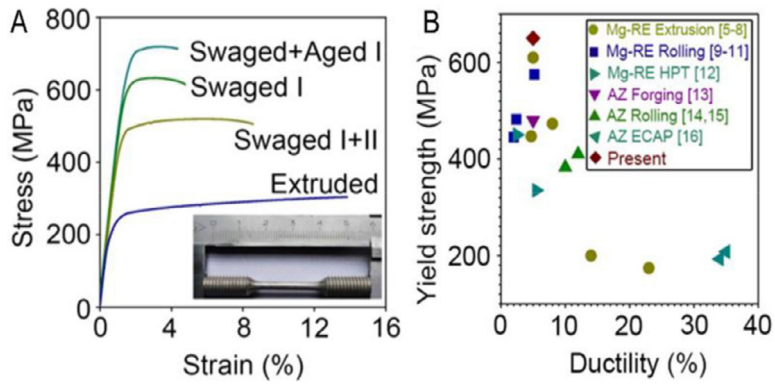

Fig. 12. Tensile properties of the swaged and aged Mg-8Gd-3Y-0.4Zr Mg alloys: (A) Tensile stress-strain curves; (B) comparison of yield strength versus ductility for processed Mg alloys [49].

Chuming Liu et al. [49] fabricated a nanocrystalline Mg-8Gd-3Y-0.4Zr alloy by rotary swaging and aging, which have a yield strength of 650 MPa and ultimate strength of 710 MPa as shown in Fig. 12. The main strengthening mechanism is nano-grain strengthening. The work provides a simple and low-cost production technique to fabricate bulk nanocrystalline Mg alloys.

Wenbo Du et al. [50] developed an ultra-high strength and ductility Mg-12Gd-1Er-1Zn-0.9Zr (wt.%) alloy by hot extrusion, pre-deformation and two-stage aging treatment, and the mechanical properties of the alloy are shown in Fig. 13. Pre-deformation can introduce high density dislocations, resulting in work hardening and inducing precipitation during the two-stage aging. The study provides an effective way to develop Mg alloys with high strength and ductility synergy.

Liming Peng et al. [51] developed a Mg-13.1Gd-1.6Ag-0.4Zr alloy with the yield strength and ultimate strength of 421 MPa, 515 MPa, respectively. The high strength is mainly attributed to the bimodal-grained structure and enhanced precipitation. Differential-thermal extrusion and subsequent aging is a suitable method for achieving high strength Mg alloys. Hucheng Pan, Jinghuai Zhang and Daqing Fang et al. [52] developed an ultra-high strength Mg-13Gd alloy via extruding and aging with the YS and UTS of 470 MPa and 508 MPa, respectively, as shown in Fig. 14. The primary strengthening mechanism is texture strengthening and precipitation strengthening. Aging precipitation was only present in the large un-DRXed grains rather than in the fine DRXed grains for the first time.

Hucheng Pan et al. [53] developed low-alloy Mg-Ca-based alloys with high strength and ductility synergy by suitable alloying addition and low-temperature extrusion. The high strength is mainly attributed to the high density of submicron grains and nano-precipitates, and the alloying element additions and higher extrusion temperatures are beneficial to the improvement of ductility. Y. Yu et al. [54] fabricated a high-strength Mg-9Gd-3Nd-1Zn-1Sn-0.5Zr (wt.%) alloy by extrusion and subsequent two-steps aging, which has an ultimate strength of 462 MPa, and yield strength and elongation were 392 MPa and 4.2%, respectively. The high strength is mainly due to the increase in the number of the β' phase and LPSO phase. Huan Liu et al. [55] developed a Mg-10.6Gd-2Ag (wt.%) alloy with excellent ductility and high strength by equal channel angular pressing (ECAP) and aging, which has an UTS of 460 MPa, and a moderate ductility of 8.9%. The fine and full DRXed microstructure improves the ductility. Jingfeng Wang et al. [56] developed the high strength-ductility balance Mg-Gd-Y-Zn-Mn alloy by altering

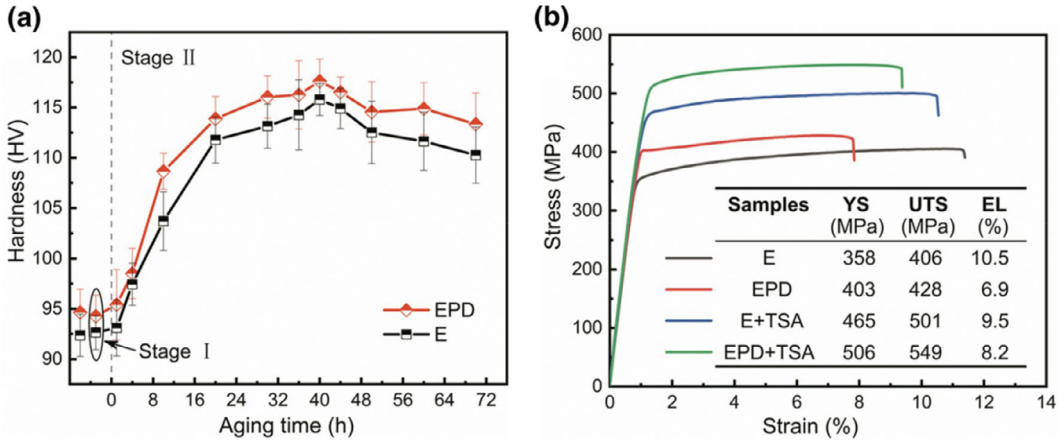

Fig. 13. (a) Age-hardening behavior of the E and EPD Mg-12Gd-1Er-1Zn-0.9Zr samples, (b) tensile engineering stress-strain curves of the various samples [50].

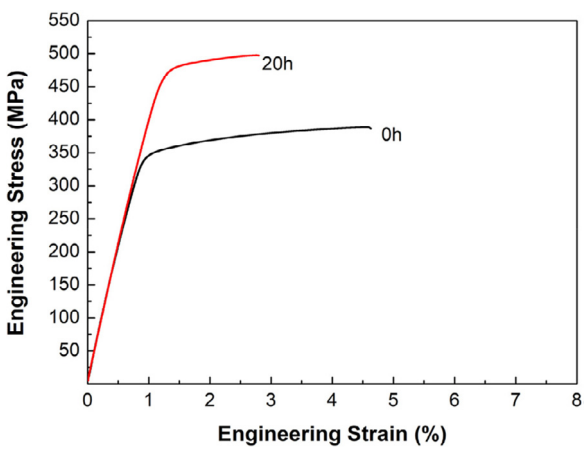

Fig. 14. Tensile stress-strain curve for the as-extruded (0 h) and peak-aged (20 h) samples along the extrusion direction (ED) [52].

dynamic recrystallization behavior during pre-aging treatment. The UTS, YS, and EL of Mg-9.2Gd-4.4Y-1Zn-0.8Mn reached 455 MPa, 382 MPa and 11%, respectively, as shown in Fig. 15. The special bimodal structure, strong fiber texture, β-Mg_5(Gd, Y) particles, lamellar, and block-shaped LPSO phases lead to the outstanding mechanical properties of the alloys.

Lu Li et al. [57] developed a Mg-6Zn-2Yb-0.5Zr alloy by axisymmetric hot extrusion, which has an UTS of ~436 MPa and a lower elongation (EL) of ~14.1%. Zhimin Zhang et al. [58] developed a high strength Mg-13Gd-4Y-2Zn-0.5Zr alloys by multi-directional forging (MDF) process with the UTS and YS of 399 MPa and 308 MPa, respectively, after 3 passes. Chuming Liu et al. [61] fabricated a high strength and ductility synergy Mg-9Al alloy by tailoring multi-directional forging. The strength is attributed to grain boundary strengthening, and the drastic morphology alteration and decreased volume fraction of the precipitates improve the ductility.

In the past year, the research of high-strength magnesium alloys has made gratifying progress. In terms of new alloy design, low-alloyed high-strength magnesium alloys have become a relatively important research direction. The strength of Mg-Ca based alloy can reach more than 400 MPa, and the high-strength alloy based on Mg-Gd, combined with the improvement of the processing technology, has been able to increase the performance to more than 700 MPa. The main strengthening mechanisms of high-strength magnesium alloys are precipitation strengthening and grain boundary strengthening.

4.3. Superlight wrought Mg alloys

Superlight wrought Mg alloys mainly focus on Mg-Li alloys with the density of 1.4–1.65 g/cm^3. The mechanical properties of the superlight wrought Mg-Li alloys developed in 2020 are summarized in Table 5.

Ruizhi Wu et al. [62] developed an as-rolled Mg-8Li-1Al alloy by combined addition of Y and Ce, which has an UTS of 279 MPa and an elongation of 15.0%. Guohua Wu and Wencai Liu et al. [63] prepared a high strength as-extruded Mg-10Li-5Zn-0.5Er alloy, and fine dispersed Mg-Li-Zn particles improve the strength. Ruizhi Wu et al. [64] developed a high specific strength Mg-16Li-2.5Zn-2.5Er alloy by extrusion and cold rolling. Dynamic recrystallization results in fine-grain strengthening during extrusion. After cold rolling, introducing the high density dislocation and uniformizing the distribution of the second phase particles further lead to the work hardening and dispersion strengthening. Fei Guo et al. [66] investigated the β-Li phase transformed into the α-Mg phase in a dual-phase Mg-9.5Li-1 Zn alloy after large strain cold rolling. High density strain-induced phase transformation improved the yield strength without sacrificing the ductility. The research indicates that strain-induced phase transformation is an efficient method for improving the mechanical properties in dual-phase Mg alloys. Yan Yang et al. [65] studied the microstructure and mechanical behavior of the extruded Mg-6Li-0.3Zn-0.6Y alloy. The results show that the Mg-6Li-0.3Zn-0.6Y alloy contains α-Mg, β-Li, W-$Mg_3Zn_3Y_2$ phase and X-Mg_{12}ZnY, and the extruded Mg-6Li-0.3Zn-0.6Y alloy possesses an UTS of 225 MPa with an EL of 18%. The effect of Y and Zn on the corrosion resistance of the superlight Mg-

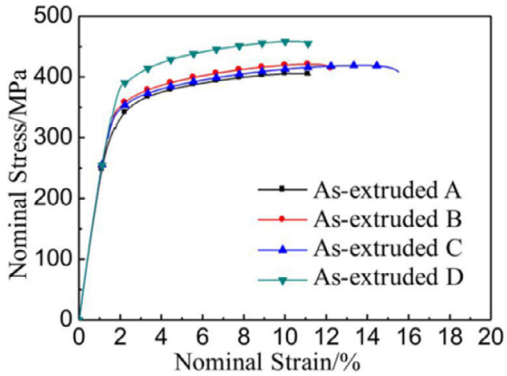

Heat treatments performed on the Mg-Gd-Y-Zn-Mn alloys.

Designation	Thermal Condition
As-annealed	1. Semi-continuous casting 2. 500 °C × 8 h + 525 °C × 5 h + annealing to 400 °C within 10 h
Pre-aged B	1. As-annealed sample 2. 225 °C × 110 h
As-quenched	1. As-cast sample 2. 500 °C × 8 h + 525 °C × 5 h + quenching
Pre-aged D	1. As-quenched sample 2. 225 °C × 110 h
As-extruded A	1. As-annealed sample 2. Hot extrusion (420 °C, 11:1, 0.3 mm/s)
As-extruded B	1. Pre-aged B sample 2. Hot extrusion (420 °C, 11:1, 0.3 mm/s)
As-extruded C	1. As-quenched sample 2. Hot extrusion (420 °C, 11:1, 0.3 mm/s)
As-extruded D	1. Pre-aged D sample 2. Hot extrusion (420 °C, 11:1, 0.3 mm/s)

Fig. 15. Tensile properties of the as-extruded samples tested along with ED at ambient temperature [56].

Table 5
Mechanical properties of the superlight wrought Mg-Li alloys developed in 2020.

Alloys	Process	YS (MPa)	UTS (MPa)	EL (%)	Ref.
Mg-8Li-1Al-0.6Y-0.6Ce	As-rolled	245	279	15.0	[62]
Mg-10Li-5Zn-0.5Er	As-extruded	249	252	35.2	[63]
Mg-16Li-2.5Zn-2.5Er	As-rolled	225±4	234±4	26±1.7	[64]
Mg-6Li-0.3Zn-0.6Y	As-extruded	180	225	18	[65]

6.5Li alloys was investigated. The corrosion results indicate that the combining addition of Y and Zn can improve the corrosion resistance of extruded Mg-6.5Li alloys with LPSO phase [67].

4.4. High plasticity wrought Mg alloys

Mg alloys with a hexagonal close-packed (hcp) crystal structure do not have sufficient independent slip systems and their basal texture is easily formed after plastic processing, which impedes the comprehensive application of Mg alloys. Improving plasticity has always been one of the research hotspots of magnesium alloys. Recently, there are many reports on the use of alloying and deformation methods to acquire high plasticity magnesium alloys [68].

On the one hand, low-alloying alloy design methods are combined with plastic processing technology to obtain magnesium alloys with higher plasticity [53]. For example, Xiaoqing Liu and Mingyi Zheng et al. [69] developed a Mg-0.68Al-0.32Ca-0.50Mn (AXM070305, wt.%) magnesium (Mg) alloy with high strength and excellent ductility through an extrusion and subsequent T6 heat treatment. After T6 aging treatment, the YS of the alloy is 248 MPa, the UTS is 288 MPa, and the EL is 21%. The Mg-0.5Zn-0.2Mn-0.2Sm/0.3La-0.4Ca alloy shows good ductility with an elongation of 27.5–30.5%, and Mg-0.5Zn-0.2Mn-0.2Sm/−0.3La-0.4Zn alloy exhibits an excellent balance of the strength and ductility: YS is 190 MPa, UTS is 239 MPa, and EL is 23.9% [68].

T.T. Sasaki and S. Kamado et al. [70] studied the role of Zn on the room temperature formability and strength in Mg-Al-Ca-Mn sheet alloys. The peak-aged Mg-1.2Al-0.5Ca-0.4Mn-1.6Zn alloy exhibits a high UTS of 210 MPa with an excellent EL of 30.1%, which is due to the dense dispersion of Guinier-Preston (G-P) zones within the Mg matrix. Yongxian Huang et al. [71] found that the strength and ductility of friction-stir-processed Mg-6Zn can be enhanced by Y and Zr co-alloying. The ultimate strength and elongation of the FSPed Mg-6Zn-1Y-0.5Zr alloy reach 310 MPa and 27.7%. H. Mirzadeh et al. [72] found that the Ca addition and hot extrusion process can improve mechanical properties of Mg-Zn alloy. The UTS and EL of extruded Mg-2Zn-1Ca are 283 MPa and 29%, respectively. Bin Jiang and Jie Fu et al. [73] investigated the influence of minor Ce additions on the microstructure and mechanical properties of Mg-1.0Sn-0.6Ca alloy. They found that the elongation of extruded Mg-1.0Sn-0.6Ca alloys reaches 27.6%, which is due to vigorously activated basal slip and homogeneously distributed tensile strain during tensile testing.

On the other hand, the severe plastic deformation method is used to make the alloy structure ultra-fine, thereby improving the plasticity of the alloy [28,74]. For example, Tingzhuang Han et al. [75] used accumulated extrusion bonding to prepare an AZ31 magnesium alloy with a grain size of 2.5 μm, the elongation of the alloy at room temperature could reach 33%. In addition, the recrystallization structure of extruded magnesium alloy can be improved by adding Mn, leading to further improved plasticity. For example, adding 0.5% Mn to the Mg-1Gd alloy can refine the recrystallization structure from 8 μm to about 7.2 μm, the elongation of the alloy can reach ~33% [76]. Moreover, J.J. Bhattacharyya and S.R. Agnew et al. [77] reported a mechanistic explanation for the excellent strength and plasticity of microalloyed Mg-Al-Ca-Mn alloys at peak aging conditions [78]. The enhanced strain-rate sensitivity is responsible for this behavior. The potential for optimizing mechanical properties can be increased by engineering the strain-rate sensitivity [77]. Weidong Xie et al. [79] reported that the elongation of the extruded Mg-0.4Al-1.5Mn is 52.5%, which is attributed to the restriction of extension twin-

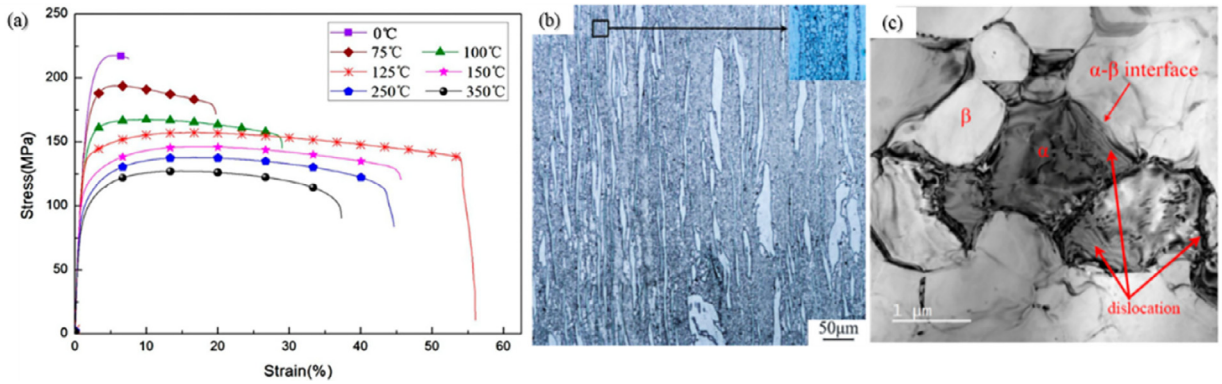

Fig. 16. (a) Stress-strain curves of 95% cold-rolled LZ91 alloys annealed at different temperatures. (b) Optical microstructure of 95% cold-rolled LZ91 alloys annealed at 125 °C and (c) a typical TEM image of 95% cold-rolled LZ91 alloys annealed at 125 °C [81].

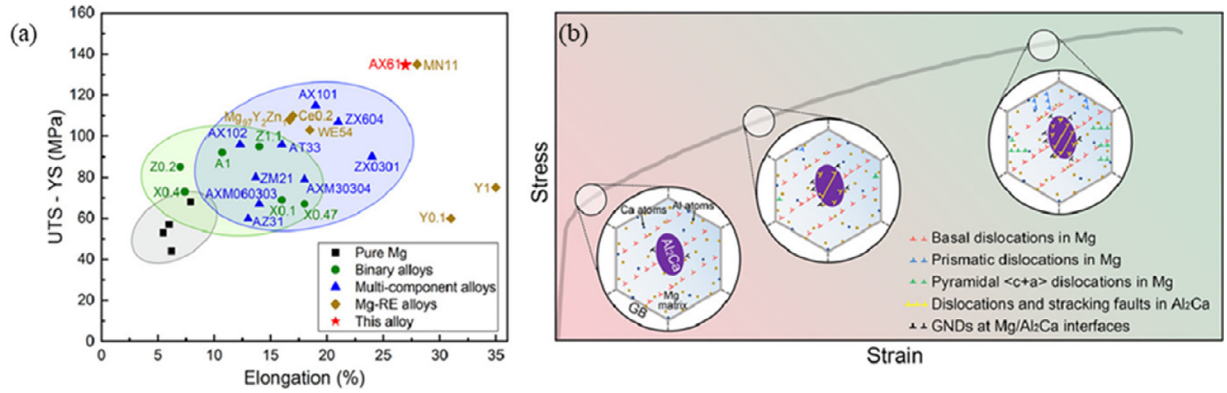

Fig. 17. (a) Tensile properties of the AX61 alloy; (b) schematic illustration of the deformation mechanisms in the AX61 alloy [82].

ning and the high SF can significantly promote the activation of non-basal slip. K.S. Shin and H. Yu et al. [80] found that the refined microstructure and weakened texture significantly improved the ductility of extruded Mg-1.32Bi-0.72Ca alloy. Fusheng Pan and Yan Yang et al. [81] studied the effects of annealing temperature on microstructure and mechanical properties of LZ91 alloy. The results show that the elongation of the cold-rolled LZ91 alloys after annealing at 125 °C reaches as high as 56.1% (Fig. 16) because of the fined DRX grains formed during the annealing. Xiaoqin Zeng and Leyun Wang et al. [82] reported a new Mg-Al-Ca alloy, which was one of the alloys with the highest tensile elongation and work hardening ability. The results show that the improvement of the elongation of Mg-6Al-1Ca is attributed to the formation of Al_2Ca and solutes Al and Ca promoting $\langle c+a \rangle$ dislocations in Mg (Fig. 17). Chuming Liu et al. [61] reported that the dynamic precipitation assisted grain refinement during multi-directional forging could improve the strength and ductility of an Mg-9Al alloy. Guilin Wu and Xiaoxu Huang et al. [83] study the grain size effect on plastic deformation behavior of Mg-3Gd (wt.%) alloy. Mg-3Gd samples with average grain sizes ranging from 3.3 μm to 114 μm were prepared by accumulative roll-bonding (ARB) and annealing. The transmission electron microscopy (TEM) characterization revealed that $\langle a \rangle$ dislocations and extension twins dominate in the samples with grain sizes larger than 10 μm, while $\langle a \rangle$ and $\langle c+a \rangle$ dislocations characterize the structures of the samples with grain sizes smaller than 5 μm. In parallel, there is a consistent and concise trend that both the strength and ductility increase with decreasing grain size. The appearance of yield-point phenomenon in the small-grained samples had a significant effect on both strength and ductility. This is illustrated by an increase in boundary (Hall-Petch) strengthening and an increase in the total elongation to 36.6%. The mechanical properties of typical high plasticity wrought Mg alloys developed in 2020 are summarized in Table 6.

In terms of high-plasticity magnesium alloys, it has been possible to refine the structure of the alloy to several microns through alloy composition design and process improvement, so that the room temperature elongation of the alloys can be increased to more than 50%. For the alloy composition design, some new low-alloy alloys, such as Mg-Bi-Ca, Mg-Al-Mn, and Mg-Li alloys have been designed. In terms of processing technology, achieving ultra-fine grains along with the weakening of basal texture is still the main development directions.

4.5. High-modulus and high-strength mg alloys

Xianhua Chen's group from Chongqing University focused on the strength of Mg alloys. A new high-modulus and high-strength Mg-Gd-Ag-Mn-Ge alloy was developed [84]. As

Table 6
The mechanical properties of typical high plasticity wrought Mg alloys at room temperature in 2020.

Alloys	Process	TYS (MPa)	UTS (MPa)	EL (%)	Ref
Mg-8.8Al-0.47Zn-0.21Mn-0.17Ag	Forging and annealing	131	344	34	[61]
Mg-0.5Zn-0.2Mn-0.2Sm-0.3La	Extrusion	190	239	23.9	[68]
Mg-1.2Al-0.5Ca-0.4Mn-1.6Zn	Hot-rolled and annealing	210	282	30.1	[70]
Mg-6Zn-1Y-0.5Zr	Friction stir processing	170	310	27.7	[71]
Mg-2Zn-1Ca	Extrusion		283	29	[72]
Mg-1.0Sn-0.6Ca-0.2Ce	Extrusion	97	264	27.6	[73]
Mg-1Gd-0.5Mn	Extrusion	146	211	33	[76]
Mg-0.4Al-1.5Mn	Extrusion	170	213	52.5	[79]
Mg-1.32Bi-0.72Ca	Extrusion			43	[80]
Mg-8.9Li-1.1Zn	Cold rolling and Annealing		157	56.1	[81]
Mg-6Al-1Ca	Extrusion	125	260	27	[82]
Mg-3Gd	Accumulative roll-bonding and annealing	173	214	36.6	[83]

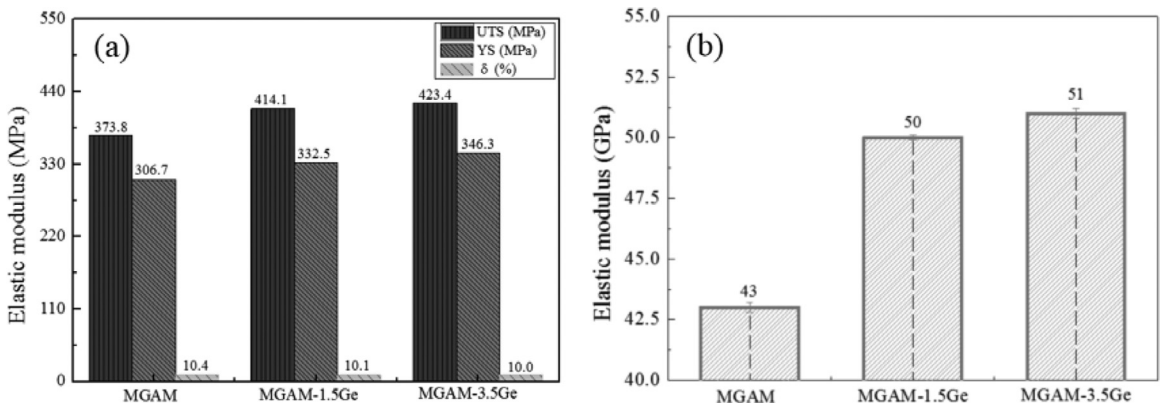

Fig. 18. (a) Tensile properties and (b) elastic modulus of the as-extruded Mg-Gd-Ag-Mn (-Ge) alloys: MGAM, MGAM-1.5Ge and MGAM-3.5Ge [84].

shown in Fig. 18, with increasing Ge content, the modulus and strength of the alloy increased significantly. In the Ge-containing alloys, the as-extruded MGAM-3.5Ge alloy exhibited the best comprehensive mechanical properties, with the elastic modulus, strength, and ductility being 51 GPa, 423 MPa, and 10%, respectively. The high-modulus is due to the formation of high-modulus MgAg, Gd_5Ge_3 phases, and the high-strength is the result of grain boundary strengthening, solid solution strengthening, and precipitation strengthening.

5. Functional Mg materials

5.1. Bio-magnesium alloys

Magnesium alloys are biocompatible and biodegradable, and the biodegradable nature offers alternative options for the materials to extend their applications in the biomedical field, thus Mg alloys have great potential in manufacturing implantable medical devices, such as bone implants, vascular stent, etc. [85,86]. Bio-magnesium alloys have attracted more and more attention. However, the stress shielding and secondary surgery-related clinical issues present a great challenge to implantable medical devices. The rapid degradation of magnesium alloys may lead to the early failure of implants. Therefore, a lot of research has been carried out in the design and preparation of new magnesium materials and the development of coatings that regulate the degradation rate or introduce other functions.

Several new types of magnesium materials including pure Mg, Mg alloys, and composites were reported in 2020. Dongguan Yi'an Science and Technology Co., Ltd of China has developed a high purity magnesium for bone screws, and the high purity magnesium screws have entered the clinical trial stage in China and obtained CE certification in July 2019. Jia She et al. [87] of Chongqing University recently developed a Mg-Zn-Mn-based alloy with alloying elements mainly composed of Zn and Mn, which has good biocompatibility. The alloy with a strength of 300–350 MPa and elongation of 20%−30% exhibits high strength, good plasticity and high work-hardening ability, which has great potential in biological structural materials, especially vascular stents.

Due to the uncertain biocompatibility of Zr element, to avoid the addition of Zr, D.H. StJohn et al. [88] discussed the possibility of obtaining a refined magnesium alloy structure by applying an ultrasonic treatment (UST) during the Mg-Zn-Ca alloy solidification process without adding Zr element. UST can produce well-refined microstructures exhibiting a lower corrosion rate without the sacrifice of mechanical properties, which means that UST is a promising technique to produce biocompatible magnesium alloys. Shaokang Guan's group [89] investigated the Mg-Zn-Y-Nd alloy and found that it has inferior mechanical properties compared to the commer-

cial esophageal stents material, 317 L stainless steel (317 L SS), while the biodegradability of Mg-Zn-Y-Nd is significantly better than that of 317 L SS. Besides, it has a strong inhibitory effect on esophageal cancer-related pathological cells, making it an ideal metal for potential esophageal stent applications. Khurram Munir and Yuncang Li et al. [90] studied the microstructure, mechanical properties, corrosion behavior, and biocompatibility of Mg-0.6Zr-0.5Sr-xSc ($x = 0.5$, 1, 2, 3 wt.%). They suggested that the high concentration of *Sc* in Mg alloy containing Sr could modify its microstructure by inhibiting the formation of intermetallic phase along the grain boundary, and by forming a chemically stable *Sc* oxide layer on the surface of Mg alloy, thus the degradation rate of Mg alloy was inhibited and the corrosion resistance was improved. Their results show that the compressive strengths of Mg-0.6Zr-0.5Sr-xSc alloys are in the range of 174–265 MPa, which is similar to that of natural cortical bone. Besides, Mg alloy containing *Sc* had no cytotoxicity on the viability of human $SaOS_2$ osteoblast-like cells, thus *Sc* can effectively enhance the potential of Mg alloys as biodegradable materials. Qiang Wang and Yang Zhang et al. [91] developed Mg-Zn-Zr-Nd/Y alloys to expand the application of future orthopedic materials. The Mg-Zn-Zr-Nd alloy exhibited similar corrosion rates to those of pure Mg, mainly due to the enhanced corrosion resistance of $Ca_3(PO_4)_2$ and $Mg_3(PO_4)_2$ formed on the sample surface. Thus, the nontoxicity, better biocompatibility as well as good overall mechanical properties of the alloy present the possibility of using it as a bone plate. In the Mg-Zn series with Ce (ZE) or Ca (ZX) as additional elements, the degradation rate (below 1.5 mm/y) was found to depend strongly on the nature of the second phase particles rather than on the grain size, but it was still suitable for biological applications [92].

Kaibo Nie et al. [93] added TiC nanoparticles to Mg-1.12Ca-0.84Zn-0.23Mn to produce ultra-fine grains of the alloy. Fine α-Mn particles and $MgZn_2$ precipitates are dynamically precipitated in the hot extrusion. The yield strength of the alloy reaches 424 MPa, and the ultimate tensile strength is 437 MPa, which is worthwhile to be studied as a candidate for biodegradable structural materials. Khurram Munir et al. [94] prepared graphene nanoplatelets (GNPs) reinforced magnesium matrix composites by powder metallurgy process. The ductility, compressive strength and corrosion resistance of Mg-GNPs composites were improved, and no obvious cytotoxicity was observed. Mg-xGNPs with $x < 0.3$ wt.% may become a new biodegradable weight-bearing implant material.

In the aspect of the design and preparation of new magnesium alloy coating, Shuai Cijun et al. [95] prepared AZ61-TiO_2/GO bio-composites by selective laser melting (SLM) method to enhance the interfacial bonding between graphene oxide (GO) coating and magnesium matrix. In the SLM, TiO_2 was reduced in situ by the magnetocaloric reaction, and the reduced Ti reacted with Al in AZ61 matrix to form $TiAl_2$ and also reacted with GO to form TiC at the interface of AZ61-GO. Due to the enhancement of interfacial bonding, the degradation rate of AZ61-TiO_2/GO bio-composites was 12.5% lower than that of AZ61-GO bio-composites, while the compressive strength was increased by 10.1%, and it also showed good cell compatibility. Deepa B. Prabhu et al. [96] prepared the chemical conversion coating on a Mg-4Zn alloy by immersion in saturated NaHCO3 at ambient temperature and obtained a dense coating after a 24-hour immersion, which had a high initial corrosion resistance in SBF. With sustained exposure to SBF, the coating dissolved and slowly cracked, and was a suitable choice for temporary biological implantation of magnesium alloy. Preeti Makkar et al. [97] used a chemical immersion technique to prepare Ca-Sr-P coating on the surface of magnesium alloy, which improved the corrosion resistance of magnesium alloy and enhanced its bioactivity, also promoted the adhesion, proliferation and osteogenic marker expression of MC3T3-E1 cells. In the rabbit model, 4 weeks after implantation, the bone formation and osseointegration around the coating were higher than those of magnesium alloy, implying that the coating could be used in magnesium-based orthopedic implants. D.H. StJohn group [88] investigated the effect of ultrasonic treatment on Mg-Zn-Ca alloys during solidification and presented the opportunity to develop low-cost alloys with at least equal biocompatibility, mechanical properties and corrosion performance. Berit Zeller-Plumhoffa et al. [98] used small angle X-ray scattering and X-ray diffraction to analyze the structure of biodegradable Mg-xGd implants, expanding the research on the ultrastructure of biodegradable Mg-based alloys. Barbeck et al. [99] prepared a new bioresorbable hydrofluoric acid (HF)-treated magnesium (Mg) mesh in a native collagen membrane for volume stable situations, which has good cyto- and biocompatibility, but should be further studied in further research.

Several new application fields of magnesium biomaterials were investigated. Xiangji Li et al. [100] implanted HA-coated magnesium into the eyes of rabbits to investigate its application in glaucoma therapy. No obvious inflammation was observed in the anterior chamber, lens and vitreous body. Sixteen weeks after the surgery, the implant was fully degraded, and the filtration channel of aqueous humor remained, implying a promising application in glaucoma therapy of magnesium-based biomaterials. Wenjiang Ding's group [101] used template technique to prepare a new type of Mg-Nd-Zn-Zr alloy (JDBM) porous brushite-coated bone defect repair scaffolds (denoted as JDBM-DCPD), the main hole (400∼450 μm) and small pores (150∼250 μm) are connected, and their pore structure can be adjusted by spacer selection technique, which is conducive to the penetration of nutrients and cell growth, and has good mechanical properties. After the JDBM-DCPD scaffolds were implanted in vivo, with the degradation of JDBM-DCPD, angiogenesis, osteogenesis and remodeling were effectively promoted, and large bone defects in rats and rabbits were repaired well, indicating that Mg-based scaffolds may be promising tissue engineering scaffolds for large bone defect repair clinically, free from any extra growth factors and live cells.

Magnesium alloys show great potential in implantable medical devices and a lot of studies on bio-magnesium alloys has been conducted in the past year. However, further

research on alloy design, coating and new applications still needs to be done in the future.

5.2. Mg battery

5.2.1. Mg-air battery

Mg-air batteries have attracted much attention as a possible alternative because of their environmental benignity, economic viability, relatively high theoretical specific energy density of 6.8 kW h kg^{-1} and voltage of 3.1 V [102]. Generally, an Mg-air battery is composed of air gas-diffusion cathodes, electrolytes and Mg-anodes. The present Mg-air battery is a primary battery (a single-use galvanic cell), which limits their commercial application due to fast anode fouling, high self-corrosion and the sluggish kinetics of the oxygen reduction reaction (ORR) in the air cathode. Indeed, the "re-fuelability or rechargeable Mg-air battery" can be achieved by replacing or supplementing the spent Mg anode and electrolyte with new Mg and electrolyte. However, for rechargeable Mg-air batteries, they are again limited by the reversibility with slow kinetics of ORR and oxygen evolution reaction (OER). Another critical challenge comes from the Mg anode, which is prone to self-corrosion in aqueous electrolytes due to the phenomenon called the negative difference effect (NDE), which will accelerate the corrosion of the Mg plate. Meanwhile, the by-products $Mg(OH)_2$ cover the surface of Mg-anode and hinders the further release of Mg ions, which leads to increased polarization loss and reduces anodic efficiency.

Therefore, to improve the performance of Mg-air batteries in practical terms, it is necessary to explore the corrosion mechanism of Mg anodes and propose effective solutions. In 2020, tremendous efforts have been attempted to improving the anode performance and efficiency of Mg-air batteries using both alloying and modification of the intrinsic properties of Mg itself. Alloying Mg with other metals, such as Li [103], Al [104,105], Mn [106], Zn [107,108], Ca [109,110], In [110], Bi [111], Y [112,113], La [114], Sm [115] or a composite of some of these elements, can reduce the corrosion rate of the Mg anode in open circuit potential (OCP) condition for enhancing the utilization efficiency. To illustrate this, Mg_xZn alloys ($x = 2$, 4, 6, and 15 wt.%) are used as an anode material for Mg-air batteries due to the high solid solubility (6.2 wt.%) of Zn in Mg in the phase diagram of Mg-Zn system and environmental friendliness. This study showed that the addition of 2 wt.% Zn could significantly increase the anode efficiency and specific capacity. It is found that the introduction of Zn into the Mg matrix can well suppress the self-corrosion phenomenon of the Mg anode and improve the anodic efficiency [107]. Qichi Le et al. [108] also systematically investigated the electrochemical performance of Mg-air batteries by using the Mg-Zn-Y alloys with different Zn-to-Y ratios as anodes. The results show that the Mg-Zn-Y alloys could endow a relatively higher open circuit potential, larger corrosion resistance and better electrochemical activity. In comparison with ZK60, the Mg-6%Zn-1%Y alloy shows that the best anodic efficiency of ~55% and discharge capacity of 1163 mAh g^{-1} at the 40 mA cm^{-2}. The experimental results about Mg alloys obtained in the past year are summarized in Table 7.

The microstructure of Mg alloys, such as the grain size (grain boundary), twins, and texture (grain orientation), has a vital influence on the discharge properties of Mg-air batteries. The relationship between microstructure and discharge properties of Mg alloys was intensively investigated by Liang Wu and Bin Jiang et al. [112,116,117] and is summarized in the present review. For example, the role of texture on the discharge properties of AZ31 alloy has been identified [116]. Moreover, the roles of grain size, twins and texture on the discharge properties of Mg-Li alloys have also been studied [117]. In addition, the effect of grain size on the discharge properties of Mg-Y alloys has been explored [112].

Overall, the better discharge properties of Mg alloys were attributed to the grain size refinement, increased content of (11–20)/(10–10) orientated grains, and introduction of twins. This could be understood as: (i) The grain boundary and twins were crystallographic defects with higher energy and acted as the preferential sites for the initial attack during the discharge process, as shown in Fig. 19, and (ii) the (11–20)/(10–10) orientated grains were more easily attacked than the (0002) orientated grains because of their lower binding energy. This finding may open up an effective design thought to strengthen the discharge properties of Mg-air batteries, by means of increasing the content of (11–20)/(10–10) orientated grains, introducing the twins, and decreasing the grain size of Mg alloys.

The characteristics of air-cathode are another critical parameter towards Mg-air batteries. The air-cathode of an Mg-air battery consists of a gas diffusion layer, a catalyst layer, a waterproof and breathable layer, and a flow collection layer. The catalyst layer plays a key role in the performance of the battery. In a neutral electrolyte, oxygen is reduced to OH^- at the gas-solid-liquid ternary phase interface of the air cathode [118]. However, there are few studies on neutral solution catalysts. Many types of catalysts have been studied to promote the ORR performance in acidic or alkaline electrolytes [119,120]. For example, Yongmin Huang et al. [121] reported the cobalt and copper oxides supported by nitrogen-doped porous carbon (CoCu/PNC-900) catalyst has good catalytic activity with the half-wave potential of 0.811 V(vs. RHE) in 0.1 M KOH and noticeable stability.

5.2.2. Rechargeable Mg batteries

Rechargeable Mg batteries are considered to be one of the most remarkable candidates for large-scale sustainable electrochemical energy storage owing to their abundant resources, good stability, low cost and eco-friendliness as well as high energy density (Fig. 20). However, the strong electrostatic interaction between the highly polarized divalent Mg^{2+} ions and the host lattice of the cathode materials usually leads to slow solid-state insertion/diffusion kinetics of Mg^{2+} ions in the lattice. In addition, the compatibility of existing electrode materials with a few optional electrolytes is also not ideal, which hinders the continuous development of rechargeable Mg batteries. Therefore, it is very challenging to find

Table 7
Energy density, specific capacity, anode efficiency of Mg alloys as an anode in the Mg-air battery.

Alloys	Current(mA·cm^{-2})	Power density(mW·cm^{-1})	Specific capacity(mAh·g^{-1})	Anode efficiency(%)	Ref.
Mg-6Al-Sn	50	54.8	1423	63.7	[104]
Mg-9Al-1Zn	2.5	/	1302	57.7	[105]
Mg-	20	23.1	/	/	[106]
Sn-	40	/	1297	59.3	
Mg-2 wt.% Zn	10	/	1186	54.4	[107]
Mg–6%Zn–1 wt.%Y	40	/	1163	55.1	[108]
Mg-0.1 wt.% Ca-0.2 wt.%In	55	39.8	/	/	[110]
Mg-1Bi-0.5Ca	80	85.5	/	52.1 ± 0.1	[111]
AZ80-La-Gd	/	/	1704	76.5	[114]
AZ80-xSm	40	/	1439	65.0	[115]

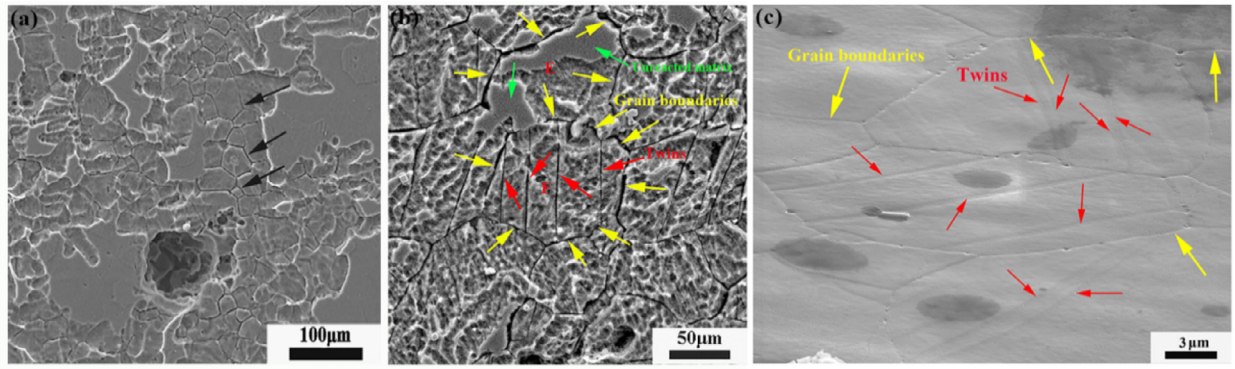

Fig. 19. Surface morphologies for the LAZ531–0% after immersed in 3.5 wt.% NaCl solution for 2 h (a), LAZ531–20% after discharge in 3.5 wt.% NaCl solution at 2.5 mA cm^{-2} for 10 h (b), and LAZ531–20% after electrochemical polishing in an AC2 electrolyte (c) [112].

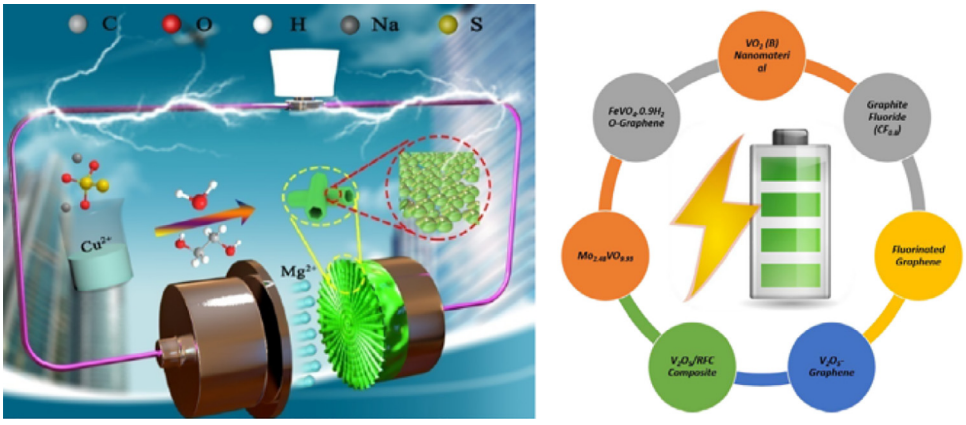

Fig. 20. The schematic illustration of rechargeable Mg battery [130,131].

a cathode and/or anode material that can reversibly intercalate Mg^{2+} ions and simultaneously possess a large specific capacity, long cycle life, and fast kinetics [122-129].

1 Cathode of magnesium-ion battery

Sunita Dey et al. [132] reported a novel cathode of one-dimensional linear chain vanadium tetrasulfide, which provided a specific capacity of about 250 mAh g^{-1}. Partial reversibility was seen to re-form the V^{5+} and S^{2-} containing intermediate on charging instead of VS_4. Zhenjiang Li et al. [128] synthesized a VS_4 with three controllable morphologies via a simple hydrothermal method as high electrochemical performance cathode material for RMB. After 400 cycles, the flower-like VS_4 showed an excellent reversible capacity of about 80 mAh g^{-1} at 50 mA g^{-1}, also with a higher capacity retention of 90%. Lauren E. Blanc et al. [134] found that the nano-sized electrode materials could alleviate the diffusion problem by shortening diffusion lengths and increasing electrode/electrolyte interaction, and then they improved the synthesis of TiS_2 as a cathode for magnesium-ion batteries. The electrochemical performance of WS-TiS_2 displayed significant improvement—yielding larger initial discharge capacities and better capacity retention—in comparison to the

Table 8
Summary of the electrochemical performance of cathode materials for Mg-ion batteries.

Cathode	Reversible capacity (mAh g^{-1})	electrochemical window (V vs. Mg/Mg^{2+})	Cycles	Ref.
VS4	198 (at 50 mA g^{-1}1)	0.2∼2.2	400	[128]
CuS Nanotube	281.2 (at 20 mA g^{-1})	0∼2.0	200	[130]
Vanadium Tetrasulfide	∼250	0∼2.0	200	[132]
WS-TiS_2	294 (at 12 mA g^{-1})	0.5∼2.4	200	[134]
Ti_3C_2 MXene	171 (at 50 mA g^{-1})	0∼2.0	100	[135]
Graphene/β-MnO_2	110 (at 25 mA g^{-1})	−1∼2.0	∼100	[136]
$MgFe_xMn_{2-x}O_4$ (x=0.67, 1, 1.33, 1.6) nanomaterials	97.8 (at 50 mA g^{-1})	0.8∼1.2	1000	[137]
Spinel-Type $MgMn_2O_4$	170 (at 27 mA g^{-1})	1.0∼3.3	–	[138]
PMTT	185 (at 500 mA g^{-1})	–	100	[139]

bulk material. At a current density of 12 mA g^{-1}, WS-TiS_2 reached an initial discharge capacity of 264 mAh g^{-1}, while micron-sized TiS_2 only reached an initial discharge capacity of 270 mAh g^{-1}, which faded considerably to 160 mAh g^{-1} upon further cycling.

Jinglian Zhu et al. [135] provided 3D interwoven MXene networks fabricated as high-performance cathode material for rechargeable magnesium battery. This star material delivered an impressive specific capacity (171 mA h g^{-1} at 50 mA g^{-1}) and good cycling performance (88% capacity retention after 100 cycles). Changliang Du et al. [130] presented a cuprous self-doping strategy to synthesize mesoporous CuS nanotubes with robust structural stability for magnesium batteries and regulated their electrochemical magnesium storage behavior. The observed discharge capacity of the mesoporous CuS nanotubes could reach about 281.2 mAh g^{-1} at 20 mA g^{-1} and 168.9 mAh g^{-1} at 500 mA g^{-1}. Gundu Venkateswarlu et al. [136] synthesized a Graphene/β-MnO_2 for the cathode of Mg-ion battery, while this composite material displayed the discharge capacity of 110 mAh g^{-1} within 60 cycles at a current density of 25 mA g^{-1}, which was an excellent rate capability, and magnesium storage performance around 100 cycles.

Yongquan Zhang et al. [137] prepared low-cost $MgFe_xMn_{2-x}O_4$ (x=0.67, 1, 1.33, 1.6) nanomaterials with a specific capacity of 88.3 mAh g^{-1} even at a high current density of 1000 mA g^{-1} after 1000 charge-discharge cycles. Spinel-type $MgMn_2O_4$ nanoplates ∼10 nm thick were prepared by Shunsuke Doi et al. [138] as a MIB cathode by the transformation of metal hydroxide nanoplates. The battery composed of this spinel-type structure reached a capacity of 170 mAh g^{-1} at 27 mA g^{-1} (1/10C). Moreover, some researchers have turned their attention to organic cathode materials. Henning Kaland et al. [139] investigated the organosulfur compound dipentamethylene thiuram tetrasulfide (PMTT) as the cathode, which delivered a discharge capacity of > 100 mAh g^{-1} after 100 cycles and excellent rate performance (185 mA h g^{-1} at 500 mA g^{-1}). The progress of the cathode materials in 2020 is summarized in Table 8.

2 Anode of Mg-ion battery

Mg possesses several advantages, such as ultrahigh theoretical volumetric energy density (3833 mAh cm^{-3}), rich natural abundance, and dendrite-free deposition during charging, thus it is an attractive material for Mg-ion batteries [140], as shown in Fig. 21. However, anode corrosion still limits their further evolution [140-144].

Min Deng et al. [145] evaluated the possibility of binary Mg-Ge alloy as an anode for primary aqueous Mg batteries. Mg-0.1Ca-0.1Ge (wt.%) anode exhibited similar voltage to Mg-0.1Ca in NaCl solution, but the highly negative OCP enabled it with enhanced voltage in the salicylate-containing electrolyte (1.7 V at 1 mA cm^{-2} versus 1.63 V of Mg-0.1Ca). All micro-alloyed Mg-Ca, Mg-Ge and Mg-Ca-Ge anodes showed similar self-discharge rates and high utilization efficiency (∼60% at 10 mA cm^{-2}). Besides, Mg-0.1Ca-0.1Ge alloy exhibits a low corrosion rate (0.2 mm y^{-1} in 3.5 wt.% NaCl solution) within 7-day exposure in the solution. Jianxin Gao et al. [146] revealed the effect of Al content on the electrochemical performance of Mg anodes for MIB. The Mg-1Al alloy possessed a larger corrosion resistance during discharge, with a significant increase in the anode utilization efficiency at 1 and 5 mA cm^{-2} compared with pure Mg. Mg-Al alloys showed decreased corrosion resistance and severe detachment of unreacted chunks by the increase in Al content, which seemed to be related to the precipitated β phase. The β phase possesses a higher positive corrosion potential and far lower anodic kinetics in the low anodic polarization range compared to the Mg matrix.

Feilure Tuerxun et al. [147] investigated the determining factor on the polarization behavior of pure Mg deposition. The [TFSA]−anion strongly bounded to Mg^{2+} in the $Mg(TFSA)_2$/2-MeTHF electrolyte, undergoes reduction decomposition easily, instead of deposition of Mg, which made the electrolyte electrochemically inactive. In the $Mg(BH_4)_2$/THF electrolyte, because the complex of $[BH_4]^-$ and Mg^{2+} was stable under the potential of Mg deposition, the deposition was not inhibited owing to the decomposition of $[BH_4]^-$. Conversely, in $Mg(TFSA)_2$/triglyme electrolyte, reversible Mg^{2+} plating and stripping can occur due to the weak bond of anions and cations. Jiahe Wang et al. [148] found that the electrostatic shielding effect could guide lateral deposition to form stable interphase toward reversible Mg anodes, which is for the first time to show that the passivation of Mg anodes could be alleviated by guiding a uniform deposition. The shielding could decelerate the vertical growth of protuberances and accelerate the deposition in the vicinity. A thin and stable interphase showed an ionic conductivity

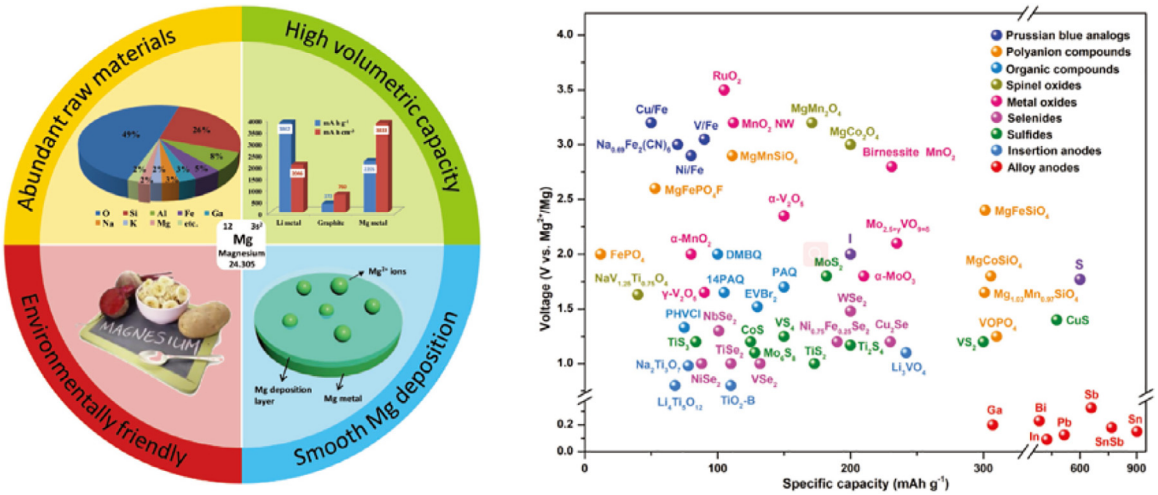

Fig. 21. The advantages of Mg-ion batteries and the development of Mg alloys as anode materials [140].

100 times of the electric conductivity. The symmetrical cell showed a low overpotential of 0.58 V at 0.1 mA cm^{-2} for 90 charge/discharge cycles.

3 Electrolytes for Mg-ion battery

As stated above, electrolytes with wide electrochemical stable windows, high ionic conductivity and good compatibility with electrode materials are the other critical points for high performance Mg-ion batteries. Generally, there are severe technological bottleneck concerns by using organic and/or aqueous electrolytes in Mg-ion batteries, and the ionic insulating passivation layer will form on the anode surface as well as poor reaction kinetics in the cathode. In addition, many organic solvents, such as PC, EC, etc., are flammable and easy to leak. Thus, except for the adoption of traditional liquid electrolytes, tremendous efforts are contributed to the solid-state electrolyte as a promising alternative for high performance Mg-ion batteries, in terms of safety, mechanical property and battery chemistry.

Generally, the ionic conductivity of solid-state electrolytes is lower than that of liquid electrolytes. Recent findings exhibit that adding ionic liquids or plasticizers can improve ionic conductivity. Biswas K et al. [149] fabricated a solid-electrolyte with an ionic conductivity of 1.62×10^{-3} S cm^{-1} at room temperature by doping PVDF-HFP with PC/$Mg(ClO_4)_2$. Thai Hoang et al. [150] followed this direction by adding PC/DOP with $Mg(ClO_4)_2$ into polymer electrolytes based on a blend of PVC and PMMA, which the ionic conductivity is 4.42×10^{-4} S cm^{-1}. Introducing inorganic fillers, such as SiO_2, TiO_2, etc., can also promote the ionic conductivity of the polymer based solid electrolyte. M. Ramesh Prabhu et al. [151] synthesized a solid $Mg(ClO_4)_2$ and a PVDF-HFP/PVAc electrolyte by employing $MgTiO_3$ as the nanofillers. In this case, high ionic conductivity of 5.80×10^{-3} S cm^{-1} at 30 °C could be achieved. Chengcheng Chen et al. [152] constructed a rechargeable quasi-solid-state electrolyte based on tailored polymer electrolytes of PVDF-HFP−nanosized SiO_2−$Mg(TFSI)_2$, which exhibits an ionic conductivity of 8.3×10^{-4} S cm^{-1}, as schematically illustrated in Fig. 22. More development details of the polymer electrolytes are shown in Table 9. We hope that the review could inspire researchers to develop applicable polymer electrolyte candidates for Mg batteries.

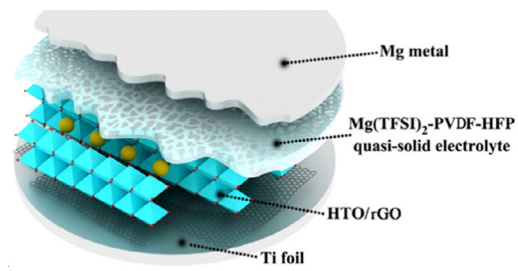

Fig. 22. Schematic diagram of the quasi-solid MIBs [152].

4 Rechargeable Mg-S batteries

Rechargeable Mg-S batteries are another promising type of Mg-ion batteries, owing to their high energy densities (3221 Wh L^{-1}), cost-effective and eco-friendly properties. Most recently, the study of Mg-S batteries was mainly focused on cathode design, electrolyte exploration, battery structure optimization and discharge behavior. Moreover, other chalcogenides were also applied in rechargeable Mg batteries. The properties of recently rechargeable Mg-S batteries are summarized in Table 10.

Rational design of cathode architectures is acquired because of the insulation properties of sulfur and magnesium sulfides, shuttle effect and slows the reaction kinetics [160,161]. In early 2020, Co@C−S demonstrated its improved performance in Mg-S battery [162]. PAN/S cathode was also studied in Mg-S batteries accompanied with electrolyte design which showed some extent of reversibility [163,164].

Table 9
Electrochemical properties of the solid-state electrolytes reported in 2020.

Salt	Polymer	Filler	IL/ Plasticizer	σ at r.t. (S/ cm)	Elec. Window (V)	t^+	Ref.
$Mg(ClO_4)_2$	PVDF -HFP	–	PC	1.62×10^{-3}	5.5	0.99	[149]
$Mg(ClO_4)_2$	PVC-g-PMMA	–	PC /DOP	4.42×10^{-4}	–	–	[150]
$Mg(ClO_4)_2$	PVDF-HFP/PVAc	$MgTiO_3$	–	5.80×10^{-3}	–	0.34	[151]
$Mg(TFSI)_2$	PVDF-HFP	SiO_2	G3/THF	8.3×10^{-4}	–	–	[152]
$Mg(ClO_4)_2$	PAN	–	PC	3.28×10^{-3}	4.6	0.6	[153]
$Mg(CF_3SO_3)_2$	PEO	–	EMIM-BF_4	9.4×10^{-5}	4	0.22	[154]
MgBr2	PVDF	–	TEGDME	1.2×10^{-6}	–	0.55	[155]
$Mg(CF_3SO_3)_2$	PEO	–	PC-DEC	3×10^{-5}	3.5	0.32	[156]
$Mg(TFSI)_2$	PVDC- AN	–	SN	1.61×10^{-6}	3.2	–	[157]
$Mg(NO_3)_2 \cdot 6H_2O$	CA	–	–	9.19×10^{-4}	3.65	0.35	[158]
–	MgCl-FTGB	–	–	4.51×10^{-5}	4.8	0.733	[159]

Table 10
Summary of rechargeable Mg-S battery.

Cathode	Electrolyte	Capacity (mAh g^{-1})	Cycling performance (mAh g^{-1})	Cycles	Ref.
NG-NCNT@NCS@S	MgCl-FTGB@GF	-	1100 (0.2 C)	50	[159]
MesoCo@C-S	MACC-DME	830 (0.1 C)	280 (0.2 C)	400	[162]
SPAN	$Mg[BH_4]_2$/$Li[BH_4]$-DME	800 (0.1 C)	800 (0.5 C)	300	[163]
SPAN	$Mg[B(hfip)_4]_2$•3 DME-DME/TEGDME	550 (C/30)	-	-	[164]
VN/60S	MTB-DME	866 (200 mA g^{-1}) 575 (500 mA g^{-1})	450 (500 mA g^{-1})	100	[165]
NG-NCNT@NCS@S	LiCl-$[Mg•6THF][AlCl_4]_2$	869 (0.1 C)	300 (0.4 C)	500	[166]
CMK/S	MMAC-IL ionic liquid (MMAC/DME/Pyr14TFSI)	762 (50 mA g−1) 267.4 (250 mA g−1)	359.8 (100 mA g−1)	50	[170]
S/NC	$Mg[B(hfip)_4]_2$-DME	899 (0.05 C)	330	100	[167]
Te-Cu	B-based Mg salts	338 (100 mA g−1)	178.5 (100 mA g−1)	400	[171]
SeS2/CMK3-Cu interlayer	OMBB	1020 (0.1 C)	299 (3 C)	1000	[172]

Another challenge of Mg-S batteries is the availability of suitable electrolyte solutions. A halogen-free electrolyte containing $Mg[BH4]_2$ and Mg[BH4] in diglyme was proposed in Mg-S batteries [163]. The tailored electrolyte features a low overpotential of 0.04 V and could remove the blocking layer on the surface of the Mg foil. On the other hand, ionic liquid Mg electrolyte of MMAC-IL [164], polymer electrolyte of magnesium chloride-(fluorinated tetraethylene glycolic) borate [159], magnesium trifluoromethanesulfonate [165], $[Mg{\cdot}6THF][AlCl_4]_2$ electrolytes with LiCl additive [166], and ($Mg[B(hfip)_4]_2$/DME) with iodine addictive [167] were also explored in Mg-S batteries.

It is important to study other components in Mg−S batteries to further improve the electrochemical performances. According to the study when using the Cu current collector and MBA-based hybrid electrolyte, green aqueous polyacrylate binder-based S@pPAN electrode exhibits a better cycling stability than other selected binders [168]. A. Robba et al. [169] demonstrated that Cu current collector cannot be considered in Mg–S batteries with sulfur cathode due to the formation of CuS//Mg redox pair which will significantly decrease energy density on the cell level.

Inspired by the application of conversion type element sulfur cathode, selenium and tellurium based materials have been explored to improve the sluggish kinetic and the inferior reversibility of Mg battery. Guanglei Cui and coworkers designed Mg-tellurium batteries aided with Cu current collector [171]. Furthermore, Mg–SeS_2 battery with a Cu foam interlayer between cathode and separator was also designed [172]. The Cu foam interlayer not only acts as the trapping layer, but also serves as a "promoter" to propel the overall charge-discharge kinetics by the reversible displacement reaction between copper sulfide (copper selenide) and Mg^{2+}.

Polysulfides shuttle generally causes the low Coulombic efficiency and short cycling life in metal-sulfur batteries. A study demonstrated that even in a geometrically identical cell setup, there are distinct differences between Li−S and Mg−S batteries [133]. The side reactions on the Mg anode surface as a limiting process cause the much more rapid self-discharge of the Mg system, while other factors, such as the mobility of dissolved species and solid-phase kinetics, play a minor role.

In summary, Mg-S batteries and other Mg-chalcogenides (Te and Se) batteries promise significant improvements in energy density while the developments in these batteries are in

an early stage. To improve the performance of the current state-of-the-art Mg-S battery, innovative efforts are required, not only in the design of active materials but also in the engineering of the full cell. Further progress in this direction can be achieved by combining theoretical calculations and in-situ characterization techniques to understand reaction mechanisms and engineer more reversible Mg-S batteries.

5.3. Hydrogen storage Mg materials

Magnesium-based hydrogen storage materials are considered to be one of the most promising solid-state hydrogen storage materials due to their high hydrogen storage capacity, simple reaction process, abundant resources and environmental protection. However, the application of magnesium-based hydrogen storage materials is greatly hindered by the slow hydrogen absorption kinetics and high thermodynamic stability. Therefore, in order to enhance the hydrogen storage performance and practical application of magnesium-based hydrogen storage materials and promote the application of magnesium-based hydrogen, the scholars from all over the world have been deepening their research based on common methods such as alloying, nano-crystallization, catalyst addition and surface modification, and developing new modification methods.

It is useful for us to understand and predict various phenomena and characteristics of materials at multiple scales by first-principles and dynamic models. Based on DFT calculations and KMC simulations, M. Abdellaoui's group [173] studied the hydrogen storage properties of intermetallic hydrides $MgNiH_3$, $MgCoH_3$ and $MgCo_{0.5}Ni_{0.5}H_3$. The unstable $MgNiH_3$ and extremely stable $MgCoH_3$ can be mixed to form the $MgCo_{0.5}Ni_{0.5}H_3$ mixtures that possess high volumetric capacity, better thermal stability (H=−45.92 kJ/mol H_2) and lower dehydrogenation temperature (T=353.33 K). It is proved theoretically that hydrogen storage mixture with excellent comprehensive performance can be obtained by two kinds of intermetallic compounds with different stability, which guides the design and preparation of new materials. At present, alloying is the most common method. Generally, the hydrogen de-/hydrogenation performances of magnesium-based hydrogen storage materials are optimized by adjusting the internal structure of the alloy. J. Cermak et al. [174] empower the hydrogen storage performance of the alloy by forming a LPSO structure in the Mg-In-C alloy, and perform dynamics studies on a series of alloys with different content ratios of solid solution phase (Mg) and β structure. The hydrogen sorption capacity varies between about 6 wt.% H_2 for (Mg) and 0.6 wt.% H_2 for β structure. In the interval from 69 to 71 wt.%, hydride decomposition enthalpy decreases to 54 ± 3 kJ (mol H_2)$^{-1}$ and 57 ± 3 kJ × (mol H_2)$^{-1}$ for ordered alloys, and even down to 51.5 kJ × (mol H_2)$^{-1}$ for amorphous β structure. The activation energy of desorption kinetics is also lowered in the ordered structure. This proves that the ordered structure can be used as dispersed catalytic phases to improve the kinetic and thermodynamic properties of the disordered structure, which indicates that we do not need to tune the hydrogen sorption via grain surface modifications by other elements, and can also significantly improve the hydrogen storage performance.

Surely, another frequently used method with a good modification effect is the combination of nanometer system with an addition of catalyst. Synergistic modification strategies via combining several modification techniques, such as system nanometer and catalyst addition, have been studied by many researchers. Hui Liang et al. [175] prepared magnesium nanoparticles (Mg NPs) by in-situ reduction of methyl magnesium chloride with lithium naphthalene. The Mg NPs can be reacted with H_2, and O_2 and H_2O molecules cannot be infiltrated into PMMA. Moreover, the Mg NPs in PMMA might release a higher amount of H_2 at below 300 °C with a rapid absorption/desorption kinetics than the material reported in the literature. Miaomiao Hu et al. [176] have successfully synthesized Mg–TiCX@C nanocomposite through a reactive gas evaporation method. The carbon confinement nanostructure and the catalysis of the TiCX have enhanced the hydrogen storage kinetics of the nanocomposite. $Mg_{88}(TiC_{0.6})_{12}$@C nanocomposite absorbed 5.5 wt.% H_2 within 25 min at 523 K and desorbed 4.5 wt.% H_2 within 60 min at 573 K. Nicola Patelli's group [177] reported on biphasic Mg-Ti-H nanoparticles that outperform the known Mg-based materials in sorption kinetics and thermodynamic stability. In this work, the bulk-immiscible MgH_2 and TiH_2 phases are mixed at the nanoscale. TiH_2 conveys catalytic activity for H_2 dissociation/recombination and accelerates hydrogen diffusion, while MgH_2 provides reversible hydrogen storage. At the remarkably low temperature of 150 °C, hydrogen absorption and desorption are completed in less than 100 s and 1000s, respectively. Pei Liu et al. [178] in-situ synthesized binary nanocatalysts Mg_2Ni and Ce_6O_{11} with oxygen vacancy defects on the Mg surface by the hydrogen activation of Mg-Ni-CeO_2. During H_2 absorption, the oxygen vacancy defects on the Ce_6O_{11} surface can trap H_2 molecules, while the Mg_2Ni on Mg/Mg_2Ni interface can promote H_2 dissociation. For H_2 desorption, the Mg_2Ni can weaken the Mg-H bond and act as a "hydrogen pump" to transfer H for the formation of H_2 with the assistance of Ce^{3+}/Ce^{4+} transformation in Ce_6O_{11}. The results showed that both hydrogen absorption kinetics and dehydriding kinetics were improved. F. J. Antiqueira et al. [179] produced Mg-8mol%Fe nanocomposites by high-energy reactive milling to improve the hydrogen storage properties. Nanocomposites with MgH_2, low Fe fraction and no Mg_2FeH_6 are suggested to have the best hydrogen storage performance.

Attention to the properties of alloys themselves is not only paid by scholars from various countries, and the traditional preparation methods, such as high-energy ball milling, are also being constantly innovated. P. de Rango et al. [180] proposed Fast Forging, which is a new SPD method for the synthesis of Mg-based alloys for hydrogen storage. The Fast Forging process operates rapidly comparison made with the long time Ball Milling process. Fast Forging can not only complete energy transfer and mechanical alloying, but also provide a large number of H active sites. The obtained bulk

samples have no risk of spontaneous combustion and are easy to realize industrialized production due to low cost.

Magnesium-based materials can not only be used as hydrogen carriers, but also be used for hydrolysis under mild conditions to produce hydrogen and increase productivity. S.A. Pighin et al. [181] prepared two samples, MgH_2 with ball grinding for 5 h and nanostructured Mg of dehydrogenation at 355 °C after ball grinding for 2.5 h. The hydrolysis performance of MgH_2 and nanostructured Mg in 0.6 M $MgCl_2$ aqueous solution was analyzed. A nanometric Mg that has a concentration of 0.6 M $MgCl_2$ can produce 910 ml/g of H_2. The hydrolysis performance is one of the best reported in magnesium-based materials and is attributed to the morphology and microstructure of the material. This study promotes our understanding of the application of magnesium-based materials and the related preparation methods in other aspects of hydrogen energy.

5.4. High modulus and high damping Mg alloys

As is known to us all, Mg and its alloys have been widely used in automotive, communication electronics, aerospace and military fields due to their excellent damping capacities [182-185] However, compared with other structural metallic materials, high-damping Mg alloys usually exhibit low elastic modulus and poor resistance to elastic deformation, which cannot meet the requirements of high-tech fields for Mg alloy materials with high elastic modulus and high damping capacity. Thus it hinders further development and application of Mg alloys. Therefore, several researchers are exploring ways to simultaneously achieve the optimal combination of elastic modulus and damping capacity.

Alloying is the most effective and economical way to improve the elastic modulus of Mg alloys, but the addition of alloying elements tends to reduce the damping capacity. Since damping is related to dislocations movement, the addition of alloying elements increases the atomic concentration in the Mg matrix, reducing the mobile dislocations. For example, the elastic modulus of Mg-2Y-2Sn was ~47.5 GPa, while its damping (Q^{-1}) capacity was only ~0.000581 at room temperature. Mg-10Al-5Ca-2Zn alloy displayed a relatively higher elastic modulus of 49.2 GPa, but its damping value was below ~ 0.000446 [186,187]. Therefore, to balance the relationship between elastic modulus and damping capacity, Xianhua Chen's group [188] developed an extruded Mg-7Gd-4Y-2Zn-0.5Mn-0.8Si alloy with excellent damping properties and elastic modulus of ~49.3 GPa. This alloy exhibited superior damping properties at room temperature to that of the extruded pure Mg at high strain amplitudes. The mechanism of the increased damping capacity was associated with the presence of abundant thermal mismatch dislocations around the phase interfaces. However, at higher temperatures, the extruded Mg-7Gd-4Y-2Zn-0.5Mn-0.8Si alloy showed a lower damping capacity than that of pure magnesium but a higher value compared with that of the Si-free alloy. The high elastic modulus was attributed to the formation of high modulus Gd_5Si_3 and SiY particles.

In addition, to further improve the elastic modulus and damping capacity of Mg alloys, Xianhua Chen's group [189] reported a new Mg-1.3Y-0.8Zn-6.4Al-16.7Li alloy (Alloy II) with a high elastic modulus of 52.9 GPa and superior damping capacity in 2020, as shown in Fig. 23. The high elastic modulus was attributed to Li in solid solute and the formation of high modulus Al-Li compounds and Al_2Y particles. At room temperature, the excellent damping capacity in the alloy was due to the presence of a large number of mobile parallel dislocations. Moreover, the alloy could be classified as a high damping metal ($Q^{-1} > 0.01$) in the strain amplitude region. The high temperature damping capacity could be explained by the movement of dislocations and grain boundary sliding.

5.5. Dissoluble magnesium alloys

Multi-stage fracturing is a key technology to improve the exploit efficiency of low permeability oil and gas resources, in which fracturing tools play a major role. Traditional fracturing tools need to be drilled and milled after fracturing, which is difficult to operate, time-consuming and laborious. New fracturing tools could degrade rapidly after fracturing. Magnesium alloys possess the characteristics of low density, high specific strength and poor corrosion resistance, which can be used as an alternative material for the preparation of fracturing tools. At present, dissoluble magnesium alloy materials are mainly concentrated in AZ series, Mg-Zn series, and magnesium-based composite materials. Although excellent mechanical properties have been obtained, it is difficult to meet the performance requirements of rapid degradation. Therefore, an effective way to simultaneously improve the strength and degradation properties of magnesium alloys is the key to extend such applications.

Jingfeng Wang et al. [190] innovatively proposed to simultaneously improve the mechanical and degradation properties of magnesium alloys by introducing the LPSO phase. Meanwhile, the effect of LPSO content on the mechanical and degradation properties of magnesium alloy was investigated. The $Mg_{97.5}Ni_1Y_{1.5}$ alloys exhibited optimal comprehensive properties with an average corrosion rate, up to 6675 mm/y at 366 K (93 °C) and ultimate compressive strength (UCS) of 410 MPa (Fig. 24), which could be used as a promising candidate material for the preparation of fracturing tools. The higher potential difference between the LPSO phase and the magnesium matrix forms a galvanic couple, and the LPSO phase act as a cathode to accelerate the degradation of the magnesium matrix. The galvanic corrosion dominated the whole corrosion process.

Kunkun Deng et al. [191] reported that the extruded Mg-4Zn-2Ni alloys presented excellent mechanical and degradation properties. Increasing extrusion temperature led to a decrease in both the UCS and degradation rate. When extruded at 200 °C, the UCS and degradation rate of Mg-4Zn-2Ni alloy were 513 MPa and 619 mm/y at 298 K (25 °C), respectively. Dislocation density and the second phase were considered to be the main factors affecting the degradation rate.

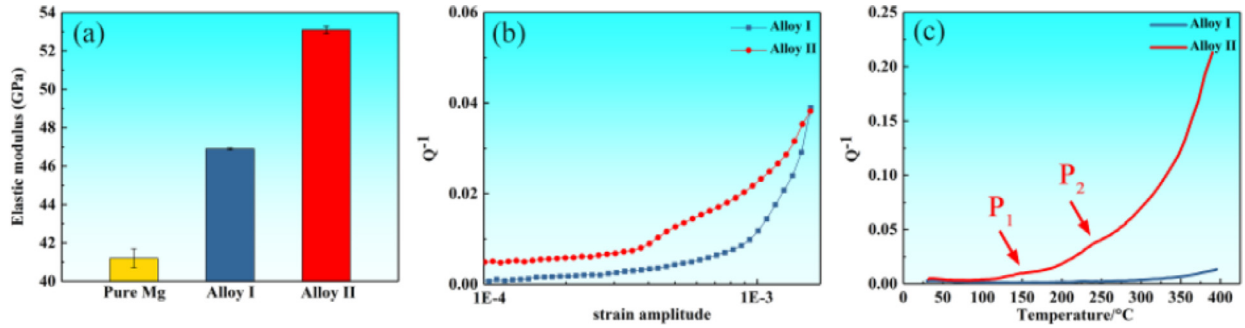

Fig. 23. (a) Elastic modulus of pure Mg, alloy I (Mg-1.3Y-0.8 Zn alloy) and alloy II (Mg-1.3Y-0.8Zn-6.4Al-16.7Li), respectively. The damping capacity of alloy I and alloy II as a function of (b) strain amplitude and (c) temperature [189].

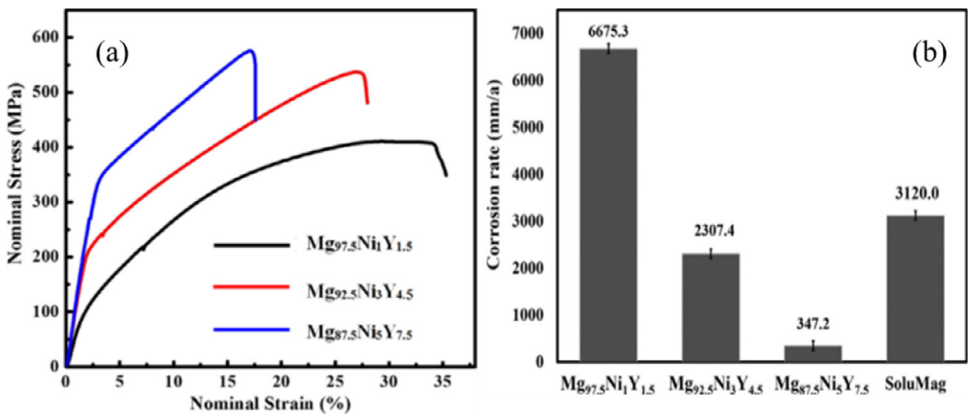

Fig. 24. Compressive stress-strain curves (a), corrosion rates (b) of as-cast Mg-Ni-Y alloys [190].

H. X. Li et al. [192] discovered that the addition of Ni in GW103 K alloy can improve the mechanical and degradation performance of magnesium alloys with the transformation of precipitation phases from Mg_5RE to 18R-LPSO. The Mg-10Gd-3Y-0.3Zr-0.8Ni alloys exhibited UCS of 597 MPa, and a degradation rate of 24.4 mg · cm^{-2} · h^{-1} at 93 °C in 3 wt.% KCl.

6. Casting and processing technologies

6.1. Casting technology for large-scale ingots of high strength Mg alloys

The Mg-RE-TM alloy exhibits excellent mechanical properties due to the LPSO phase. However, it is difficult for the fabrication of large-scale ingots of high strength Mg alloys, due to the high rare earth content. The large size and high-quality ingots are the basis of producing wrought magnesium alloys. Therefore, developing large-scale magnesium alloy ingots with high quality is necessary and urgent. The casting technology of large-scale ingots for high-strength Mg alloys was developed in the past year.

Mingyi Zheng et al. [193] prepared the Mg-8.2Gd-3.8Y-1.0Zn-0.4 Zr (wt.%) alloy ingot with a diameter of 280 mm. Jingfeng Wang et al. [16] prepared the high-quality large-scale Mg-Gd-Y-Zn-Mn alloy ingot through semi-continuous casting with a diameter of 315 mm and a length of 2410 mm, as shown in Fig. 25. It plays an important role in promoting the application of Mg alloys. And then, they investigated the acquiring a bimodal microstructure in Mg-Gd-Y-Zn-Mn alloy and found that the as-extruded alloy has excellent mechanical properties with an UTS of 455 MPa, YS of 382 MPa and EL of 11.0%. The mechanism is mainly attributed to the presence of bimodal microstructure, strong fiber texture, β-Mg_5(Gd, Y) particles, lamellar and block-shaped LPSO phases [16].

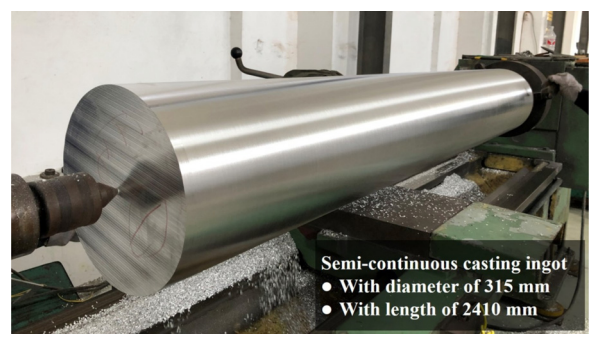

Fig. 25. Large-scale alloy ingot fabricated by semi-continuous casting [16].

6.2. Processing technologies of wrought Mg alloys

In the past year, magnesium alloy plastic processing technology also made good progress. By changing the tangential strain in the extrusion deformation process of the die struc-

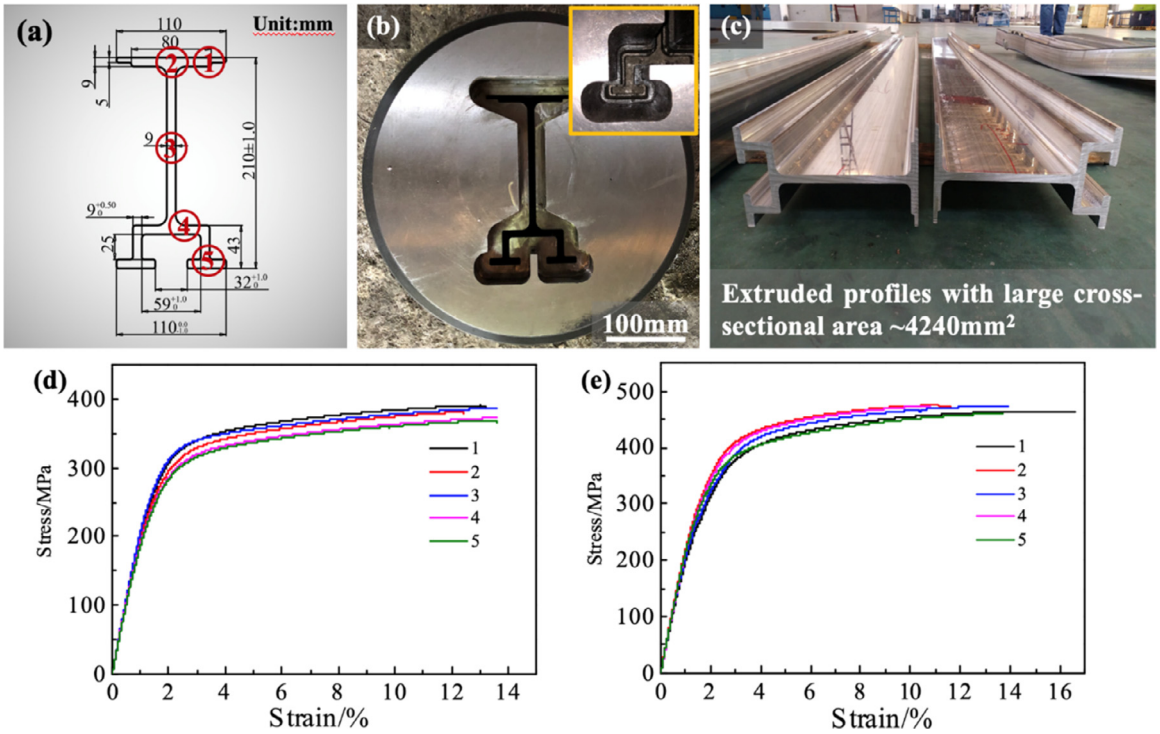

Fig. 26. (a) Geometry and main dimensions of the profile with a large cross-section; (b) extrusion die; (c) extruded profiles; (d) tensile stress-strain curves of as-extruded profiles; (e) tensile stress-strain curves of peak-aged profiles [194].

ture, and increasing the strain by increasing the stage of die shape, the structure and base texture of the wrought magnesium alloy can be improved.

6.2.1. Extrusion of large-size profiles

As a predominant plastic forming process of Mg alloys, hot extrusion can be used to produce solid and hollow profiles with improved microstructure and mechanical properties. In the past, the pony-size and simple-cross-section Mg profiles with poor mechanical properties have been commercialized. However, the extrusion technologies of large-size and complex-cross-section Mg profiles especially with high strength are still undeveloped.

Jingfeng Wang et al. [16] used HyperXtrude software to simulate the profile structure of a large-size high-strength and high-touch Mg-9Gd-4Y-1Zn-0.8Mn alloy rail transit support beam. Under the premise of ensuring the successful extrusion of large-size high-strength and tough magnesium alloy support beam profiles, the preferred process was determined. Furthermore, the large-size high-strength and tough magnesium alloy support beam profile used in rail transit with good surface quality, uniform composition and homogeneous structure were successfully prepared, which show outstanding mechanical properties with an UTS of over 470 MPa, El of over 10% (Fig. 26).

In addition to the solid profiles, hollow profiles can greatly reduce the weight of the formed products, showing a better prospect [195], among which the wide thin-walled hollow magnesium alloy profile of the large size is under conventional technology, the research and development cycle is long, the test mold cost is high, and the preparation is extremely difficult. Jingfeng Wang et al. [196] optimized the structure of the wide-form thin-walled hollow profile of the large size by Deform-3D numerical simulation software and the extrusion process of the profile by HyperXtrude numerical simulation software. After the optimization, a bright and straight large-size wide-walled hollow AZ31 alloy profile was prepared successfully, with a profile cross-section size of 502 mm × 60 mm, which is currently the world's largest wide-walled thin-walled hollow magnesium alloy profile (Fig. 27). Microstructure observation and mechanical performance testing were carried out in the regions of the profile. The regional tissues were uniform, the average grain size was about 10−30 μm, the tensile strength was above 250 MPa, and the elongation was more than 15%.

6.2.2. Development of extrusion technology

Yanpeng Wang et al. [29] provide a staggered extrusion (SE) method to simplify the preparation process of magnesium alloy bent products. The curvature of extruded products can be quantitatively controlled by adjusting the staggering distance at the end of the stem. They provided a scientific basis for forming AZ31 Mg alloy bending products with excellent microstructure by the SE process. The continuous variable channel direct extrusion has been developed. The alloy ingot has been developed successively [40]: smaller-thicker-smaller-thicker-smaller, five strain processes are obtained for extruded products, the prepared AZ31 magnesium alloy sheet has a weak base texture and a strength of above 250 MPa, and its elongation can reach more than 30%. One magne-

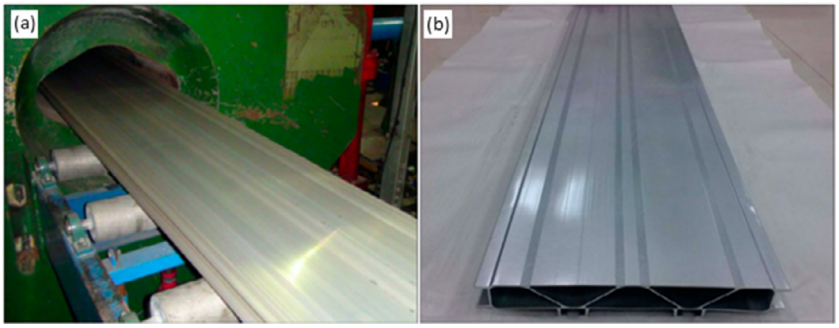

Fig. 27. Extrusion results of a wide profile: (a) extrusion result at the scene after repairing; (b) extrusion profile after repairing [196].

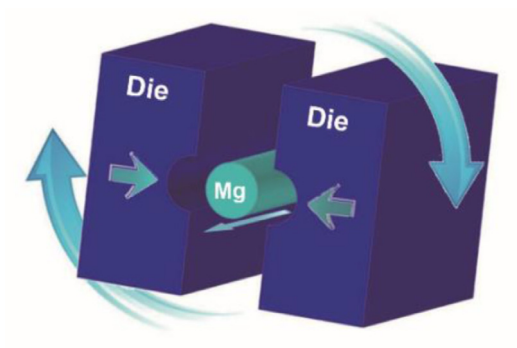

Fig. 28. Schematic illustration of the rotary swaging technique [49].

sium alloy ingot is solidified in the middle of another magnesium alloy ingot by casting so that the structure of the central part of the ingot is greatly different from the other parts, and the interface of the ingot can be increased. The two parts in the extrusion process can be perfectly welded together, causing greater strain, and finally, a refined structure is obtained [197]. Through this process, the plasticity and anisotropy of the magnesium alloy can be effectively improved, and the elongation of the prepared AZ31 magnesium alloy can reach 21%, CYS/TYS (compressive yield strength / tensile yield strength) can reach 0.84. Yingchun Wan et al. [49] prepared Mg–Gd–Y–Zr alloys with an average grain size of 80 nm and a dimension of $\Phi 3$ mm $\times$ 1000 mm using the rotary swaging method. The schematic of the rotary swaging is shown in Fig. 28. The further-aged Mg alloy exhibits a yield strength of 650 MPa and an ultimate tensile strength of 710 MPa, being the highest reported for bulk Mg alloys.

Bin Jiang et al. [197] proposed a novel approach entitled bimetal casting-co-extrusion to reduce the room-temperature (RT) compression-tension yield asymmetry of Mg alloys. The schematic diagram of the fabrication for the Mg-3Al-1 Zn/Mg-1Y (AZ31/W1, wt.%) composite rod is shown in Fig. 29. A well metallurgical bonding interface with a diffusion zone of $\sim$1 μm was observed, which provided a guarantee for good mechanical properties of AZ31/W1 composite rod. Compared with the AZ31 alloy rod, AZ31/W1 composite rod demonstrated a higher yield symmetry from 0.57 to 0.84 at RT, which resulted from the activation of a basal slip in tension and the restriction of {10–12} extension twinning in compression. Therefore, this work offers an insightful opinion to control the activated proportion between slip and twinning during deformation and improves the RT yield asymmetry of Mg alloys by bimetal casting-co-extrusion processing method.

6.2.3. Large-strain high-efficiency rolling

Due to the hexagonal close-packed crystal structure, the Mg alloys show limited slip systems at room temperature which cannot satisfy the von-Mises criterion for homogeneous plastic deformation. The Mg alloys with a relatively high strength are especially difficult for plastic deformation, which requires a relatively small rolling reduction pre-pass and high processing temperature. The per-pass rolling reduction of high-strength Mg-RE alloys is normally no more than 30% [198]. Therefore, the low strain of the rolling process can further be improved to enhance the rolling efficiency without compromising the mechanical properties of Mg alloy sheets.

A novel asymmetric rolling process has been introduced into a hard-to-deform Mg-8.8Gd-3.4Y-1Zn-0.8Mn (wt.%) alloy by Jingfeng Wang' group [199], which results in a large strain with $\sim$91% total reduction by only 2 rolling passes. Fig. 30 shows a schematic illustration of the novel asymmetric rolling process which was implemented by a hard-plate rolling process (HPR). As a promising structural material, the Mg-Gd-Y-Zn-Mn alloy exhibits excellent mechanical properties as well as improved anisotropy of strength and plasticity (Tension//RD: TYS of 362 MPa, UTS of 415 MPa and El of 8.3%; Tension//TD: TYS of 371 MPa, UTS of 434 MPa and El of 10.7%). The outstanding mechanical properties should be attributed to the refined grains, the homogeneously dispersed LPSO phase and β phase and the weakened texture.

6.2.4. Online heating rolling

Edge crack is a common defect in the case of rolling for magnesium alloy sheets. Fusheng Pan et al. developed an on-line heating rolling (O-LHR) technology, which showed largely reduced edge cracking susceptibility, high surface quality, improved mechanical properties of magnesium alloys [200]. The O-LHR provides in-situ heating which accelerates the deformation of magnesium alloys. The concept of ON-LHR is to heat the sheets and working rolls simultaneously. There is no need to anneal the sheets between passes compared with the conventional rolling. Qiang Liu and Jiangfeng

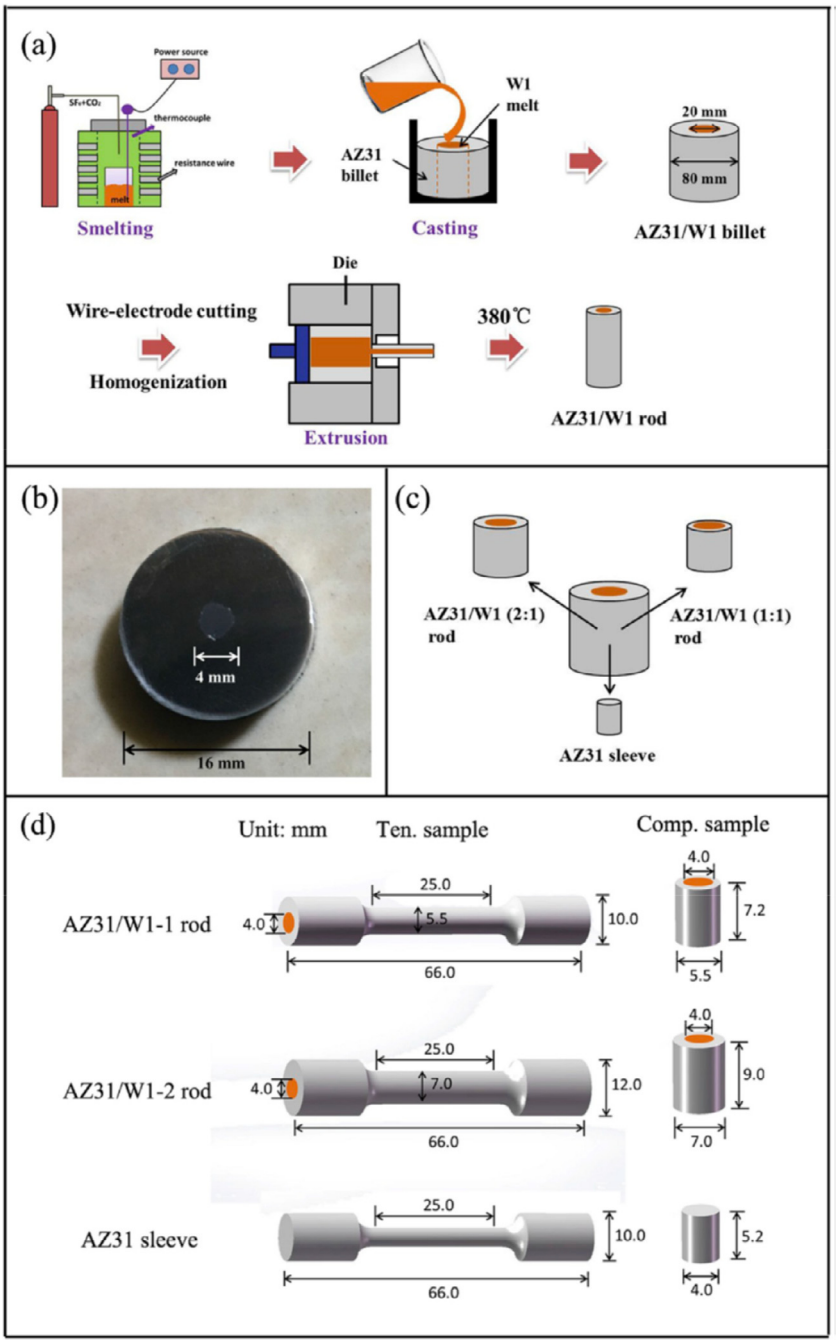

Fig. 29. (a) Schematic diagram showing the fabrication of AZ31/W1 rod by a bimetal casting-co-extrusion process; (b) size of AZ31/W1 rod, where AZ31 sleeve was ~4 mm in external diameter and W1 core was ~16 mm in inner diameter; (c) sample preparations for tension and compression tests; (d) detailed sizes of tensile and compressive samples for AZ31/W1–1 rod, AZ31/W1–2 rod and AZ31 sleeve [197].

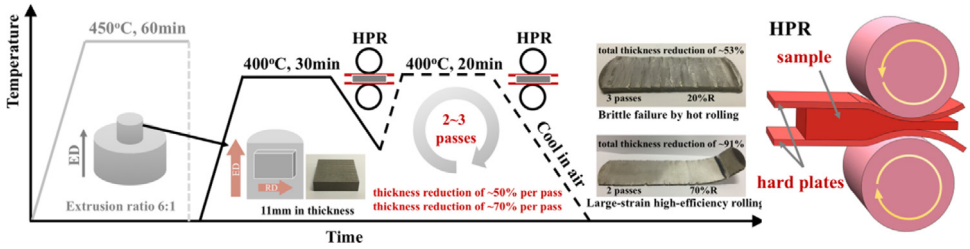

Fig. 30. Schematic representation of the large-strain high-efficiency rolling [199].

Song et al. [201] found that no visible edge cracking occurred on AZ31 sheets with O-LHR rolling at 250 °C, while conventional rolling of AZ31 sheets exhibited several edge cracks with a maximum crack depth of 4.2 mm.

In addition, the tension was imposed on the magnesium alloy sheet during the rolling process. Jiangfeng Song et al. [202] found that there is an optimum tension in consideration of both shape quality and edge crack of magnesium alloy sheet. The imposed tension helps to improve the shape quality of the sheet. However, excessive tension will increase the edge cracking susceptibility of the AZ31 sheets.

6.3. Additive manufacturing technology of Mg alloys

Compared with conventional manufacturing technologies, additive manufacturing (AM) technology has many advantages such as no mold, free-forming, and near net shape, which provides an efficient way for the complex structural components. With the development of AM technology and the growing demand for high-performance magnesium alloy complex components, the research on magnesium alloy additive manufacturing has made some progress in 2020.

Yongho Sohn et al. [203] prepared the dense WE43 Mg alloy by laser powder bed fusion. The as-built microstructure consisted of fine (<10 μm) α-Mg (hcp) grains with globular β_1-Mg_3Nd precipitates and (Y, Zr)$_2O_3$ oxides. After heat treatment, the globular β_1-Mg_3Nd precipitates were dissolved and re-precipitated into thin sheets. The (Y, Zr)$_2O_3$ oxides were not found to dissolve or coalesce, but agglomerated within the α-Mg (hcp) matrix. Under compression, the as-built LPBF WE43 had yield strength, compressive strength and strain to failure of 224 MPa, 417 MPa and 9.5% respectively. In tension, the as-built LPBF WE43 had, on average, yield strength of 215 MPa, tensile strength of 251 MPa and strain at failure of 2.6%.

Wire and arc additive manufacturing ((WAAM)) exhibits a great potential for additive manufacturing of Mg alloys due to low heat input of cold metal transmission as a heat source. Jianrui Liu et al. [204] revealed the relationship between the microstructure and mechanical properties of WAAMed AZ31 material. The schematic diagram of the experimental setup developed for WAAM-CMT and the external view of the AZ31 thin wall deposited by the WAAM-CMT method are shown in Fig. 31. The manufactured AZ31 thin-walled deposit was mainly composed of columnar dendrite arrays, including dendritic α-Mg matrix, inter-dendritic eutectics (α-Mg and β-$Mg_{17}Al_{12}$) and some dispersive η-Al_8Mn_5 phases. The tensile properties present obvious anisotropic characteristics because of the epitaxial columnar dendritic growth along the building direction.

M. Esmaily et al. [205] prepared the WE43 alloy by selective laser melting (SLM) and investigated the microstructure and corrosion behavior of the specimens after hot isostatic pressing (HIP), and solutionizing heat treatment, whilst assessed and contrast relative to the conventionally cast alloy counterpart. The SLM prepared specimens possessed a unique microstructure comprising fine grains growing with a strong [0001] texture along the building direction with a low fraction of process-induced and metallurgical defects, reaching < 0.1%, after optimizing the SLM parameters and HIP treatment. Electrochemical measurements demonstrated that the WE43 prepared by SLM was cathodically more active as compared with its cast counterpart.

Table 11
Corrosion rates calculated from weight loss of Mg specimens immersed in basic $Mg(OH)_2$ saturated solution containing different individual constituents for 72 h [207].

Solution	Weight Loss(mm/y)
$(NH_4)_2SO_4$	2.84 ± 0.13
Haze-contaminated solution	2.09 ± 0.35
NH_4NO_3	1.06 ± 0.06
NH_4Cl	0.49 ± 0.08
NaCl	0.37 ± 0.02
KCl	0.37 ± 0.01
Na_2SO_4	0.35 ± 0.03
$MgCl_2$	0.38 ± 0.04
$CaSO_4$	0.37 ± 0.01
$Mg(OH)_2$	0.34 ± 0.01
$Ca(NO_3)_2$	0.25 ± 0.01

7. Corrosion and protection of Mg alloy

7.1. Corrosion behavior of Mg alloys

7.1.1. Environmental corrosion of Mg alloys

The poor corrosion resistance of Mg and its alloys can be mainly attributed to: (i) the highly negative electromotive force (emf = −2.363 V), and (ii) the poorly protective properties of the surface film formed on Mg, which easily leads to pitting, galvanic corrosion, stress corrosion cracking and other corrosion forms. However, the corrosion of Mg and its alloys in a specific environment may be a combination of multiple corrosion forms. Chaofang Dong et al. [206] studied the long-term corrosion behavior of AZ31 exposed to a dry tropical desert environment, and found that cracks appeared in the uniform corrosion product layer on the surface of AZ31 with the extension of exposure time, as shown in Fig. 32. The corrosion form of the alloy changed from early uniform corrosion to severe local corrosion, and the corrosion accelerated. In the face of the increasingly severe smog problem, Guangling Song et al. [207] investigated the corrosion rate of pure magnesium in an $Mg(OH)_2$ saturated solution containing different individual constituents of PM 2.5 in a haze like Table 11, and considered that the industrial service environment of magnesium is relatively complex, and the corrosion properties of magnesium obtained from the conventional solution cannot be used directly, and more systematic research is needed. P. Volovitch et al. [208] studied the corrosion behavior of Mg-Li(-Al-Y-Zr)-alloy in aqueous solution and reported that the in-situ development film on Mg-Li(-Al-Y-Zr)-alloy was composed of Li-doped MgO on a Li-depleted metallic matrix, which was beneficial to the protection of the alloy.

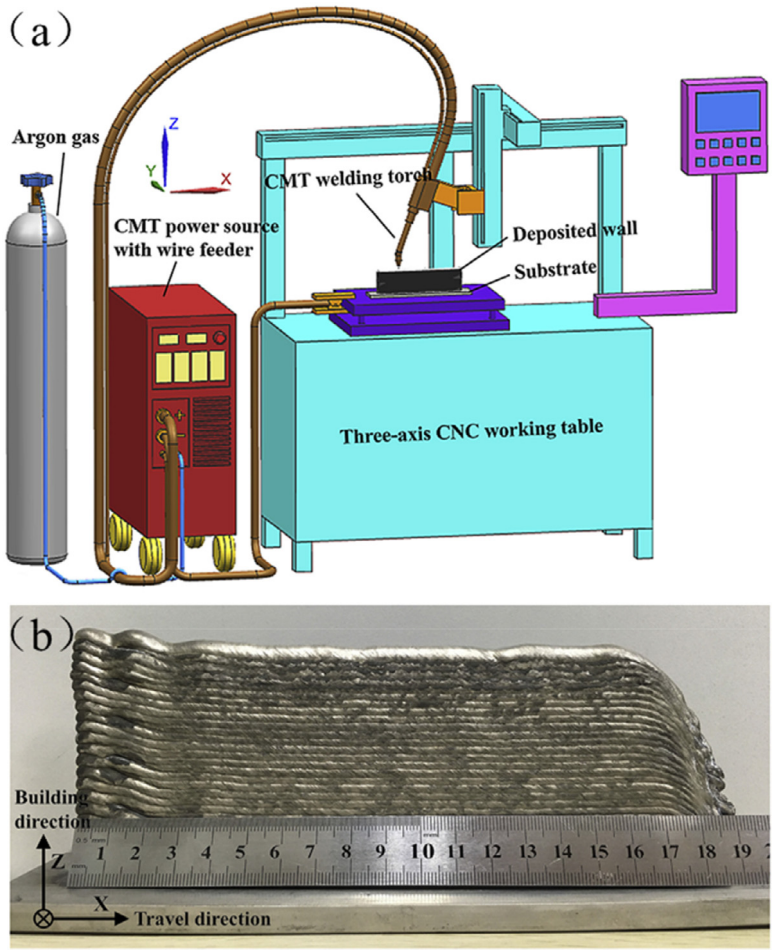

Fig. 31. (a) The schematic diagram of the experimental setup developed for WAAM-CMT; (b) the external view of the AZ31 thin wall deposited by WAAM-CMT method [204].

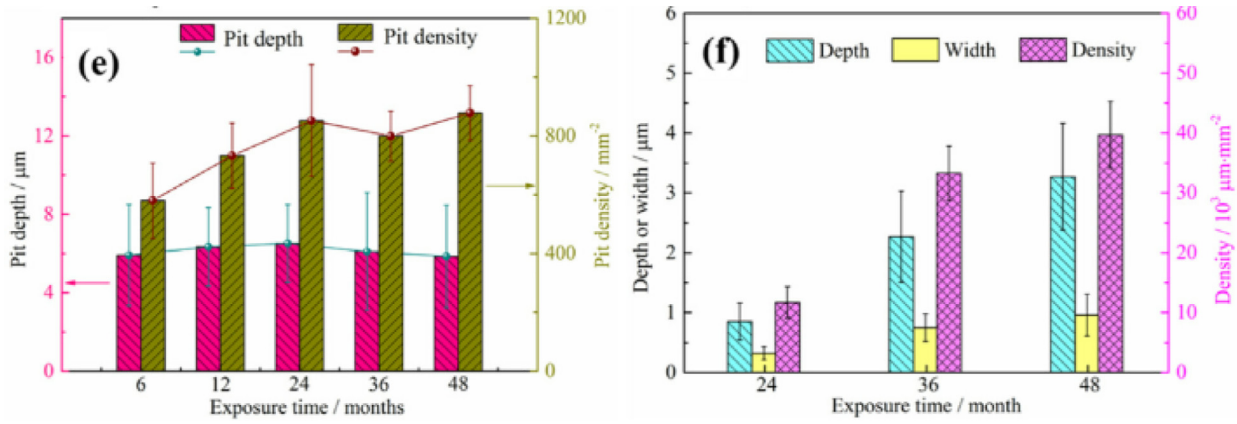

Fig. 32. The size and distribution of the pits and trenches [206].

7.1.2. Corrosion mechanism of Mg alloys

Corrosion is the result of the interaction of materials and media. The microstructure of the matrix has a significant influence on the corrosion resistance of magnesium alloys, such as grain size, second phase and impurities, etc. Kwang Seon Shin et al. [209] studied the influence of grain size on the corrosion rate of magnesium alloys and developed a new model for predicting the corrosion rate based on microstructure parameters. They concluded that in the case of single grains like single crystals or bi-crystals, corrosion rate increases with increasing grain size, while for very fine grains (less than 50 μm) corrosion rate with decreasing grain size, as shown in

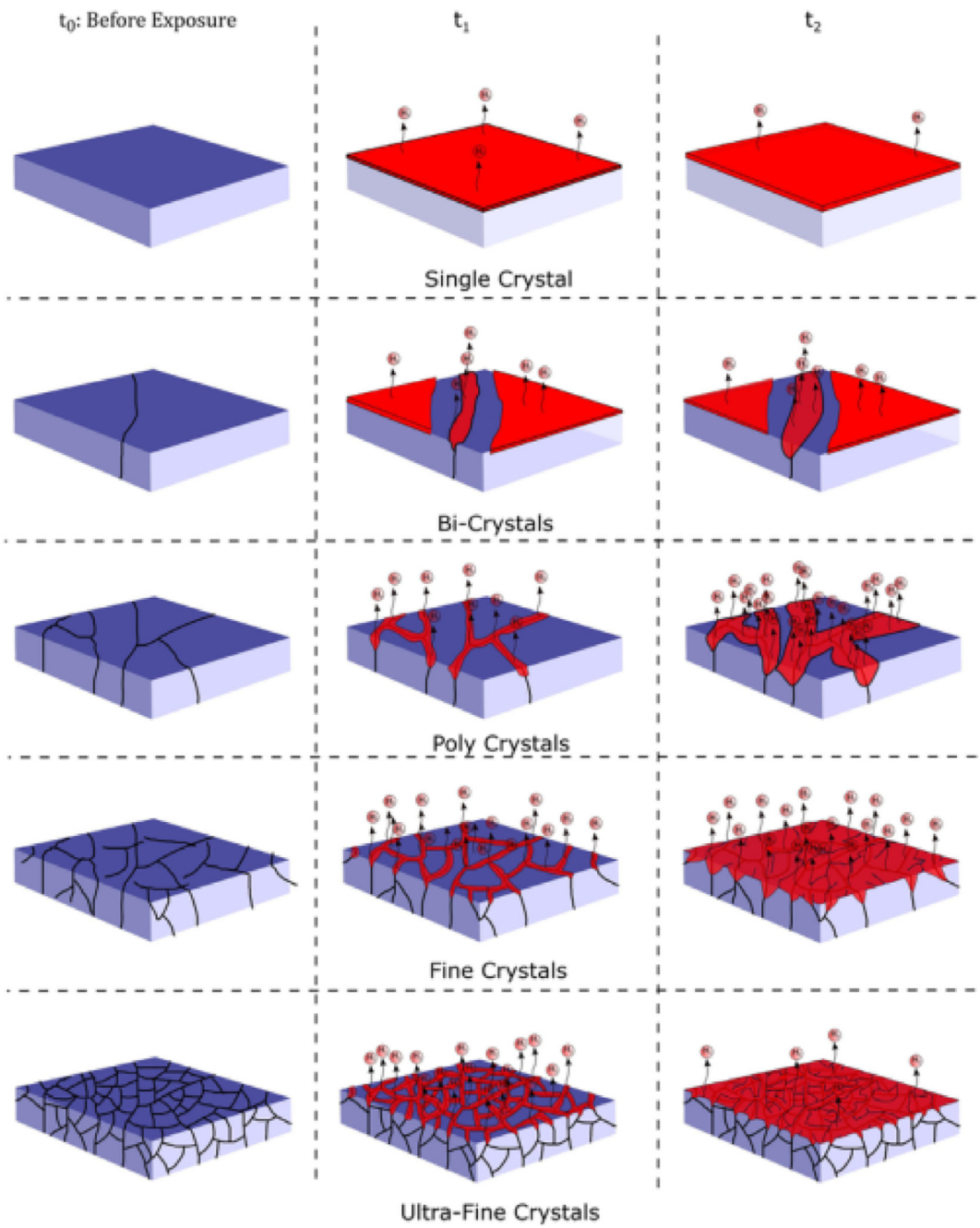

Fig. 33. Schematic representation of the effect of grain size refinement on the corrosion propagation [209].

Fig. 33. The alloys with an ultrafine particle size have a lower corrosion rate. Xianhua Chen et al. [210] studied the influence of Fe content (10 ppm - 150 ppm) on the corrosion resistance of AZ61 and found that more micro-galvanic cells are formed among the impurity particles, second-phase particles and the matrix with increasing Fe content. When Fe content drops from 150 ppm to 10 ppm, the corresponding corrosion rates in the as-cast and solution treatment conditions are reduced from 8.54 mm/a and 8.61 mm/a to 2.54 mm/a and 0.21 mm/a, respectively.

The latest research progress on the corrosion mechanism of Mg-Li alloy has been made. P. Volovitch et al. [208] studied the corrosion behavior of Mg-Li(-Al-Y-Zr)-alloy in aqueous solution and proposed a new corrosion mechanism, as shown in Fig. 34. It can be divided into 5 steps: 1) adsorption of aggressive anions; 2) surface hydroxylation; 3) oxide dissolution; 4) electron trapped by cathodic catalysis and 5) charge compensation via doping by Li^+. In recent years, there has been a lot of research on the corrosion behavior of magnesium alloys in biological environments.

7.1.3. Bio corrosion behavior of Mg alloys

Mg and its alloys have become the research hotspot of a new generation of biomedical biodegradable metal implant materials due to their excellent mechanical compatibility, biocompatibility and degradability. A. S. Gnedenkov et al.

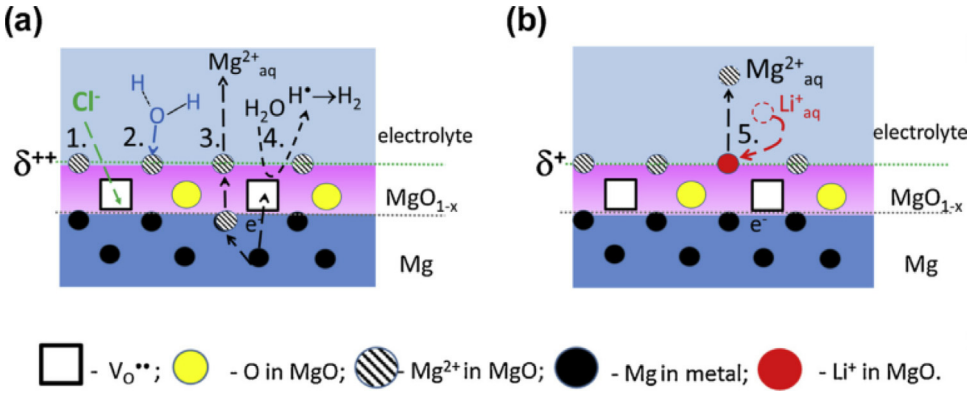

Fig. 34. Schematic representation of (a) common and (b) specific for Li-doped charge compensation mechanisms in Mg_1O_{1-X} (δ^+ and δ^{++} indicate the positive surface charge, assuming higher charge for δ^{++}) [208].

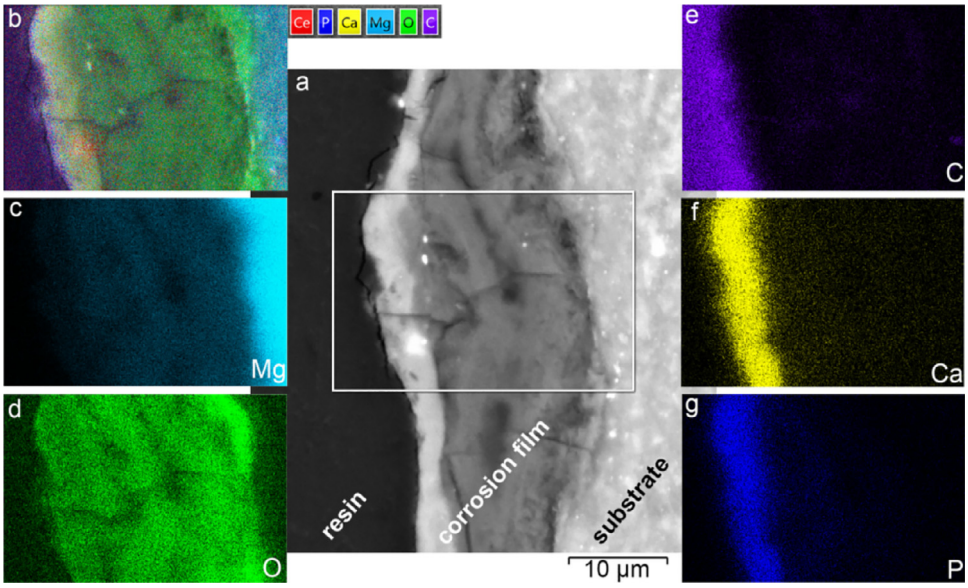

Fig. 35. SEM-EDX maps of the cross-section of the MA8 Mg alloy sample after 30 days of immersion in MEM: SEM (a) and SEM-EDX (b) images of the corrosion film as well as corresponding EDX maps of the element distribution Mg (c), O (d), C (e), Ca (f), P (g) [211].

[211] studied the corrosion resistance of the MA8 Mg alloy in mammalian cell culture medium (MEM) and 0.83 wt.% NaCl solution, and proposed a model of corrosion mechanism for MA8 Mg alloy in the MEM. The corrosion current density after exposure in MEM for 1 h was two times lower than that for exposing to NaCl solution due to Ca and P rich deposits formed in the corrosion layer on the Mg alloy surface in MEM, as shown in Fig 35.

Jinghua Jiang et al. [212] investigated the effect of different phase constitutions of LPSO structures on the corrosion rate of bio-medical Mg-Y-Zn alloys. The as-cast $Mg_{98.5}Y_1Zn_{0.5}$ alloys containing only 18R structures exhibited the highest corrosion resistance with a corrosion rate of 2.78 mm/y. The Mg-Y-Zn alloys with a single LPSO structure (either 18R or 14H) exhibited better corrosion resistance. Lu Li et al. [213] developed a new Mg-5.8Zn-0.5Zr-2Yb alloy with good mechanical and bio-corrosive properties in simulated body fluids (SBF). The corrosion rate of ZYbK620 alloys in T4 and T6 states after immersion in SBF at 37 °C for 10 days are 1.49 and 2.27 mm/y, respectively. However, under the simultaneous action of the human body corrosive environment and mechanical load, magnesium alloy is prone to corrosion fatigue and stress corrosion cracking. Shaokang Guan et al. [214] investigated the fatigue behavior of the extruded Mg-Zn-Y-Nd alloy in air and in simulated body fluid (SBF) and found that the samples under low-stress amplitude have a longer fatigue life in SBF. Nevertheless, in order to prolong the implant integrity, the application of protective biocompatible coatings is desirable. This is one of the future studies for biomedical magnesium alloys.

7.2. Corrosion resistance improvement of Mg alloys

7.2.1. High-efficiency corrosion inhibitors of Mg alloys

The addition of high-efficiency corrosion inhibitors can significantly inhibit the corrosion of magnesium alloys. Xiaopeng Lu et al. [215] studied the corrosion behavior of AZ91 in 3.5 wt.% NaCl solution. By adding sodium dodecyl sulfate (SDS) to the solution, the active Mg surface is covered by a hydrophobic outer corrosion layer and a passive inner ox-

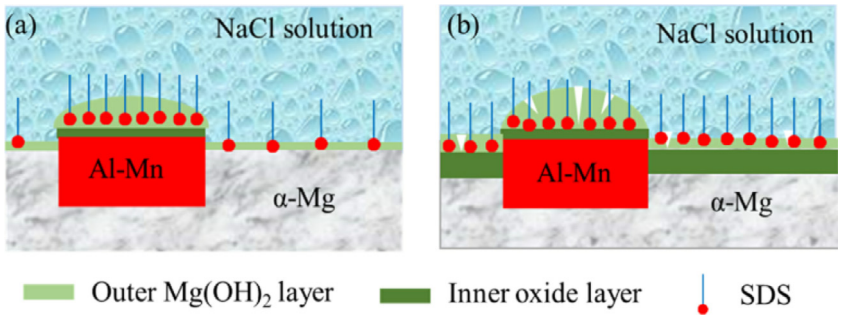

Fig. 36. Schematic illustration of the inhibition mechanism of SDS: (a) initial stage and (b) later stage of the corrosion of Mg in SDS containing NaCl solution [215].

ide layer, which suppresses the cathodic hydrogen evolution and anodic dissolution of the substrate, as shown in Fig. 36. The electrochemical reaction kinetics is inhibited due to the adsorption of SDS in the corrosion products, while the oxidation reaction of the substrate is facilitated by the hydrophobic outer corrosion layer.

7.2.2. Improvement of corrosion resistance by microalloying

Magnesium (Mg) has relatively poor corrosion resistance due to the negative electrode potential (−2.363 V) and loose corrosion products film ($Mg(OH)_2$). Alloying is a valid method to improve the corrosion resistance of Mg alloys.

The effect of micro-alloyed Ca (0.05, 0.1 and 0.2 wt.%) on the microstructure and corrosion properties of extruded AZ31 alloy was investigated by Liang Wu et al. [216]. AZ31–0.05Ca alloy contains a small number of Mg-Al-Ca phase particles, which may lead to severe micro-galvanic corrosion and a higher corrosion rate than that of AZ31 alloy. But AZ31–0.1Ca and AZ31–0.2Ca possessed many dispersed fine Al_2Ca particles, which could be beneficial to form a more protective film. Thus, the addition of 0.1 and 0.2 wt.% Ca was beneficial to improve the corrosion resistance of AZ31 alloy.

Further, Liang Wu et al. [217] also investigate the effect of Sc element (0.1∼1.5 wt.%) on the microstructure and corrosion behavior of pure Mg. The Mg-Sc binary alloys had a single-phase microstructure for Sc concentrations between 0.1∼0.3 wt.%. As shown in Fig. 37, the Sc additions improved the corrosion resistance of pure Mg due to the refinement of microstructure and the formation of a more protective corrosion product film. Mg-0.3Sc showed the lowest corrosion rate, and hydrogen evolution rate and weight loss rate of 1.52 mm y^{-1} and 2.17 mm y^{-1}, respectively. The corrosion rate of the pure Mg was 3 times higher than that of Mg-0.3Sc. Mg-0.3Sc alloy is expected to be one kind of high corrosion resistance magnesium alloy in the future.

Cheng Zhang and Liang Wu et al. studied the effect of Al on the microstructure, corrosion behavior and mechanical properties of Mg-4Li alloy [218]. The addition of Al resulted in the precipitation of some Mg-Al phase and Al_3Li phase particles. The addition of 3 wt.% Al increased the tensile strength by solid solution strengthening, precipitation strengthening, grain refinement strengthening and texture strengthening. However, Mg-4Li-3Al showed a higher corrosion rate than that of Mg-4Li due to the precipitate particles in Mg-4Li-3Al causing microgalvanic corrosion and the change of grain orientation. Huseyin Zengin et al. [219] studied the effect of Y on the corrosion resistance of the magnesium alloy. The results showed that Y addition up to 1 wt.% improved the corrosion resistance of the alloy due to the formation of finer grains, fine and uniform distribution of second phase particles and more stable oxide film. Liangyu Wei and Jingyuan Li et al. [18] analyzed the microstructure and degradation behavior of Mg-xZn-0.1Mn-0.2Ca alloys, and found that the corrosion resistance first increased and then decreased with increasing zinc content. The Mg-xZn-0.1Mn-0.2Ca alloys with 0.2 and 2 wt.% Zn additions were more likely to generate the localized corrosion. The Mg-1Zn-0.1Mn-0.2Ca alloy exhibited a relatively uniform surface morphology due to the protection of the Mg_2Ca phase distributed in the Mg matrix, and has the best corrosion resistance with a corrosion rate of 6.09 mm/y.

7.2.3. Surface treatment for Mg alloys

Surface modification is an effective way to improve the corrosion resistance of magnesium alloys. Kemin Zhang et al. [220] used a high-current pulsed electron beam (HCPEB) to process as-cast WE43 Mg alloy, and its surface presented a concave and wavy morphology, which greatly improved the corrosion resistance in vitro. Compared with this traditional method, chemical methods have gradually become a research hotspot [208]. Shaojun Yuan et al. [221] and F. Zhang et al. [222] used stearic acid (SA) and 1-dodecanethiol (DT) to modify AZ31 magnesium alloy respectively, the superhydrophobic structure (as shown in Fig. 38) greatly improved the corrosion resistance of the matrix. Besides, the superhydrophobic coating composed of the mixture of magnesium compounds and zinc substance was also a simple method [223]. Wenhua Yao et al. fabricated a nanocomposite coating composed of polyvinylidene fluoride and chemically modified SiO_2 nanoparticles via a spraying method on the Mg alloy. The final coating presented an excellent superhydrophobic (CA=151.8°) and good corrosion resistance (i_{corr}=23.1 μA cm^{-2}) [224].

Also, many scholars have studied the use of conversion coating to improve its corrosion protection, such as Ce/Mn conversion coating [225], LDH coating [226]. As shown in Fig. 39, Zhihui Xie et al. developed novel composite coatings consisting of underlying MgAl-LDH layer and outer films of

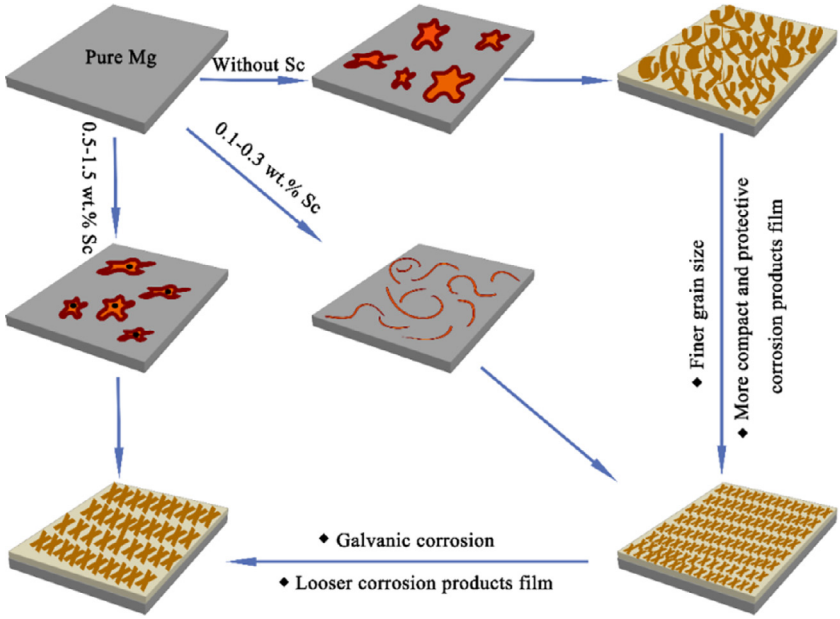

Fig. 37. Schematic diagram of corrosion mechanism of the Mg-xSc ($x = 0$, 0.1, 0.3, 0.5, 1.0 and 1.5 wt.%) alloys after immersion in the NaCl solution [217].

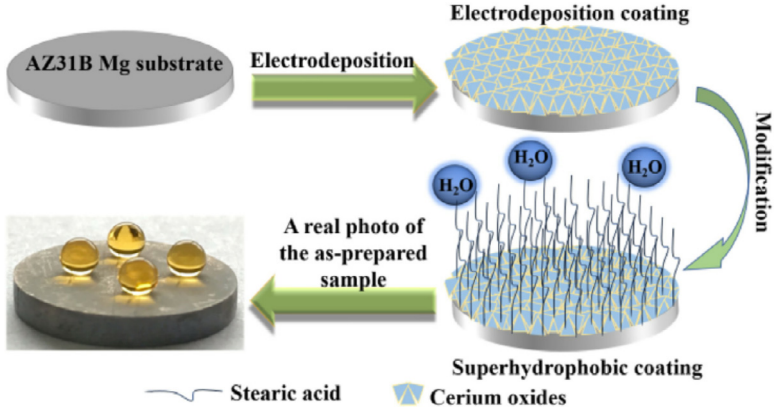

Fig. 38. A schematic diagram of the preparation process of the superhydrophobic coating formed on the AZ31B Mg substrate [221].

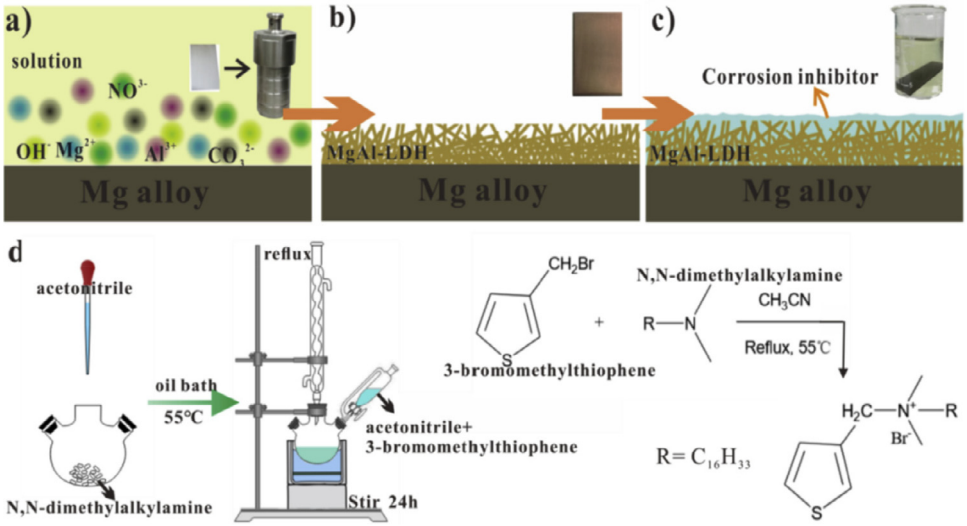

Fig. 39. The schematic diagrams of the (a, b, and c) in-situ growth of MgAl-LDH film and the preparation of CIs@MgAl-LDH coatings on Mg alloy and (d) synthesis of NTA inhibitor [227].

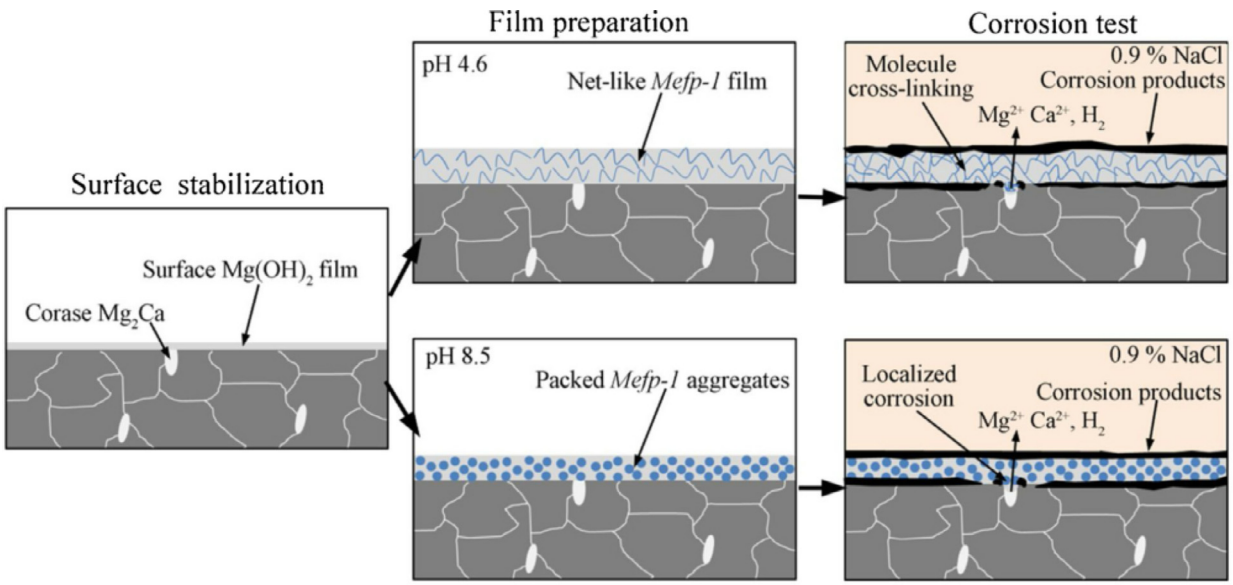

Fig. 40. Schematic illustration for the protein film formation and its inhibition for the corrosion of Mg-1.0Ca alloy [239].

different corrosion inhibitors (CIs) by a hydrothermal method. The results provided new insights into the interactions of NTA with MgAl-LDH depositions and Mg alloy substrate and can serve as guidelines in designing thiophene contained CIs for the modification of MgAl-LDH primer and thus achieve superior corrosion protection [227].

Yuxin Zhang et al. prepared some anti-corrosion coatings via the in-situ growth of different kinds of corrosion inhibitors intercalated MgAl-LDHs. The replacement of MoO_4^{2-} further improves the corrosion resistance of Mg-Al LDH/LA. The results show that the synergistic effect of molybdate and lauric acid leads to a better corrosion resistance performance [228].

The porous layer produced by PEO on the surface of magnesium alloys was loaded with Ta_2O_5 [229], inhibitors (sodium salts of glycolic, 4-aminosalicylic and 2,6-pyridinedicarboxylic acids) [230], graphene oxide [231], Nd sulfate salt [232], Ce [233], further improving its corrosion resistance. Junlei Tang et al. [234] fabricated SiC_p/Al 5056 composite coatings on a magnesium substrate using cold spraying, and loaded SiC particles to modify it. The addition of SiC particles increases the galvanic potential and decreases the galvanic reduction current of the coating/substrate couple. Therefore, the combination of composite coating technology, corrosion inhibition technology, nanotechnology and other methods is the general trend [235-238].

The uncontrolled degradation of magnesium alloys limits its application in clinical medicine and surface treatment is an effective way to improve the corrosion resistance and biocompatibility of biomedical magnesium alloys. Changjian Lin et al. [239] studied the formation and properties of the pre-formed Mefp-1 film on Mg-1.0Ca (wt.%) alloy at different pH values. They found that the Mefp-1 film pre-formed at pH 4.6 shows a network-like structure, whereas it is more packed at pH 8.5, as shown in Fig. 40. The Mefp-1 films formed at both pH values can effectively inhibit the localized corrosion of Mg-1.0Ca alloy. Moreover, the film pre-formed at pH 4.6 provides an increasing corrosion inhibition to Mg-1.0Ca alloy during 7 days of exposure.

Deepa B. Prabhu et al. [96] prepared a protective layer of $MgCO_3 \cdot 3H_2O$ on the surface of Mg-4Zn alloy via chemical conversion coating by treatment with saturated $NaHCO_3$ as a simple room temperature procedure. The combined effects of slow first hydrogen evolution rate and precipitation of phosphates, and similarities to the carbonate coating developed in vivo, makes the films a suitable choice for Mg alloys for temporary bio implant applications.

8. International standards on magnesium

In early 2020, five ISO standards on magnesium were successfully registered as new projects. All of the five standards proposed by China were still under development and have been proceeded to WD (working draft) and CD (committee draft) stage, as listed in Table 12. ISO/CD 4155, ISO/WD 4177, ISO/CD 4181, ISO/CD 4188 and ISO/CD 4189 were proposed to measure the content of nickel, chromium, strontium, arsenic, and sodium with inductively coupled plasma atomic emission spectrometry, respectively.

In addition, ISO/CD 8287 (Magnesium and magnesium alloys — Unalloyed magnesium — Chemical composition) has been promoted to ISO/DIS 8287, ISO/WD 23694 (Wrought Magnesium and Magnesium alloys – Extruded Rods, Bars and Tubes) and ISO/WD 23700 (Wrought Magnesium and Magnesium alloys – Rolled Plates and Sheets) have been promoted to ISO/FDIS (final draft of International Standard) 23694 and ISO/FDIS 23700, respectively. It is anticipated that the establishment of these important international standards will pave the way for the further development and applications of magnesium and magnesium alloys in a variety of industrial sectors.

Table 12
Newly registered ISO standards on magnesium and magnesium alloys in 2020.

No.	Standard No.	Name	New Project approved at
1	ISO/CD 4155	Magnesium and magnesium alloys—Determination of nickel— inductively couple plasma atomic emission spectrometry	2020–02–21
2	ISO/WD 4177	Magnesium and magnesium alloys—Determination of chromium— inductively couple plasma atomic emission spectrometry	2020–02–21
3	ISO/CD 4181	Magnesium and magnesium alloys—Determination of Strontium— inductively couple plasma atomic emission spectrometry	2020–02–21
4	ISO/CD 4188	Magnesium and magnesium alloys—Determination of Arsenic— inductively couple plasma atomic emission spectrometry	2020–02–21
5	ISO/CD 4189	Magnesium and magnesium alloys—Determination of sodium— inductively couple plasma atomic emission spectrometry	2020–02–21

Note: CD-Committee draft, WD-Working draft

9. Summary and outlook

Research on magnesium alloys has continuously received considerable attention, with over 3000 papers on magnesium and magnesium alloys published and indexed in SCI in the past year alone. Based on the bibliometric analysis, the control of microstructures of Mg alloys in relation to their mechanical properties based on the development of new alloys and advanced processing technology is still a main research focus, and the corrosion and protection of Mg alloys are still widely concerned. The emerging research hot spots involve mainly functional magnesium materials, such as Mg ion batteries, hydrogen storage Mg materials, and bio-magnesium alloys.

With further development on the control of microstructures of Mg alloys by new alloy design and advanced processing, some remarkable results on the mechanical properties of magnesium alloys were achieved in 2020. For high-strength magnesium alloys, the ultimate tensile strength and yield strength of Mg-8Gd-3Y-0.4Zr alloy via rotary swaging and aging have exceeded 710 MPa and 650 MPa, respectively. The development of RE-free or low-RE high-strength magnesium alloys is more prominent, such as the extruded Mg-1.0Ca-1.0Al-0.2Zn-0.1Mn alloy exhibits an ultimate tensile strength of 425 MPa and an elongation to failure of 11%. High plasticity wrought Mg alloys with an elongation of above 50% were developed in 2020. The elongation of an extruded Mg-0.4Al-1.5Mn is 52.5%, while the elongation of a cold-rolled LZ91 alloy after annealing at 125 °C reaches 56.1%. For high-modulus and high-strength Mg alloys, Mg-Gd-Ag-Mn-Ge alloy with Young's modulus, UTS, and elongation of 51 GPa, 423 MPa and 10%, respectively, were developed.

Functional magnesium materials are becoming an emerging focus and being anticipated to grow significantly in new magnesium materials. A lot of studies on functional magnesium materials were carried out in 2020, including Mg batteries, and hydrogen storage Mg materials, bio-Mg materials, high modulus and high damping Mg alloys, and dissoluble magnesium alloys, etc. In the aspect of Mg batteries, a significant contribution to rechargeable magnesium batteries (RMBs) is achieved by introducing heterogeneous enolization chemistry to overcome the dissociation and diffusion difficulties of electrolyte ions at the electrochemical interface, finally enabling fast and reversible redox processes. By coupling with weakly coordinating boron cluster-based electrolyte, an Mg battery with a specific power of up to 30.4 kW kg^{-1} and a life-span of 200 cycles can be constructed. A new Mg-1.3Y-0.8Zn-6.4Al-16.7Li alloy with a high Young's modulus of 52.9 GPa and superior damping capacity is developed. A dissoluble $Mg_{97.5}Ni_1Y_{1.5}$ alloys with optimal comprehensive properties, an average corrosion rate of up to 6675 mm/y at 366 K (93 °C) and an ultimate compressive strength (UCS) of 410 MPa was developed in the past year.

The preparation and processing technologies for magnesium alloys were further improved last year. Cast technology for large-scale ingots of high-strength Mg alloys and large-size profile extrusion technology were developed. Some of the new preparation and processing technologies show important prospects, such as rotary swaging extrusion, low temperature extrusion, bimetal casting-co-extrusion process and online heating rolling, etc. The high-quality and large-scale Mg-Gd-Y-Zn-Mn alloy ingots were prepared through semi-continuous casting. The large-size high-strength and tough Mg-9Gd-4Y-1Zn-0.8Mn alloy support beam profile used in rail transport with good surface quality, uniform composition and homogeneous microstructure, and outstanding mechanical properties with an UTS of over 470 MPa, an El of over 10% was successfully extruded. The widest thin-walled hollow magnesium alloy profile with a cross-section of 502 mm × 60 mm in the world has been successfully prepared as well.

Although the research and development on magnesium alloys have been widely conducted, a lot of problems still need to be solved. For the load-bearing structural Mg alloys, the comprehensive properties of magnesium alloys need to be further improved so as to replace more and more steel or aluminum alloys. For example, the ultimate tensile strength and plasticity of ultra-high strength cast magnesium alloys should be increased to more than 400 MPa, 7–10%, respectively. The ultimate tensile strength and the plasticity of ultra-high strength wrought magnesium alloys should be increased to more than 600 MPa and 7–10%, respectively. The elastic modulus of high elastic modulus magnesium alloys should be enhanced to the level close to that of aluminum alloys. The corrosion resistance of high corrosion-resistant magne-

sium alloys should be improved to meet the application requirements on most occasions. The processing technology for the large-scale Mg parts, the welding and joining technology, the additive manufacturing and the characterization of fatigue properties in Mg alloy parts are also needed to be further developed to meet the demand of wider applications.

Close attention needs to be paid to functional Mg materials such as Mg batteries, hydrogen storage Mg materials, structural-functional materials and bio-magnesium materials. For example, the uncontrolled degradation of magnesium alloys limits its applications in clinical medicine. The surface treatment as an effective method to improve the corrosion resistance and biocompatibility of biomedical magnesium alloys needs to be further developed to achieve the control of degradation of Mg alloys and accelerate the development of Mg implant materials. For Mg battery materials, the most important and urgent tasks for the future development of rechargeable magnesium batteries are to develop suitable electrolytes with characters of wider electrochemical window, higher ionic conductivity, passivation free property and chemical safety, and to uncover the interfacial kinetics between electrode and electrolytes, which can further guide the design of cathode and anode materials as well as electrolyte selection.

Acknowledgments

The authors would like to thank the experts worldwide (including Dr. Chaohe Xu and Dr. Liying Qiao, etc.) who have contributed to this review by providing important information and commenting on the preparation. The review is financially supported by the National Key Research and Development Program of China (Project No. 2016YFB0301100 & Project No. 2016YFB0700403), the Chongqing Academician Special Fund (Project No. cstc2018jcyj-yszxX0007 & Project No. cstc2020yszx-jcyjX0001), Chongqing Research Program of Basic Research and Frontier Technology (Project No. cstc2019jcyj-msxm0438), the 111 Project (Project No. B16007) by the Ministry of Education and the State Administration of Foreign Experts Affairs of China.

References

[1] T. Xu, Y. Yang, X. Peng, J. Song, F. Pan, Overview of advancement and development trend on magnesium alloy, Journal of Magnesium and Alloys 7 (3) (2019) 536–544.

[2] M. Yeganeh, N. Mohammadi, Superhydrophobic surface of Mg alloys: A review, Journal of Magnesium and Alloys 6 (1) (2018) 59–70.

[3] K. Luo, L. Zhang, G. Wu, W. Liu, W. Ding, Effect of Y and Gd content on the microstructure and mechanical properties of Mg–Y–RE alloys, Journal of Magnesium and Alloys 7 (2) (2019) 345–354.

[4] Y. Ali, D. Qiu, B. Jiang, F. Pan, M. Zhang, Current research progress in grain refinement of cast magnesium alloys: A review article, J Alloy Compd 619 (2015) 639–651.

[5] J. Song, J. She, D. Chen, F. Pan, Latest research advances on magnesium and magnesium alloys worldwide, Journal of Magnesium and Alloys 8 (1) (2020) 1–41.

[6] B. Zhou, W. Liu, G. Wu, L. Zhang, X. Zhang, H. Ji, W. Ding, Microstructure and mechanical properties of sand-cast Mg-6Gd-3Y-0.5Zr alloy subject to thermal cycling treatment, J Mater Sci Technol 43 (2020) 208–219.

[7] L. Zhang, Y. Zhang, J. Zhang, R. Zhao, J. Zhang, C. Xu, Effect of Alloyed Mo on Mechanical Properties, Biocorrosion and Cytocompatibility of As-Cast Mg–Zn–Y–Mn Alloys, Acta Metallurgica Sinica (English Letters) 33 (4) (2020) 500–513.

[8] S. Lv, X. Lü, F. Meng, Q. Yang, X. Qiu, P. Qin, Q. Duan, J. Meng, Microstructures and mechanical properties in a Gd-modified high-pressure die casting Mg–4Al–3La−0.3Mn alloy, Materials Science and Engineering: A 773 (2020) 138725.

[9] T. Le, Q. Wei, J. Wang, P. Jin, M. Chen, J. Ma, Effect of different casting techniques on the microstructure and mechanical properties of AE44-2 magnesium alloy, Mater Res Express 7 (11) (2020).

[10] H. Xie, Z. Liu, X. Liu, F. Liu, Y. Shi, X. Wu, J. Li, Microstructure, generation of intermetallic compounds and mechanical strengthening mechanism of as-cast Mg–4Y–xZn alloys, Materials Science and Engineering: A 797 (2020) 139948.

[11] J. Lyu, J. Kim, H. Liao, J. She, J. Song, J. Peng, F. Pan, B. Jiang, Effect of substitution of Zn with Ni on microstructure evolution and mechanical properties of LPSO dominant Mg–Y–Zn alloys, Materials Science and Engineering: A 773 (2020) 138735.

[12] R. Zhao, W. Zhu, J. Zhang, L. Zhang, J. Zhang, C. Xu, Influence of Ni and Bi microalloying on microstructure and mechanical properties of as-cast low RE LPSO-containing Mg–Zn–Y–Mn alloy, Materials Science and Engineering: A 788 (2020) 139594.

[13] J. Liu, K. Zhang, J. Han, X. Li, Y. Li, M. Ma, J. Yuan, M. Li, Homogenization heat treatment of Mg–7.0 wt%Y–1.0 wt%Nd–0.5 wt%Zr alloy, Rare Met. 39 (10) (2020) 1196–1201.

[14] Y. Liu, J. Wen, J. He, H. Li, Enhanced mechanical properties and corrosion resistance of biodegradable Mg–Zn–Zr–Gd alloy by Y microalloying, J Mater Sci 55 (4) (2020) 1813–1825.

[15] H. Zengin, Y. Turen, H. Ahlatci, Y. Sun, Microstructure, mechanical properties and corrosion resistance of as-cast and as-extruded Mg–4Zn–1La magnesium alloy, Rare Met. 39 (8) (2020) 909–917.

[16] K. Wang, J. Wang, X. Dou, Y. Huang, N. Hort, S. Gavras, S. Liu, Y. Cai, J. Wang, F. Pan, Microstructure and mechanical properties of large-scale Mg-Gd-Y-Zn-Mn alloys prepared through semi-continuous casting, J Mater Sci Technol 52 (2020) 72–82.

[17] N. Mo, I. McCarroll, Q. Tan, A. Ceguerra, J. Cairney, H. Dieringa, Y. Huang, B. Jiang, F. Pan, M. Bermingham, M. Zhang, Roles of Nd and Mn in a new creep-resistant magnesium alloy, Materials Science and Engineering: A 779 (2020) 139152.

[18] L. Wei, J. Li, Y. Zhang, H. Lai, Effects of Zn content on microstructure, mechanical and degradation behaviors of Mg-xZn-0.2Ca-0.1Mn alloys, Mater Chem Phys 241 (2020) 122441.

[19] T. Sakai, T. Nakata, T. Miyamoto, S. Kamado, J. Liao, Tensile creep behavior of a die-cast Mg–6Al-0.2Mn–2Ca-0.3Si (wt.%) alloy, Materials Science and Engineering: A 774 (2020) 138841.

[20] T. Rzychoń, The microstructure and creep properties of as-cast Mg-Sn-Si-(Al) magnesium alloys, Arch Civ Mech Eng 20 (3) (2020).

[21] K. GUO, C. XU, X. LIN, J. YE, C. ZHANG, D. HUANG, Microstructure and strengthening mechanism of Mg—5.88Zn—0.53Cu—0.16Zr alloy solidified under high pressure, T Nonferr Metal Soc 30 (1) (2020) 99–109.

[22] S. Lv, X. Lu, Y. Li, F. Meng, X. Hua, Q. Yang, X. Qiu, J. Meng, Q. Duan, Crystallographic orientation relationships between the aggregated intermetallic phases in a casting Mg-Ag-Al alloy, Mater Design 190 (2020) 108561.

[23] Q. Yang, S. Lv, P. Qin, F. Meng, X. Qiu, X. Hua, K. Guan, W. Sun, X. Liu, J. Meng, Interphase boundary segregation induced phase transformation in a high-pressure die casting Mg-Al-La-Ca-Mn alloy, Mater Design 190 (2020) 108566.

[24] K. Takagi, M. Yamasaki, Y. Mine, K. Takashima, Temperature dependence of prismatic slip in a single-crystalline long-period stacking ordered Mg–Zn–Y alloy, Scripta Mater 178 (2020) 498–502.

[25] J. Cui, T. Luo, C. Wang, Y. Li, X. Feng, Q. Huang, Y. Yang, Evolution of the Microstructure and Microsegregation in Subrapidly Solidified Mg-6Al-4Zn-1.2Sn Magnesium Alloy, Adv Eng Mater (2020).

[26] Y. Wang, S. Jia, M. Wei, L. Peng, Y. Wu, Y. Ji, L. Chen, X. Liu, Coupling in situ synchrotron X-ray radiography and phase-field simulation

to study the effect of low cooling rates on dendrite morphology during directional solidification in Mg–Gd alloys, J Alloy Compd 815 (2020) 152385.
[27] Y. Zhang, J. Zheng, Y. Xia, H. Shou, W. Tan, W. Han, Q. Liu, Porosity quantification for ductility prediction in high pressure die casting AM60 alloy using 3D X-ray tomography, Materials Science and Engineering: A 772 (2020) 138781.
[28] B. Xu, J. Sun, Z. Yang, L. Xiao, H. Zhou, J. Han, H. Liu, Y. Wu, Y. Yuan, X. Zhuo, D. Song, J. Jiang, A. Ma, Microstructure and anisotropic mechanical behavior of the high-strength and ductility AZ91 Mg alloy processed by hot extrusion and multi-pass RD-ECAP, Materials Science and Engineering: A 780 (2020) 139191.
[29] Y. Wang, F. Li, Y. Wang, X. Li, W. Fang, Effect of extrusion ratio on the microstructure and texture evolution of AZ31 magnesium alloy by the staggered extrusion (SE), Journal of Magnesium and Alloys 8 (4) (2020) 1304–1313.
[30] D. Zhao, X. Chen, X. Wang, F. Pan, Effect of impurity reduction on dynamic recrystallization, texture evolution and mechanical anisotropy of rolled AZ31 alloy, Materials Science and Engineering: A 773 (2020) 138741.
[31] J. Peng, Z. Zhang, J. Huang, P. Guo, W. Zhou, Y. Wu, The effect of grain size on texture evolution and mechanical properties of an AZ31 magnesium alloy during cold-rolling process, J Alloy Compd 817 (2020) 153302.
[32] H. Su, Z. Chu, C. Xue, Y. Li, L. Ma, Relationship among Initial Texture, Deformation Mechanism, Mechanical Properties, and Texture Evolution during Uniaxial Compression of AZ31 Magnesium Alloy, Crystals 10 (9) (2020) 738.
[33] K.J. Tam, M.W. Vaughan, L. Shen, M. Knezevic, I. Karaman, G. Proust, Modelling the temperature and texture effects on the deformation mechanisms of magnesium alloy AZ31, Int J Mech Sci 182 (2020) 105727.
[34] Y. Chen, L. Hu, L. Shi, T. Zhou, J. Tu, Q. Chen, M. Yang, Effect of texture types on microstructure evolution and mechanical properties of AZ31 magnesium alloy undergoing uniaxial tension deformation at room temperature, Materials Science and Engineering: A 769 (2020) 138497.
[35] H. Su, Z. Chu, C. Xue, Y. Li, L. Ma, Effect of initial texture on the {10–12} twinning variants selection mechanism in AZ31 magnesium alloy, Mater Res Express 7 (8) (2020) 86503.
[36] F. Zhang, Z. Liu, Y. Wang, P. Mao, X. Kuang, Z. Zhang, Y. Ju, X. Xu, The modified temperature term on Johnson-Cook constitutive model of AZ31 magnesium alloy with {0002} texture, Journal of Magnesium and Alloys 8 (1) (2020) 172–183.
[37] Y. Wang, F. Li, X.W. Li, W.B. Fang, Unusual texture formation and mechanical property in AZ31 magnesium alloy sheets processed by CVCDE, J Mater Process Tech 275 (2020) 116360.
[38] L. Shi, L. Liu, L. Hu, T. Zhou, M. Yang, Y. Lian, J. Zhang, Effect of Final Rolling Temperature on Microstructures and Mechanical Properties of AZ31 Alloy Sheets Prepared by Equal Channel Angular Rolling and Continuous Bending, Materials 13 (15) (2020) 3346.
[39] D. Xia, J. Zhang, X. Chen, G. Huang, B. Jiang, A. Tang, S. Gavras, Y. Huang, N. Hort, F. Pan, Effect of biaxial compressive stress state on the microstructure evolution and deformation compatibility of rolled sheet Mg alloy AZ31 at room temperature, Materials Science and Engineering: A 789 (2020) 139599.
[40] Q. Yang, B. Jiang, B. Song, D. Yu, S. Chai, J. Zhang, F. Pan, Mechanical behavior and microstructure evolution for extruded AZ31 sheet under side direction strain, Progress in Natural Science: Materials International 30 (2) (2020) 270–277.
[41] C. Paramatmuni, F.P.E. Dunne, Effect of twin crystallographic orientation on deformation and growth in Mg alloy AZ31, Int J Plasticity 135 (2020) 102775.
[42] X. Wang, P. Mao, R. Wang, Z. Liu, Z. Wang, F. Wang, L. Zhou, Z. Wei, Role of{101¯2} twinning in the anisotropy and asymmetry of AZ31 magnesium alloy under high strain rate deformation, Materials Science and Engineering: A 772 (2020) 138814.
[43] H. Son, S. Hyun, Periodic formations of deformation twins and dislocation arrays via grain boundary sliding at serrated grain boundary in cold-shear-strained AZ31 alloy, Int J Plasticity 135 (2020) 102815.
[44] K. Zhang, Z. Shao, J. Jiang, Effects of twin-twin interactions and deformation bands on the nucleation of recrystallization in AZ31 magnesium alloy, Mater Design 194 (2020) 108936.
[45] H. Wu, T. Yan, L. Wang, X. Li, Y. Wei, S. Li, X. Wang, R. Wu, Effect of Yb addition on the microstructure and mechanical properties of ZK60 alloy during extrusion, Materials Science and Engineering: A 777 (2020) 139033.
[46] T. Zhang, H. Cui, X. Cui, H. Chen, E. Zhao, L. Chang, Y. Pan, R. Feng, S. Zhai, S. Chai, Effect of addition of small amounts of samarium on microstructural evolution and mechanical properties enhancement of an as-extruded ZK60 magnesium alloy sheet, Journal of Materials Research and Technology 9 (1) (2020) 133–141.
[47] M. Sun, M. Liu, B. Zhang, Z. Chen, H. Jiang, Microstructures and Mechanical Properties of As-Extruded AZ31−xSm Magnesium Alloy, J Mater Eng Perform 29 (8) (2020) 5273–5281.
[48] Z. Shan, J. Yang, J. Fan, H. Zhang, Q. Zhang, Y. Wu, H. Dong, Microstructure evolution and mechanical properties of an AZ61 alloy processed with TS-ECAP and EPT, Materials Science and Engineering: A 780 (2020) 139195.
[49] Y. Wan, B. Tang, Y. Gao, L. Tang, G. Sha, B. Zhang, N. Liang, C. Liu, S. Jiang, Z. Chen, X. Guo, Y. Zhao, Bulk nanocrystalline high-strength magnesium alloys prepared via rotary swaging, Acta Mater 200 (2020) 274–286.
[50] L. Jia, W. Du, J. Fu, Z. Wang, K. Liu, S. Li, X. Du, Obtaining Ultra--High Strength and Ductility in a Mg–Gd–Er–Zn–Zr Alloy via Extrusion, Pre-deformation and Two-Stage Aging, Acta Metallurgica Sinica (English Letters) (2020).
[51] Y. Zhang, W. Rong, Y. Wu, L. Peng, Achieving ultra-high strength in Mg–Gd–Ag–Zr wrought alloy via bimodal-grained structure and enhanced precipitation, J Mater Sci Technol 54 (2020) 160–170.
[52] R.G. Li, H.R. Li, H.C. Pan, D.S. Xie, J.H. Zhang, D.Q. Fang, Y.Q. Dai, D.Y. Zhao, H. Zhang, Achieving exceptionally high strength in binary Mg-13Gd alloy by strong texture and substantial precipitates, Scripta Mater 193 (2021) 142–146.
[53] H. Pan, R. Kang, J. Li, H. Xie, Z. Zeng, Q. Huang, C. Yang, Y. Ren, G. Qin, Mechanistic investigation of a low-alloy Mg–Ca-based extrusion alloy with high strength–ductility synergy, Acta Mater 186 (2020) 278–290.
[54] Z. Yan, Y. Yu, J. Qian, J. Luo, Y. Sang, Fabrication of High-Strength Mg–Gd–Nd–Zn–Sn–Zr Alloy via Extrusion and Aging, Met Mater Int (2020).
[55] J. Sun, B. Xu, Z. Yang, H. Zhou, J. Han, Y. Wu, D. Song, Y. Yuan, X. Zhuo, H. Liu, A. Ma, Achieving excellent ductility in high-strength Mg-10.6Gd-2Ag alloy via equal channel angular pressing, J Alloy Compd 817 (2020) 152688.
[56] K. Wang, X. Dou, J. Wang, Y. Huang, S. Gavras, N. Hort, S. Liu, H. Hu, J. Wang, F. Pan, Achieving enhanced mechanical properties in Mg-Gd-Y-Zn-Mn alloy by altering dynamic recrystallization behavior via pre-ageing treatment, Materials Science and Engineering: A 790 (2020) 139635.
[57] L. Li, Y. Wang, C. Zhang, T. Wang, H. Lv, W. Yu, Ultrafine-grained Mg–Zn–Yb–Zr alloy with simultaneously improved strength and ductility processed by axisymmetric hot extrusion, Vacuum 173 (2020) 109157.
[58] B. Dong, Z. Zhang, J. Yu, X. Che, M. Meng, J. Zhang, Microstructure, texture evolution and mechanical properties of multi-directional forged Mg-13Gd-4Y–2Zn-0.5Zr alloy under decreasing temperature, J Alloy Compd 823 (2020) 153776.
[59] Y. Zhao, D. Zhang, J. Feng, X. Chen, T. Deng, B. Jiang, F. Pan, Effect of Gd addition on the age hardening response of Mg–6Zn-1Mn alloy, Journal of Materials Research and Technology 9 (4) (2020) 8834–8841.
[60] R.G. Li, H.R. Li, D.Y. Zhao, Y.Q. Dai, D.Q. Fang, J.H. Zhang, L. Zong, J. Sun, High strength commercial AZ91D alloy with a uniformly fine-grained structure processed by conventional extrusion, Materials Science and Engineering 780 (Apr.7) (2020) 139191–139193.
[61] J. Wei, S. Jiang, Z. Chen, C. Liu, Increasing strength and ductility

of a Mg–9Al alloy by dynamic precipitation assisted grain refinement during multi-directional forging, Materials Science and Engineering: A 780 (2020) 139192.
[62] F. Zhong, H. Wu, Y. Jiao, R. Wu, J. Zhang, L. Hou, M. Zhang, Effect of Y and Ce on the microstructure, mechanical properties and anisotropy of as-rolled Mg-8Li-1Al alloy, J Mater Sci Technol 39 (2020) 124–134.
[63] H. Ji, G. Wu, W. Liu, X. Liang, G. Liao, D. Ding, Microstructure characterization and mechanical properties of the as-cast and as-extruded Mg-xLi-5Zn-0.5Er (x = 8, 10 and 12 wt%) alloys, Mater Charact 159 (2020) 110008.
[64] Q. Ji, Y. Wang, R. Wu, Z. Wei, X. Ma, J. Zhang, L. Hou, M. Zhang, High specific strength Mg-Li-Zn-Er alloy processed by multi deformation processes, Mater Charact 160 (2020) 110135.
[65] J. Su, Y. Yang, X. Fu, Q. Ma, F. Ren, X. Peng, Microstructure and Mechanical Properties of Duplex Structured Mg-Li-Zn-Y Alloys, Arch. Foundry Eng. 18 (1) (2018) 181–185.
[66] F. Guo, L. Jiang, Y. Ma, L. Liu, Z. Zhang, M. Yang, D. Zhang, F. Pan, Strengthening a dual-phase Mg–Li alloy by strain-induced phase transformation at room temperature, Scripta Mater 179 (2020) 16–19.
[67] J. Li, Y. Yang, H. Deng, M. Li, J. Su, F. Hu, X. Xiong, X. Peng, Microstructure and corrosion behavior of as-extruded Mg-6.5Li-xY-yZn alloys, J Alloy Compd 823 (2020) 153839.
[68] L. Fu, Q. Le, W. Hu, J. Zhang, J. Wang, Strengths and ductility enhanced by micro-alloying Sm/La/Ca to Mg–0.5Zn–0.2Mn alloy, Journal of Materials Research and Technology 9 (3) (2020) 6834–6849.
[69] X. Liu, X. Qiao, Z. Li, M. Zheng, High strength and excellent ductility of dilute Mg-0.68Al-0.32Ca-0.50Mn (wt%) extrusion alloy obtained by T6 treatment, Mater Charact 162 (2020) 110197.
[70] Z.H. Li, T.T. Sasaki, M.Z. Bian, T. Nakata, Y. Yoshida, N. Kawabe, S. Kamado, K. Hono, Role of Zn on the room temperature formability and strength in Mg–Al–Ca–Mn sheet alloys, J Alloy Compd 847 (2020) 156347.
[71] J. Li, Y. Huang, F. Wang, X. Meng, L. Wan, Z. Dong, Enhanced strength and ductility of friction-stir-processed Mg–6Zn alloys via Y and Zr co-alloying, Materials Science and Engineering: A 773 (2020) 138877.
[72] Z. Zareian, M. Emamy, M. Malekan, H. Mirzadeh, W.J. Kim, A. Bahmani, Tailoring the mechanical properties of Mg–Zn magnesium alloy by calcium addition and hot extrusion process, Materials Science and Engineering: A 774 (2020) 138929.
[73] Y. Chai, C. He, B. Jiang, J. Fu, Z. Jiang, Q. Yang, H. Sheng, G. Huang, D. Zhang, F. Pan, Influence of minor Ce additions on the microstructure and mechanical properties of Mg-1.0Sn-0.6Ca alloy, J Mater Sci Technol 37 (2020) 26–37.
[74] X. Chen, L. Xiao, Y. Liu, M. Xu, T. Xu, B. Gao, Z. Hu, H. Zhou, High strength-ductility of heterogeneous sandwich Mg–Y alloys produced by high pressure torsion, Vacuum 179 (2020) 109568.
[75] T. Han, J. Zou, G. Huang, L. Ma, C. Che, W. Jia, L. Wang, F. Pan, Improved strength and ductility of AZ31B Mg alloy sheets processed by accumulated extrusion bonding with artificial cooling, Journal of Magnesium and Alloys (2020).
[76] P. Peng, A. Tang, J. She, J. Zhang, S. Zhou, K. Song, F. Pan, Significant improvement in yield stress of Mg-Gd-Mn alloy by forming bimodal grain structure, Materials Science and Engineering: A 803 (2021) 140569.
[77] J.J. Bhattacharyya, T. Nakata, S. Kamado, S.R. Agnew, Origins of high strength and ductility combination in a Guinier-Preston zone containing Mg-Al-Ca-Mn alloy, Scripta Mater 163 (2019) 121–124.
[78] T. Nakata, C. Xu, R. Ajima, K. Shimizu, S. Hanaki, T.T. Sasaki, L. Ma, K. Hono, S. Kamado, Strong and ductile age-hardening Mg-Al-Ca-Mn alloy that can be extruded as fast as aluminum alloys, Acta Mater 130 (2017) 261–270.
[79] F. Hu, S. Zhao, G. Gu, Z. Ma, G. Wei, Y. Yang, X. Peng, W. Xie, Strong and ductile Mg-0.4Al alloy with minor Mn addition achieved by conventional extrusion, Materials Science and Engineering: A 795 (2020) 139926.
[80] S.J. Meng, H. Yu, S.D. Fan, Y.M. Kim, S.H. Park, W.M. Zhao, B.S. You, K.S. Shin, A high-ductility extruded Mg-Bi-Ca alloy, Mater Lett 261 (2020) 127066.
[81] Y. Yang, M. Li, H. Deng, F. Ren, H. Zhang, B. Jiang, X. Peng, F. Pan, Effects of annealing temperature on microstructure and mechanical properties of LZ91 alloy, Mater Sci Tech-Lond 36 (18) (2020) 2010–2017.
[82] G. Zhu, L. Wang, J. Wang, J. Wang, J. Park, X. Zeng, Highly deformable Mg–Al–Ca alloy with Al2Ca precipitates, Acta Mater 200 (2020) 236–245.
[83] X. Luo, Z. Feng, T. Yu, J. Luo, T. Huang, G. Wu, N. Hansen, X. Huang, Transitions in mechanical behavior and in deformation mechanisms enhance the strength and ductility of Mg-3Gd, Acta Mater 183 (2020) 398–407.
[84] T. Tu, X. Chen, T. Chen, Y. Yuan, F. Pan, New high-modulus and high-strength Mg-Gd-Ag-Mn-Ge alloys, Materials Science and Engineering: A (2020) 140559.
[85] M.D. Costantino, A. Schuster, H. Helmholz, A. Meyer-Rachner, R. Willumeit-Römer, B.J.C. Luthringer-Feyerabend, Inflammatory response to magnesium-based biodegradable implant materials, Acta Biomater 101 (2020) 598–608.
[86] W. Wang, H. Wu, Y. Sun, J. Yan, L. Zhang, S. Zhang, J. Ni, Y. Song, X. Zhang, Local intragranular misorientation accelerates corrosion in biodegradable Mg, Acta Biomater 101 (2020) 575–585.
[87] J. She, P. Peng, L. Xiao, A.T. Tang, Y. Wang, F.S. Pan, Development of high strength and ductility in Mg–2Zn extruded alloy by high content Mn-alloying, Materials Science and Engineering: A 765 (2019) 138203.
[88] M.S. Dargusch, N. Balasubramani, J. Venezuela, S. Johnston, G. Wang, C. Lau, M. Bermingham, D. Kent, D.H. StJohn, Improved biodegradable magnesium alloys through advanced solidification processing, Scripta Mater 177 (2020) 234–240.
[89] S. Wang, X. Zhang, J. Li, C. Liu, S. Guan, Investigation of Mg–Zn–Y–Nd alloy for potential application of biodegradable esophageal stent material, Bioactive Materials 5 (1) (2020) 1–8.
[90] K. Munir, J. Lin, C. Wen, P.F.A. Wright, Y. Li, Mechanical, corrosion, and biocompatibility properties of Mg-Zr-Sr-Sc alloys for biodegradable implant applications, Acta Biomater 102 (2020) 493–507.
[91] S. Jin, D. Zhang, X. Lu, Y. Zhang, L. Tan, Y. Liu, Q. Wang, Mechanical properties, biodegradability and cytocompatibility of biodegradable Mg-Zn-Zr-Nd/Y alloys, J Mater Sci Technol 47 (2020) 190–201.
[92] J. Bohlen, S. Meyer, B. Wiese, B.J.C. Luthringer-Feyerabend, R. Willumeit-Römer, D. Letzig, Alloying and Processing Effects on the Microstructure, Mechanical Properties, and Degradation Behavior of Extruded Magnesium Alloys Containing Calcium, Cerium, or Silver, Materials 13 (2) (2020) 391.
[93] Z.H. Zhu, K.B. Nie, K.K. Deng, J.G. Han, Fabrication of biodegradable magnesium matrix composite with ultrafine grains and high strength by adding TiC nanoparticles to Mg-1.12Ca-0.84Zn-0.23Mn (at.%) alloy, Materials Science and Engineering: C 107 (2020) 110360.
[94] K. Munir, C. Wen, Y. Li, Graphene nanoplatelets-reinforced magnesium metal matrix nanocomposites with superior mechanical and corrosion performance for biomedical applications, Journal of Magnesium and Alloys 8 (1) (2020) 269–290.
[95] C. Shuai, B. Wang, S. Bin, S. Peng, C. Gao, TiO2-Induced In Situ Reaction in Graphene Oxide-Reinforced AZ61 Biocomposites to Enhance the Interfacial Bonding, Acs Appl Mater Inter 12 (20) (2020) 23464–23473.
[96] D.B. Prabhu, P. Gopalakrishnan, K.R. Ravi, Morphological studies on the development of chemical conversion coating on surface of Mg–4Zn alloy and its corrosion and bio mineralisation behaviour in simulated body fluid, J Alloy Compd 812 (2020) 152146.
[97] P. Makkar, H.J. Kang, A.R. Padalhin, O. Faruq, B. Lee, In-vitro and in-vivo evaluation of strontium doped calcium phosphate coatings on biodegradable magnesium alloy for bone applications, Appl Surf Sci 510 (2020) 145333.
[98] B. Zeller-Plumhoff, C. Malich, D. Krüger, G. Campbell, B. Wiese, S. Galli, A. Wennerberg, R. Willumeit-Römer, D.C.F. Wieland, Analysis of the bone ultrastructure around biodegradable Mg–xGd implants

using small angle X-ray scattering and X-ray diffraction, Acta Biomater 101 (2020) 637–645.
[99] M. Barbeck, L. Kühnel, F. Witte, J. Pissarek, C. Precht, X. Xiong, R. Krastev, N. Wegner, F. Walther, O. Jung, Degradation, Bone Regeneration and Tissue Response of an Innovative Volume Stable Magnesium-Supported GBR/GTR Barrier Membrane, Int J Mol Sci 21 (9) (2020) 3098.
[100] L. Xiangji, R. Filek, Z. Xiaomin, G. Huanhuan, Q. Liying, L. Hong, X. Lin, W. Yong, P. Fusheng, C.M. Hutnik, Bio-modulation of scarring Glaucoma Filtration Surgery using a novel application of coated magnesium, Journal of Magnesium and Alloys (2020).
[101] W. Wang, G. Jia, Q. Wang, H. Huang, X. Li, H. Zeng, W. Ding, F. Witte, C. Zhang, W. Jia, G. Yuan, The in vitro and in vivo biological effects and osteogenic activity of novel biodegradable porous Mg alloy scaffolds, Mater Design 189 (2020) 108514.
[102] B. Vaghefinazari, D. Höche, S.V. Lamaka, D. Snihirova, M.L. Zheludkevich, Tailoring the Mg-air primary battery performance using strong complexing agents as electrolyte additives, J Power Sources 453 (2020) 227880.
[103] H. Yang, L. Wu, B. Jiang, W. Liu, F. Pan, Clarifying the roles of grain boundary and grain orientation on the corrosion and discharge processes of α-Mg based Mg-Li alloys for primary Mg-air batteries, Journal of Materials Science and Technology -Shenyang- 62 (2020) 128–138.
[104] H. Liu, Y. Yan, X. Wu, H. Fang, X. Chu, J. Huang, J. Zhang, J. Song, K. Yu, Effects of Al and Sn on microstructure, corrosion behavior and electrochemical performance of Mg–Al-based anodes for magnesium-air batteries, J Alloy Compd (2020) 157755.
[105] B. Xiao, G. Song, D. Zheng, F. Cao, A corrosion resistant die-cast Mg-9Al-1Zn anode with superior discharge performance for Mg-air battery, Mater Design 194 (2020) 108931.
[106] X.J. Gu, W.L. Cheng, S.M. Cheng, Y.H. Liu, H.X. Wang, Tailoring the microstructure and improving the discharge properties of dilute Mg-Sn-Mn-Ca alloy as anode for Mg-air battery through homogenization prior to extrusion, J. Mater. Sci. Technol. (2020) 60.
[107] F. Tong, X. Chen, Q. Wang, S. Wei, W. Gao, Hypoeutectic Mg–Zn binary alloys as anode materials for magnesium-air batteries, J Alloy Compd (2020).
[108] X. Chen, Q. Zou, Q. Le, J. Hou, R. Guo, H. Wang, C. Hu, L. Bao, T. Wang, D. Zhao, F. Yu, A. Atrens, The quasicrystal of Mg–Zn–Y on discharge and electrochemical behaviors as the anode for Mg-air battery, J Power Sources 451 (2020) 227807.
[109] L. Wang, D. Snihirova, M. Deng, B. Vaghefinazari, S.V. Lamaka, D. Höche, M.L. Zheludkevich, Tailoring electrolyte additives for controlled Mg-Ca anode activity in aqueous Mg-air batteries, J Power Sources 460 (2020) 228106.
[110] M. Deng, L. Wang, D. Höche, S.V. Lamaka, P. Jiang, D. Snihirova, N. Scharnagl, M.L. Zheludkevich, Ca/In micro alloying as a novel strategy to simultaneously enhance power and energy density of primary Mg-air batteries from anode aspect, J Power Sources 472 (2020) 228528.
[111] S. Cheng, W. Cheng, X. Gu, H. Yu, Z. Wang, H. Wang, L. Wang, Discharge properties of low-alloyed Mg–Bi–Ca alloys as anode materials for Mg–air batteries: Influence of Ca alloying, J Alloy Compd 823 (2020) 153779.
[112] H. Yang, L. Wu, B. Jiang, B. Lei, W. Liu, J. Song, G. Huang, D. Zhang, F. Pan, Effects of Grain Size on the Corrosion and Discharge Behaviors of Mg-Y Binary Alloys for Mg-Air Batteries, J Electrochem Soc 167 (13) (2020).
[113] X. Chen, H. Wang, Q. Le, Y. Jia, X. Zhou, F. Yu, A. Atrens, The role of long-period stacking ordered phase on the discharge and electrochemical behaviors of magnesium anode Mg-Zn-Y for the primary Mg-air battery, Int J Energ Res 44 (11) (2020) 8865–8876.
[114] X. Chen, Y. Jia, Q. Le, H. Wang, X. Zhou, F. Yu, A. Atrens, Discharge properties and electrochemical behaviors of AZ80-La-Gd magnesium anode for Mg-air battery, Journal of Magnesium and Alloys (2020).
[115] X. Chen, Q. Liao, Q. Le, Q. Zou, A. Atrens, The influence of samarium (Sm) on the discharge and electrochemical behaviors of the magnesium alloy AZ80 as an anode for the Mg-air battery, Electrochim Acta (2020) 136315.
[116] H. Yang, B. Lei, L. Wu, B. Jiang, W. Liu, Q. Yang, J. Song, G. Huang, D. Zhang, F. Pan, Effects of Texture and Discharge Products on the Discharge Performance of Mg Anodes for Mg Air Batteries, J Electrochem Soc 167 (13) (2020).
[117] H. Yang, L. Wu, B. Jiang, B. Lei, W. Liu, J. Song, A. Atrens, G. Huang, D. Zhang, F. Pan, Enhancement of Corrosion Resistance and Discharge Performance of Mg-5Li-3Al-1Zn Sheet for Mg-air Battery via Rolling, J Electrochem Soc 167 (11) (2020) 110529.
[118] K. Wang, Y. Xiao, X. Liu, Z. Zhang, J. Chen, Y. Zuo, S. Zhao, Performance Improvement of Underwater Mg-Oxygen Battery with Parameter Optimization, J Electrochem Soc 167 (14) (2020).
[119] G. Li, M. Jiang, Q. Liao, R. Ding, Y. Gao, L. Jiang, D. Zhang, S. Chen, H. He, Directly anchoring Ag single atoms on α-MnO 2 nanorods as efficient oxygen reduction catalysts for Mg-air fuel cell, J Alloy Compd (2020).
[120] L. Zhang, Q. Shao, J. Zhang, An overview of non-noble metal electrocatalysts and their associated air cathodes for Mg-air batteries, Materials Reports: Energy (2020) 100002.
[121] X. Huang, X. Zhang, W. Hu, S. Lv, Y. Huang, Altering the MOF-74 derivatives for efficient oxygen electrocatalysis through synergistic multi-metals and nitrogen modification, J Mater Sci 55 (24) (2020) 10773–10784.
[122] L. Wei, R. Lian, Y. Zhao, Y. Meng, L. He, Y. Yu, G. Chen, Y. Wei, Experimental Investigation and First-Principles Calculations of a Ni3Se4 Cathode Material for Mg-Ion Batteries, Acs Appl Mater Inter 12 (8) (2020) 9316–9321.
[123] K. Kisu, S. Kim, M. Inukai, H. Oguchi, S. Takagi, S. Orimo, Magnesium Borohydride Ammonia Borane as a Magnesium Ionic Conductor, ACS Applied Energy Materials 3 (4) (2020) 3174–3179.
[124] E. Sheha, F. Liu, T. Wang, M. Farrag, J. Liu, N. Yacout, M.A. Kebede, N. Sharma, L. Fan, Dual Polymer/Liquid Electrolyte with BaTiO3 Electrode for Magnesium Batteries, ACS Applied Energy Materials 3 (6) (2020) 5882–5892.
[125] X. Cheng, Z. Zhang, Q. Kong, Q. Zhang, T. Wang, S. Dong, L. Gu, X. Wang, J. Ma, P. Han, H. Lin, C. Chen, G. Cui, Highly Reversible Cuprous Mediated Cathode Chemistry for Magnesium Batteries, Angew. Chem. Int. Ed. 59 (28) (2020).
[126] Y. Zhang, J. Gui, T. Li, Z. Chen, S. Cao, F. Xu, A novel Mg/Na hybrid battery based on Na2VTi(PO4)3 cathode: Enlightening the Na-intercalation cathodes by a metallic Mg anode and a dual-ion Mg2+/Na+ electrolyte, Chem Eng J 399 (2020) 125689.
[127] N. Wu, Y. Yang, Q. Zhang, X. Zhang, X. Du, A layered titanium-based transition metal oxide as stable anode material for magnesium-ion batteries, J Mater Sci 55 (35) (2020) 16674–16682.
[128] Z. Li, S. Ding, J. Yin, M. Zhang, C. Sun, A. Meng, Morphology-dependent electrochemical performance of VS4 for rechargeable magnesium battery and its magnesiation/demagnesiation mechanism, J POWER SOURCES 451 (2020) 227815.
[129] R. Sun, X. Ji, C. Luo, S. Hou, P. Hu, X. Pu, L. Cao, L. Mai, C. Wang, Water-Pillared Sodium Vanadium Bronze Nanowires for Enhanced Rechargeable Magnesium Ion Storage, Small 16 (30) (2020) 2000741.
[130] C. Du, Y. Zhu, Z. Wang, L. Wang, W. Younas, X. Ma, C. Cao, Cuprous Self-Doping Regulated Mesoporous CuS Nanotube Cathode Materials for Rechargeable Magnesium Batteries, Acs Appl Mater Inter 12 (31) (2020) 35035–35042.
[131] M. Rashad, M. Asif, I. Ahmed, Z. He, L. Yin, Z.X. Wei, Y. Wang, Quest for carbon and vanadium oxide based rechargeable magnesium-ion batteries, Journal of Magnesium and Alloys 8 (2) (2020) 364–373.
[132] S. Dey, J. Lee, S. Britto, J.M. Stratford, E.N. Keyzer, M.T. Dunstan, G. Cibin, S.J. Cassidy, M. Elgaml, C.P. Grey, Exploring Cation–Anion Redox Processes in One-Dimensional Linear Chain Vanadium Tetrasulfide Rechargeable Magnesium Ion Cathodes, J Am Chem Soc 142 (46) (2020) 19588–19601.
[133] R. Richter, J. Häcker, Z. Zhao-Karger, T. Danner, N. Wagner, M. Ficht-

ner, K.A. Friedrich, A. Latz, Insights into Self-Discharge of Lithium– and Magnesium–Sulfur Batteries, ACS Applied Energy Materials 3 (9) (2020) 8457–8474.
[134] L.E. Blanc, X. Sun, A. Shyamsunder, V. Duffort, L.F. Nazar, Direct Nano-Synthesis Methods Notably Benefit Mg-Battery Cathode Performance, Small Methods 4 (5) (2020) 2000029.
[135] J. Zhu, R. Shi, Y. Liu, Y. Zhu, J. Zhang, X. Hu, L. Li, 3D interwoven MXene networks fabricated by the assistance of bacterial celluloses as high-performance cathode material for rechargeable magnesium battery, Appl Surf Sci 528 (2020) 146985.
[136] G. Venkateswarlu, D. Madhu, J. Vatsala Rani, Graphene/β-MnO2 composites—Synthesis and its electroanalytical properties study in the Mg storage battery, Int J Energ Res 44 (13) (2020) 10238–10250.
[137] Y. Zhang, G. Liu, C. Zhang, Q. Chi, T. Zhang, Y. Feng, K. Zhu, Y. Zhang, Q. Chen, D. Cao, Low-cost MgFexMn2-xO4 cathode materials for high-performance aqueous rechargeable magnesium-ion batteries, Chem Eng J 392 (2020) 123652.
[138] S. Doi, R. Ise, T. Mandai, Y. Oaki, S. Yagi, H. Imai, Spinel-Type MgMn2 O4 Nanoplates with Vanadate Coating for a Positive Electrode of Magnesium Rechargeable Batteries, Langmuir 36 (29) (2020) 8537–8542.
[139] H. Kaland, J. Hadler-Jacobsen, F.H. Fagerli, N.P. Wagner, K. Wiik, Dipentamethylene Thiuram Tetrasulfide-Based Cathodes for Rechargeable Magnesium Batteries, ACS Applied Energy Materials 3 (11) (2020) 10600–10610.
[140] J. Niu, Z. Zhang, D. Aurbach, Alloy Anode Materials for Rechargeable Mg Ion Batteries, Adv Energy Mater 10 (23) (2020) 2000697.
[141] H. Park, H. Lim, S.H. Oh, J. Park, H. Lim, K. Kang, Tailoring Ion-Conducting Interphases on Magnesium Metals for High-Efficiency Rechargeable Magnesium Metal Batteries, Acs Energy Lett 5 (12) (2020) 3733–3740.
[142] L. Wang, S.S. Welborn, H. Kumar, M. Li, Z. Wang, V.B. Shenoy, E. Detsi, High-Rate and Long Cycle-Life Alloy-Type Magnesium-Ion Battery Anode Enabled Through (De)magnesiation-Induced Near–Room-Temperature Solid–Liquid Phase Transformation, Adv Energy Mater 9 (45) (2019).
[143] J. Lüder, S. Manzhos, First-Principle Insights Into Molecular Design for High-Voltage Organic Electrode Materials for Mg Based Batteries, Front Chem 8 (2020).
[144] F. Tuerxun, K. Yamamoto, M. Hattori, T. Mandai, Y. Uchimoto, Determining Factor on Polarization Behavior of Magnesium Deposition for Magnesium Battery Anode, Acs Appl Mater Inter 23 (12) (2020) 25775–25785.
[145] M. Deng, L. Wang, D. Höche, S.V. Lamaka, D. Snihirova, P. Jiang, M.L. Zheludkevich, Corrosion and discharge properties of Ca/Ge micro-alloyed Mg anodes for primary aqueous Mg batteries, Corros Sci 177 (2020) 108958.
[146] J. Gao, S. Gao, E. Wang, Y. Song, G. Sun, Revealing the effect of aluminum content on the electrochemical performance of magnesium anodes for aqueous batteries, Mater. Corros. 71 (11) (2020) 1812–1823.
[147] F. Tuerxun, K. Yamamoto, M. Hattori, T. Mandai, K. Nakanishi, A. Choudhary, Y. Tateyama, K. Sodeyama, A. Nakao, T. Uchiyama, M. Matsui, K. Tsuruta, Y. Tamenori, K. Kanamura, Y. Uchimoto, Determining Factor on the Polarization Behavior of Magnesium Deposition for Magnesium Battery Anode, Acs Appl Mater Inter 12 (23) (2020) 25775–25785.
[148] J. Wang, W. Zhao, H. Dou, B. Wan, Y. Zhang, W. Li, X. Zhao, X. Yang, Electrostatic Shielding Guides Lateral Deposition for Stable Interphase toward Reversible Magnesium Metal Anodes, Acs Appl Mater Inter 12 (17) (2020) 19601–19606.
[149] R. Singh, S. Janakiraman, A. Agrawal, S. Ghosh, K. Biswas, An amorphous poly(vinylidene fluoride-co-hexafluoropropylene) based gel polymer electrolyte for magnesium ion battery, J Electroanal Chem (2019).
[150] N.T.K. Dung, N.T.D. Linh, D.Q. Tham, N.T. Chinh, M.M. Tan, T.T. Mai, N.T.T. Trang, D.M. Thanh, N.Q. Tung, T. Hoang, Effect Of Magnesium Perchlorate Content on the Mechanical, Thermal Stability, and Dielectric Properties of Plasticized PMMA/PVC-g-PMMA Electrolytes, Adv Polym Tech (2020) (2020) 1–9.
[151] S. Ponmani, K. Selvakumar, M.Ramesh Prabhu, The effect of the geikeilite (MgTiO3) nanofiller concentration in PVdF-HFP/PVAc–based polymer blend electrolytes for magnesium ion battery, Ionics 26 (5) (2020) 2353–2369.
[152] J. Sun, Y. Zou, S. Gao, L. Shao, C. Chen, Robust Strategy of Quasi–Solid-State Electrolytes to Boost the Stability and Compatibility of Mg Ion Batteries, Acs Appl Mater Inter 12 (49) (2020) 54711–54719.
[153] R. Singh, S. Janakiraman, M. Khalifa, S. Anandhan, S. Ghosh, A. Venimadhav, K. Biswas, A high thermally stable polyacrylonitrile (PAN)-based gel polymer electrolyte for rechargeable Mg-ion battery, J. Mater. Sci. Mater. Electron. 31 (24) (2020) 22912–22925.
[154] C. Maheshwaran, D.K. Kanchan, K. Gohel, K. Mishra, D. Kumar, Effect of Mg(CF3SO3)2 concentration on structural and electrochemical properties of ionic liquid incorporated polymer electrolyte membranes, J. Solid State Electrochem. (2020).
[155] M. Mesallam, E.M. Kamar, N. Sharma, E. Sheha, Synthesis and characterization of polyvinylidene fluoride/magnesium bromide polymer electrolyte for magnesium battery application, Phys Scripta 95 (11) (2020).
[156] C. Maheshwaran, D.K. Kanchan, K. Mishra, D. Kumar, K. Gohel, Flexible magnesium-ion conducting polymer electrolyte membranes: mechanical, structural, thermal, and electrochemical impedance spectroscopic properties, Journal of Materials Science Materials in Electronics 31 (3) (2020) 15013–15027.
[157] D. Hambali, Z. Osman, L. Othman, K.B.M. Isa, N. Harudin, Magnesium (II) bis(trifluoromethanesulfonimide) doped PVdC-co-AN gel polymer electrolytes for rechargeable batteries, J Polym Res 27 (6) (2020).
[158] M. Mahalakshmi, S. Selvanayagam, S. Selvasekarapandian, M.V.L. Chandra, P. Sangeetha, R. Manjuladevi, Magnesium ion–conducting solid polymer electrolyte based on cellulose acetate with magnesium nitrate (Mg(NO3)2·6H2O) for electrochemical studies, Ionics 26 (9) (2020) 4553–4565.
[159] H. Fan, Y. Zhao, J. Xiao, J. Zhang, M. Wang, Y. Zhang, A non-nucleophilic gel polymer magnesium electrolyte compatible with sulfur cathode, Nano Res 13 (10) (2020) 2749–2754.
[160] D. Nguyen, R. Horia, A.Y.S. Eng, S. Song, Z.W. Seh, Material design strategies to improve the performance of rechargeable magnesium–sulfur batteries, Mater Horiz (2021).
[161] M. Rashad, M. Asif, Z. Ali, Quest for magnesium-sulfur batteries: Current challenges in electrolytes and cathode materials developments, Coordin Chem Rev 415 (2020) 213312.
[162] J. Sun, C. Deng, Y. Bi, K. Wu, S. Zhu, Z. Xie, C. Li, R. Amal, J. Luo, T. Liu, D. Wang, In Situ Sulfurized Carbon-Confined Cobalt for Long-Life Mg/S Batteries, ACS Applied Energy Materials 3 (3) (2020) 2516–2525.
[163] P. Wang, J. Trück, S. Niesen, J. Kappler, K. Küster, U. Starke, F. Ziegler, A. Hintennach, M.R. Buchmeiser, High-Performance Magnesium-Sulfur Batteries Based on a Sulfurated Poly(acrylonitrile) Cathode, a Borohydride Electrolyte, and a High-Surface Area Magnesium Anode, Batteries & Supercaps 3 (11) (2020) 1239–1247.
[164] P. Wang, J. Kappler, B. Sievert, J. Häcker, K. Küster, U. Starke, F. Ziegler, M.R. Buchmeiser, Characteristics of magnesium-sulfur batteries based on a sulfurized poly(acrylonitrile) composite and a fluorinated electrolyte, Electrochim Acta 361 (2020) 137024.
[165] D. Huang, S. Tan, M. Li, D. Wang, L. Mai, A high-efficient non-nucleophilic Mg(CF3SO3)2-based electrolyte for high-power Mg/S battery, Acs Appl Mater Inter 12 (15) (2020) 17474–17480.
[166] H. Fan, Z. Zheng, L. Zhao, W. Li, J. Wang, M. Dai, Y. Zhao, J. Xiao, G. Wang, X. Ding, H. Xiao, J. Li, Y. Wu, Y. Zhang, Extending Cycle Life of Mg/S Battery by Activation of Mg Anode/Electrolyte Interface through an LiCl-Assisted MgCl2 Solubilization Mechanism, Adv Funct Mater 30 (9) (2019) 1909370.
[167] V. Bhaghavathi Parambath, Z. Zhao-Karger, T. Diemant, M. Jäckle, Z. Li, T. Scherer, A. Gross, R.J. Behm, M. Fichtner, Investigation on the formation of Mg metal anode/electrolyte interfaces in Mg/S

batteries with electrolyte additives, J Mater Chem A 8 (43) (2020) 22998–23010.
[168] S. Zhang, Y. Huang, Y. NuLi, B. Wang, J. Yang, J. Wang, Sodium Polyacrylate as a Promising Aqueous Binder of S@pPAN Cathodes for Magnesium–Sulfur Batteries, The Journal of Physical Chemistry C 124 (38) (2020) 20712–20721.
[169] A. Robba, M. Menar, A. Vizintin, J. Bitenc, J. Bobnar, I. Aron, R. Vitanova, R. Dominko, Role of Cu current collector on electrochemical mechanism of Mg–S battery, J Power Sources, 450.
[170] Y. Bi, S. He, C. Fan, J. Luo, B. Yuan, T.L. Liu, A robust ionic liquid magnesium electrolyte enabling Mg/S batteries, J Mater Chem a 8 (25) (2020) 12301–12305.
[171] T. Lu, Z. Zhang, B. Chen, S. Dong, C. Wang, A. Du, L. Wang, J. Ma, G. Cui, A superior electronic conducting tellurium electrode enabled high rate capability rechargeable Mg batteries, Materials Today Energy 17 (2020) 100450.
[172] A. Du, Y. Zhao, Z. Zhang, S. Dong, Z. Cui, K. Tang, C. Lu, P. Han, X. Zhou, G. Cui, Selenium sulfide cathode with copper foam interlayer for promising magnesium electrochemistry, Energy Storage Materials 26 (2020) 23–31.
[173] M. Abdellaoui, M. Lakhal, H. Benzidi, O. Mounkachi, A. Benyoussef, A.E. Kenz, M. Loulidi, The hydrogen storage properties of Mg-intermetallic-hydrides by ab initio calculations and kinetic Monte Carlo simulations, Int J Hydrogen Energ 45 (19) (2020) 11158–11166.
[174] J. Cermak, L. Kral, P. Roupcova, Significantly decreased stability of MgH2 in the Mg-In-C alloy system: Long-period-stacking-ordering as a new way how to improve performance of hydrogen storage alloys? Renew Energ 150 (2020) 204–212.
[175] H. Liang, D. Chen, M. Chen, W. Li, R. Snyders, Study of the synthesis of PMMA-Mg nanocomposite for hydrogen storage application, Int J Hydrogen Energ 45 (7) (2020) 4743–4753.
[176] M. Hu, X. Xie, M. Chen, C. Zhu, T. Liu, TiCX-decorated Mg nanoparticles confined in carbon shell: Preparation and catalytic mechanism for hydrogen storage, J Alloy Compd 817 (2020) 152813.
[177] N. Patelli, A. Migliori, V. Morandi, L. Pasquini, Interfaces within biphasic nanoparticles give a boost to magnesium-based hydrogen storage, Nano Energy 72 (2020) 104654.
[178] P. Liu, J. Lian, H. Chen, X. Liu, Y. Chen, T. Zhang, H. Yu, G. Lu, S. Zhou, In-situ synthesis of Mg2Ni-Ce6O11 catalyst for improvement of hydrogen storage in magnesium, Chem Eng J 385 (2020) 123448.
[179] F.J. Antiqueira, D.R. Leiva, G. Zepon, B.F.R.F. de Cunha, S.J.A. Figueroa, W.J. Botta, Fast hydrogen absorption/desorption kinetics in reactive milled Mg-8 mol% Fe nanocomposites, Int J Hydrogen Energ 45 (22) (2020) 12408–12418.
[180] P. de Rango, D. Fruchart, V. Aptukov, N. Skryabina, Fast Forging: A new SPD method to synthesize Mg-based alloys for hydrogen storage, Int J Hydrogen Energ 45 (14) (2020) 7912–7916.
[181] S.A. Pighin, G. Urretavizcaya, J.L. Bobet, F.J. Castro, Nanostructured Mg for hydrogen production by hydrolysis obtained by MgH2 milling and dehydriding, J Alloy Compd 827 (2020) 154000.
[182] A. Tehranchi, B. Yin, W.A. Curtin, Solute strengthening of basal slip in Mg alloys, Acta Mater 151 (2018) 56–66.
[183] X.J. Wang, D.K. Xu, R.Z. Wu, X.B. Chen, Q.M. Peng, L. Jin, Y.C. Xin, Z.Q. Zhang, Y. Liu, X.H. Chen, G. Chen, K.K. Deng, H.Y. Wang, What is going on in magnesium alloys? J Mater Sci Technol 34 (2) (2018) 245–247.
[184] J.P. Weiler, A review of magnesium die-castings for closure applications, Journal of Magnesium and Alloys 7 (2) (2019) 297–304.
[185] Z. Zeng, N. Stanford, C.H.J. Davies, J. Nie, N. Birbilis, Magnesium extrusion alloys: a review of developments and prospects, Int Mater Rev 64 (1) (2019) 27–62.
[186] S.Güne Elik, N. Sarkaya, P. Karaday, A.A. Kaya, Changes in Elasticity Modulus and Damping in Some Novel Magnesium Alloys at Room and High Temperatures, IMMC 2016 18th International Metallurgy & Materials Congress, 2016.
[187] A.A. Kaya, Y.Türe Elik, A. Ataman, D. Turan, New Magnesium Alloys with High Elastic Modulus, MTM2017, 2017.
[188] D. Zhao, X. Chen, J. Ye, T. Chen, Y. Dai, C. Liu, Z. Luo, S. Gao, J. Zhang, J. Yao, A. Atrens, A. Tang, F. Pan, Simultaneously improving elastic modulus and damping capacity of extruded Mg-Gd-Y-Zn-Mn alloy via alloying with Si, J Alloy Compd 810 (2019) 151857.
[189] D. Zhao, X. Chen, Y. Yuan, F. Pan, Development of a novel Mg–Y–Zn–Al–Li alloy with high elastic modulus and damping capacity, Materials Science and Engineering: A 790 (2020) 139744.
[190] J. Wang, S. Gao, X. Liu, X. Peng, K. Wang, S. Liu, W. Jiang, S. Guo, F. Pan, Enhanced mechanical properties and degradation rate of Mg–Ni–Y alloy by introducing LPSO phase for degradable fracturing ball applications, Journal of Magnesium and Alloys 8 (1) (2020) 127–133.
[191] H. Niu, K. Deng, K. Nie, C. Wang, W. Liang, Y. Wu, Degradation behavior of Mg-4Zn-2Ni alloy with high strength and high degradation rate, Mater Chem Phys 249 (2020) 123131.
[192] J. Wang, T. Li, H.X. Li, Y.Z. Ma, J.S. Zhang, Effect of trace Ni addition on microstructure, mechanical and corrosion properties of the extruded Mg–Gd–Y–Zr–Ni alloys for dissoluble fracturing tools, Journal of Magnesium and Alloys (2020).
[193] C. Xu, M.Y. Zheng, Y.Q. Chi, X.J. Chen, K. Wu, E.D. Wang, G.H. Fan, P. Yang, G.J. Wang, X.Y. Lv, Microstructure and mechanical properties of the Mg–Gd–Y–Zn–Zr alloy fabricated by semi-continuous casting, Materials Science & Engineering A 549 (JUL.15) (2012) 128–135.
[194] J. Wang, X. Peng, K. Wang, H. Hu, S. Gao, J. Wang, F. Pan, Numerical Simulation and Experimental Study on Extrusion Forming of High Strength Tough Magnesium Alloy Large Size Profiles, Xiyou Jinshu Cailiao Yu Gongcheng/Rare Metal Materials and Engineering 49 (2020) 1665–1673.
[195] J. Tang, L. Chen, G. Zhao, C. Zhang, X. Chu, Formation mechanism and evolution of surface coarse grains on a ZK60 Mg profile extruded by a porthole die, J Mater Sci Technol 47 (2020) 88–102.
[196] J. WANG, X. PENG, K. WANG, Q. WANG, S. GAO, H. HU, F. PAN, Numerical simulation and experimental study on extrusion forming of ultra-large size wide thin-walled hollow magnesium alloy profiles, The Chinese Journal of Nonferrous Metals 30 (12) (2020) 1–11.
[197] Q. Wang, Y. Song, B. Jiang, J. Fu, A. Tang, H. Sheng, J. Song, D. Zhang, Z. Jiang, G. Huang, F. Pan, Fabrication of Mg/Mg composite with sleeve-core structure and its effect on room-temperature yield asymmetry via bimetal casting-co-extrusion, Materials Science and Engineering: A 769 (2020) 138476.
[198] C. Xu, M.Y. Zheng, K. Wu, E.D. Wang, G.H. Fan, S.W. Xu, S. Kamado, X.D. Liu, G.J. Wang, X.Y. Lv, M.J. Li, Y.T. Liu, Effect of final rolling reduction on the microstructure and mechanical properties of Mg–Gd–Y–Zn–Zr alloy sheets, Materials Science and Engineering: A 559 (2013) 232–240.
[199] K. Wang, J. Wang, X. Peng, S. Gao, H. Hu, L. Zeng, F. Pan, Microstructure and mechanical properties of Mg-Gd-Y-Zn-Mn alloy sheets processed by large-strain high-efficiency rolling, Materials Science and Engineering: A 748 (2019) 100–107.
[200] F. Pan, B. Zeng, B. Jiang, M. Zhang, H. Dong, Enhanced mechanical properties of AZ31B magnesium alloy thin sheets processed by on-line heating rolling, J Alloy Compd 693 (2017) 414–420.
[201] Q. Liu, J. Song, H. Zhao, B. Xiao, X. Zheng, F. Pan, Improved Edge Quality for AZ31 Sheets Using Online Heating Rolling Technique, J Mater Eng Perform 29 (7) (2020) 4212–4221.
[202] Y. Huang, B. Xiao, J. Song, H. Zhao, Q. Liu, B. Jiang, F. Pan, Effect of tension on edge crack of on-line heating rolled AZ31B magnesium alloy sheet, Journal of Materials Research and Technology 9 (2) (2020) 1988–1997.
[203] H. Hyer, L. Zhou, G. Benson, B. McWilliams, K. Cho, Y. Sohn, Additive manufacturing of dense WE43 Mg alloy by laser powder bed fusion, Additive Manufacturing 33 (2020) 101123.
[204] X. Yang, J. Liu, Z. Wang, X. Lin, F. Liu, W. Huang, E. Liang, Microstructure and mechanical properties of wire and arc additive manufactured AZ31 magnesium alloy using cold metal transfer process, Materials Science and Engineering: A 774 (2020) 138942.
[205] M. Esmaily, Z. Zeng, A.N. Mortazavi, A. Gullino, S. Choudhary, T. Derra, F. Benn, F. D'Elia, M. Müther, S. Thomas, A. Huang, A. Allanore, A. Kopp, N. Birbilis, A detailed microstructural and corrosion

analysis of magnesium alloy WE43 manufactured by selective laser melting, Additive Manufacturing 35 (2020) 101321.
[206] C. Man, C. Dong, L. Wang, D. Kong, X. Li, Long-term corrosion kinetics and mechanism of magnesium alloy AZ31 exposed to a dry tropical desert environment, Corros Sci 163 (2020) 108274.
[207] C. Zhao, F. Cao, G. Song, Corrosivity of haze constituents to pure Mg, Journal of Magnesium and Alloys 8 (1) (2020) 150–162.
[208] Y.M. Yan, A. Maltseva, P. Zhou, X.J. Li, Z.R. Zeng, O. Gharbi, K. Ogle, M.La Haye, M. Vaudescal, M. Esmaily, N. Birbilis, P. Volovitch, On the in-situ aqueous stability of an Mg-Li-(Al-Y-Zr) alloy: Role of Li, Corros Sci 164 (2020) 108342.
[209] A. Bahmani, S. Arthanari, K.S. Shin, Formulation of corrosion rate of magnesium alloys using microstructural parameters, Journal of Magnesium and Alloys 8 (1) (2020) 134–149.
[210] Y. Dai, X. Chen, T. Yan, A. Tang, D. Zhao, Z. Luo, C. Liu, R. Cheng, F. Pan, Improved Corrosion Resistance in AZ61 Magnesium Alloys Induced by Impurity Reduction, Acta Metallurgica Sinica (English Letters) 33 (2) (2020) 225–232.
[211] A.S. Gnedenkov, S.V. Lamaka, S.L. Sinebryukhov, D.V. Mashtalyar, V.S. Egorkin, I.M. Imshinetskiy, A.G. Zavidnaya, M.L. Zheludkevich, S.V. Gnedenkov, Electrochemical behaviour of the MA8 Mg alloy in minimum essential medium, Corros Sci 168 (2020) 108552.
[212] L. Wang, J. Jiang, H. Liu, B. Saleh, A. Ma, Microstructure characterization and corrosion behavior of Mg–Y–Zn alloys with different long period stacking ordered structures, Journal of Magnesium and Alloys 8 (4) (2020) 1208–1220.
[213] L. Li, T. Wang, Y. Wang, C. Zhang, H. Lv, H. Lin, W. Yu, C. Huang, Effects of ytterbium addition and heat treatment on the mechanical properties and biocorrosion behaviors of Mg–Zn–Zr alloy, Journal of Magnesium and Alloys 8 (2) (2020) 499–509.
[214] M. Liu, J. Wang, S. Zhu, Y. Zhang, Y. Sun, L. Wang, S. Guan, Corrosion fatigue of the extruded Mg–Zn–Y–Nd alloy in simulated body fluid, Journal of Magnesium and Alloys 8 (1) (2020) 231–240.
[215] Y. Li, X. Lu, K. Wu, L. Yang, T. Zhang, F. Wang, Exploration the inhibition mechanism of sodium dodecyl sulfate on Mg alloy, Corros Sci 168 (2020) 108559.
[216] C. Zhang, L. Wu, G. Huang, Y. Huang, B. Jiang, A. Atrens, F. Pan, Effect of microalloyed Ca on the microstructure and corrosion behavior of extruded Mg alloy AZ31, J Alloy Compd 823 (2020) 153844.
[217] C. Zhang, L. Wu, H. Liu, G. Huang, B. Jiang, A. Atrens, F. Pan, Microstructure and corrosion behavior of Mg-Sc binary alloys in 3.5wt.% NaCl solution, Corros Sci 174 (2020) 108831.
[218] C. Zhang, L. Wu, Z. Zhao, G. Huang, B. Jiang, A. Atrens, F. Pan, Effect of Al on the microstructure, corrosion behavior and mechanical properties of Mg-4Li, Anti-Corros Method M 67 (1) (2020) 31–37.
[219] H. Zengin, Y. Turen, Effect of Y addition on microstructure and corrosion behavior of extruded Mg–Zn–Nd–Zr alloy, Journal of Magnesium and Alloys 8 (3) (2020) 640–653.
[220] X. Zhang, K. Zhang, J. Zou, P. Yan, L. Song, Y. Liu, Surface microstructure modifications and in-vitro corrosion resistance improvement of a WE43 Mg alloy treated by pulsed electron beams, Vacuum 173 (2020) 109132.
[221] X. Liu, T.C. Zhang, H. He, L. Ouyang, S. Yuan, A stearic Acid/CeO2 bilayer coating on AZ31B magnesium alloy with superhydrophobic and self-cleaning properties for corrosion inhibition, J Alloy Compd 834 (2020) 155210.
[222] W. Wu, F. Zhang, Y. Li, L. Song, D. Jiang, R. Zeng, S.C. Tjong, D. Chen, Corrosion resistance of dodecanethiol-modified magnesium hydroxide coating on AZ31 magnesium alloy, Appl. Phys. A 126 (1) (2020).
[223] J. Xie, J. Hu, L. Fang, X. Liao, R. Du, F. Wu, L. Wu, Facile fabrication and biological properties of super-hydrophobic coating on magnesium alloy used as potential implant materials, Surf. Coat. Technol. 384 (2020) 125223.
[224] Y. Luo, W. Yao, W. Fu, L. Wu, D. Zhang, F. Pan, Preparing superhydrophobic nanocomposite coating with SiO2 nanoparticles on magnesium alloy, Surf Eng (2020) 1–8.
[225] S. Jian, C. Yang, J. Chang, Robust corrosion resistance and self-healing characteristics of a novel Ce /Mn conversion coatings on EV31 magnesium alloys, Appl Surf Sci 510 (2020) 145385.
[226] D. Yan, Y. Wang, J. Liu, D. Song, T. Zhang, J. Liu, F. He, M. Zhang, J. Wang, Self-healing system adapted to different pH environments for active corrosion protection of magnesium alloy, J Alloy Compd 824 (2020) 153918.
[227] L. Li, Z. Xie, C. Fernandez, L. Wu, D. Cheng, X. Jiang, C. Zhong, Development of a thiophene derivative modified LDH coating for Mg alloy corrosion protection, Electrochim Acta 330 (2020) 135186.
[228] X. Wang, C. Jing, Y. Chen, X. Wang, G. Zhao, X. Zhang, L. Wu, X. Liu, B. Dong, Y. Zhang, Active corrosion protection of super-hydrophobic corrosion inhibitor intercalated Mg–Al layered double hydroxide coating on AZ31 magnesium alloy, Journal of Magnesium and Alloys 8 (1) (2020) 291–300.
[229] C. Li, C. Yu, R. Zeng, B. Zhang, L. Cui, J. Wan, Y. Xia, In vitro corrosion resistance of a Ta2O5 nanofilm on MAO coated magnesium alloy AZ31 by atomic layer deposition, Bioactive Materials 5 (1) (2020) 34–43.
[230] Y. Chen, X. Lu, S.V. Lamaka, P. Ju, C. Blawert, T. Zhang, F. Wang, M.L. Zheludkevich, Active protection of Mg alloy by composite PEO coating loaded with corrosion inhibitors, Appl Surf Sci 504 (2020) 144462.
[231] W. Shang, F. Wu, Y. Wang, A. Rabiei Baboukani, Y. Wen, J. Jiang, Corrosion Resistance of Micro-Arc Oxidation/Graphene Oxide Composite Coatings on Magnesium Alloys, ACS Omega 5 (13) (2020) 7262–7270.
[232] L. Pezzato, R. Babbolin, P. Cerchier, M. Marigo, P. Dolcet, M. Dabalà, K. Brunelli, Sealing of PEO coated AZ91magnesium alloy using solutions containing neodymium, Corros Sci 173 (2020) 108741.
[233] M. Mohedano, P. Pérez, E. Matykina, B. Pillado, G. Garcés, R. Arrabal, PEO coating with Ce-sealing for corrosion protection of LPSO Mg–Y–Zn alloy, Surf. Coat. Technol. 383 (2020) 125253.
[234] Y. Wang, B. Normand, H. Liao, G. Zhao, N. Mary, J. Tang, SiCp/Al5056 Composite Coatings Applied to A Magnesium Substrate by Cold Gas Dynamic Spray Method for Corrosion Protection, Coatings 10 (4) (2020) 325.
[235] L. Guo, C. Gu, J. Feng, Y. Guo, Y. Jin, J. Tu, Hydrophobic epoxy resin coating with ionic liquid conversion pretreatment on magnesium alloy for promoting corrosion resistance, J Mater Sci Technol 37 (2020) 9–18.
[236] L. Cui, S. Cheng, L. Liang, J. Zhang, S. Li, Z. Wang, R. Zeng, In vitro corrosion resistance of layer-by-layer assembled polyacrylic acid multilayers induced Ca–P coating on magnesium alloy AZ31, Bioactive Materials 5 (1) (2020) 153–163.
[237] Z. Zhang, R. Zeng, C. Lin, L. Wang, X. Chen, D. Chen, Corrosion resistance of self-cleaning silane/polypropylene composite coatings on magnesium alloy AZ31, J Mater Sci Technol 41 (2020) 43–55.
[238] B.K. Jiang, A.Y. Chen, J.F. Gu, J.T. Fan, Y. Liu, P. Wang, H.J. Li, H. Sun, J.H. Yang, X.Y. Wang, Corrosion resistance enhancement of magnesium alloy by N-doped graphene quantum dots and polymethyltrimethoxysilane composite coating, Carbon 157 (2020) 537–548.
[239] R. Hou, F. Zhang, P. Jiang, S. Dong, J. Pan, C. Lin, Corrosion inhibition of pre-formed mussel adhesive protein (Mefp-1) film to magnesium alloy, Corros Sci 164 (2020) 108309.